

1-1-2011

# Atrial Arrhythmogenic Substrates: The Role of Structure and Molecular Remodeling

Christina Ambrosi

Washington University in St. Louis

Follow this and additional works at: <https://openscholarship.wustl.edu/etd>

---

## Recommended Citation

Ambrosi, Christina, "Atrial Arrhythmogenic Substrates: The Role of Structure and Molecular Remodeling" (2011). *All Theses and Dissertations (ETDs)*. 548.

<https://openscholarship.wustl.edu/etd/548>

This Dissertation is brought to you for free and open access by Washington University Open Scholarship. It has been accepted for inclusion in All Theses and Dissertations (ETDs) by an authorized administrator of Washington University Open Scholarship. For more information, please contact [digital@wumail.wustl.edu](mailto:digital@wumail.wustl.edu).

WASHINGTON UNIVERSITY IN ST. LOUIS

School of Engineering and Applied Science

Department of Biomedical Engineering

Dissertation Examination Committee:

Igor R. Efimov, Chair

Dan Moran

Jeanne M. Nerbonne

Joseph A. O'Sullivan

Richard B. Schuessler

Frank C-P. Yin

Atrial Arrhythmogenic Substrates: The Role of Structure and

Molecular Remodeling

by

Christina Marie Ambrosi

A dissertation presented to the  
Graduate School of Arts and Sciences  
of Washington University in  
partial fulfillment of the  
requirements for the degree  
of Doctor of Philosophy

August 2011

Saint Louis, Missouri

copyright by  
Christina Marie Ambrosi  
2011

## ABSTRACT OF THE DISSERTATION

Atrial Arrhythmogenic Substrates: The Role of Structure and Molecular Remodeling

by

Christina Marie Ambrosi

Doctor of Philosophy in Biomedical Engineering

Washington University in St. Louis, August 2011

Igor R. Efimov, Chair

Atrial tachyarrhythmias, specifically atrial flutter (AFL) and fibrillation (AF), affect over 2.2 million Americans, leading to more hospitalizations than any other cardiac arrhythmia. These arrhythmias are defined by the presence of reentrant circuits of excitation leading to high atrial rates and uncoordinated activation of the ventricles. The underlying mechanisms of AFL/AF have proven complex and, despite a century of research, no one effective treatment has been developed. Surgical ablation and pharmacological therapies are both fraught with risks and potential pro-arrhythmic side effects. Electrical cardioversion, on the other hand, is extremely effective in terminating these arrhythmias, but the high-energy shocks required for termination cause substantial pain to the patient.

In this dissertation, we first investigate the underlying molecular and structural mechanisms of AF in two clinically-relevant models – the human and canine hearts. We identify structural and molecular substrates responsible for the generation and maintenance of AFL/AF. We then explore the application of a novel low-voltage

defibrillation therapy to a rabbit model of atrial tachyarrhythmias and show significant reductions in the defibrillation threshold for both AF and AFI. We utilize a variety of experimental techniques, such as high throughput quantitative PCR, optical coherence tomography, and optical mapping. Only truly integrative approaches to arrhythmia research, combining a variety of experimental models and techniques, can continue to unravel the complexities of underlying molecular, structural, and electrophysiological mechanisms and develop effective, safe therapies, as we demonstrate in this dissertation with regards to atrial tachyarrhythmias.

## Acknowledgements

First, and foremost, I would like to thank my advisor, Dr. Igor Efimov, for his endless support and enthusiasm during the last five years. Upon my entrance to graduate school, after working in industry for two years, I was seeking a research environment with a truly translational approach to cardiac electrophysiology. I found exactly what I was looking for in the Efimov lab.

I would also like to thank Dr. Frank C-P. Yin for his constant support and encouragement during the cumulative ten years of my education at Wash U. Back in early 2001 Dr. Yin gave me a chance as an undergraduate researcher in his lab and I am forever grateful for that experience and the love of research it instilled in me.

I would also like to thank other members of the Efimov lab who, over the years, have positively impacted my work, scientific development, and the many hours I have spent in lab. I would especially like to thank Dr. Vadim Fedorov, a brilliant scientist and experimentalist, who, before departing Wash U to start his own lab, taught me a tremendous amount about electrophysiological experimental techniques. Dr. Deborah Janks provided a tremendous amount of overall support and enthusiasm for all projects in this dissertation and is also always a wonderful sounding board. I would also like to thank my fellow graduate students (both past and present) in the lab, especially Bill Hucker, Crystal Ripplinger, Qing Lou, Jake Laughner, Di Lang, Matt Sulkin, and Katherine Holzem, for their kindness and support over the last several years.

I am also very grateful for the support of my thesis committee: Dr. Dan Moran, Dr. Jeanne Nerbonne, Dr. Joseph O'Sullivan, Dr. Richard Schuessler, and Dr. Frank Yin. This work also would never have been completed with the support and friendship of Glen Reitz, Amanda Carr, and Karen Teasdale. I would also like to thank the National Institutes of Health and the American Heart Association for funding these projects.

The new friendships I have made and the old friendships I have strengthened during my time in graduate school have also been a tremendous source of support and fun over the last five years. I am grateful for new friends I have met through running and I am especially grateful for my dear friend Sara Oswald and her amazing family for so much over the years.

Finally, I would like to dedicate this dissertation to my family, especially my parents, whose unwavering love and support are neverending.

Christina M. Ambrosi  
*Washington University in St. Louis*  
*August 2011*

# Table of Contents

<b>Abstract of the Dissertation.....</b>	<b>ii</b>
<b>Acknowledgements.....</b>	<b>iv</b>
<b>List of Figures.....</b>	<b>viii</b>
<b>List of Tables.....</b>	<b>x</b>
<b>1 Introduction.....</b>	<b>1</b>
1.1 Historical Identification of Atrial Fibrillation.....	2
1.2 Elucidating the Mechanisms of Atrial Fibrillation.....	3
1.2.1 Critical Mass Hypothesis.....	5
1.2.2 Atrial Remodeling in Fibrillation.....	5
1.3 Atrial Fibrillation and Atrial Flutter.....	7
1.4 Atrial Fibrillation and Heart Failure.....	8
1.5 Tools for Understanding the Structure-Function Relationship of Atrial Flutter and Fibrillation.....	9
1.5.1 Experimental Models.....	10
1.5.1.1 Human.....	10
1.5.1.2 Dog.....	11
1.5.1.3 Rabbit.....	11
1.5.2 Experimental Techniques.....	12
1.5.2.1 Quantitative PCR.....	12
1.5.2.2 Optical Coherence Tomography.....	14
1.5.2.3 Optical Mapping.....	16
1.6 Scope and Procedure of the Dissertation.....	17
<b>2 Gender Dependent Differences in Molecular Electrophysiological Targets in Failing and Nonfailing Human Hearts.....</b>	<b>19</b>
2.1 Abstract.....	19
2.2 Introduction.....	20
2.3 Materials and Methods.....	22
2.3.1 Human Tissue Samples.....	22
2.3.2 RNA Extraction and Preparation.....	25
2.3.3 Low-Density Taqman Gene Arrays.....	26
2.3.4 Statistics and Data Analysis.....	26
2.4 Results.....	27
2.4.1 Hierarchical Cluster Analysis.....	27
2.4.2 Ventricular Remodeling in Heart Failure.....	28
2.4.3 Regional Specificity of Target Expression.....	30
2.5.3.1 Regional Specificity of $I_{KATP}$ Subunits.....	31
2.4.4 Gender Dependent Atrial/Ventricular Bias.....	34
2.4.5 Gender Dependent Atrial Remodeling.....	35

	2.4.6	Gender Dependent Ventricular Remodeling.....	39
	2.4.7	Gender Dependent Transmural Heterogeneity.....	40
	2.5	Discussion.....	41
	2.6	Conclusion.....	47
<b>3</b>		<b>Virtual Histology of the Human Heart Using Optical Coherence Tomography.....</b>	<b>48</b>
	3.1	Abstract.....	48
	3.2	Introduction.....	49
	3.3	Materials and Methods.....	51
	3.3.1	Experimental Preparations.....	51
	3.3.2	OCT Imaging.....	52
	3.3.3	Histology.....	53
	3.3.4	Computational Analysis and Statistics.....	53
	3.4	Results.....	54
	3.4.1	OCT of the Atria and Ventricles.....	54
	3.4.2	OCT of the Sinoatrial Node.....	58
	3.4.3	OCT of the Atrioventricular Junction.....	61
	3.5	Discussion.....	62
	3.6	Conclusion.....	64
<b>4</b>		<b>Quantification of Fiber Orientation in the Canine Atrial Pacemaker Complex Using Optical Coherence Tomography.....</b>	<b>65</b>
	4.1	Abstract.....	66
	4.2	Introduction.....	67
	4.3	Materials and Methods.....	69
	4.3.1	Experimental Preparation.....	69
	4.3.2	OCT Imaging.....	70
	4.3.3	Histology and Immunohistochemistry.....	70
	4.3.4	OCT Image Processing and Analysis.....	71
	4.4	Results.....	72
	4.4.1	Identification of the Atrial Pacemaker Complex.....	72
	4.4.2	Quantification of Fiber Orientation.....	75
	4.4.3	Fiber Orientation in the Block Zone.....	80
	4.5	Discussion.....	81
	4.6	Conclusion.....	84
<b>5</b>		<b>Termination of Sustained Atrial Flutter and Fibrillation Using Low-Voltage Multiple-Shock Therapy.....</b>	<b>85</b>
	5.1	Abstract.....	85
	5.2	Introduction.....	86
	5.3	Materials and Methods.....	90
	5.3.1	Experimental Preparation.....	90
	5.3.2	Optical Mapping and Defibrillation Setup.....	91
	5.3.3	Experimental Protocol.....	92
	5.3.4	Data Analysis.....	93



5.4	Results.....	93
5.4.1	Initiation of Arrhythmias.....	93
5.4.2	Application of Antitachycardia Pacing.....	95
5.4.3	Far Field Excitation Threshold.....	97
5.4.4	Termination of Atrial Flutter by Low-Voltage Multiple-Shock Therapy.....	98
5.4.5	Termination of Atrial Fibrillation by Low-Voltage Multiple-Shock Therapy.....	100
5.4.6	Mechanisms of Termination.....	101
5.4.7	Therapy Safety.....	103
5.5	Discussion.....	104
5.5.1	Antitachycardia Pacing.....	104
5.5.2	Monophasic versus Biphasic Shocks.....	105
5.5.3	Arrhythmia Organization and Defibrillation.....	105
5.5.4	Patient Pain Perception.....	106
5.5.5	Safety.....	107
5.6	Conclusion.....	108
<b>6</b>	<b>Concluding Remarks and Future Directions.....</b>	<b>110</b>
<b>Appendix A</b>	<b>Relative Quantification Data from Failing and Nonfailing Human Hearts of Both Genders.....</b>	<b>116</b>
<b>Appendix B</b>	<b>Master-8 Pacing and Acquisition Control Program.....</b>	<b>119</b>
B.1	Components of the Low-Voltage Defibrillation Setup.....	119
B.2	LabVIEW Software Configuration.....	121
B.2.1	User Interface.....	121
B.2.2	LabVIEW Code.....	122
B.3	Conclusion and Additional Applications.....	123
	<b>References.....</b>	<b>125</b>
	<b>CV.....</b>	<b>150</b>

## List of Figures

Figure 1.1	Electrocardiograms recorded by Thomas Lewis, 1912.....	3
Figure 1.2	Concept of reentry proposed by George Mines, 1913.....	4
Figure 1.3	Summary of human heart clinical characteristics.....	10
Figure 1.4	Mechanism of qPCR using the Taqman probe.....	12
Figure 1.5	Example qPCR amplification plot.....	13
Figure 1.6	Principles of OCT.....	15
Figure 1.7	Typical OCT data set.....	15
Figure 1.8	Typical optical mapping set up.....	17
Figure 2.1	Study population.....	23
Figure 2.2	Tissue sample locations in the human heart.....	24
Figure 2.3	RNA quality assessment.....	25
Figure 2.4	Hierarchical cluster analysis.....	28
Figure 2.5	Ventricular remodeling in heart failure.....	30
Figure 2.6	Regional specificity in failing and nonfailing hearts.....	31
Figure 2.7	Effect of $K_{ATP}$ channel openers on the action potential duration in isolated human hearts.....	33
Figure 2.8	Transcript-level expression of $K_{ATP}$ channel subunits in the failing and nonfailing human heart.....	34
Figure 2.9	Gender dependent comparison of relative expression levels of all genes.....	35
Figure 2.10	Gender dependent atrial remodeling in failing and nonfailing hearts.....	36
Figure 2.11	Relative expression levels of failing left atrial samples of both genders.....	37
Figure 2.12	Gender dependent adrenergic receptor remodeling in failing and nonfailing hearts.....	38
Figure 2.13	Relative expression levels of adrenergic receptors in failing left atrial samples of both genders.....	38
Figure 2.14	Gender dependent ventricular remodeling in failing and nonfailing hearts.....	39
Figure 2.15	Relative expression levels of failing left ventricular samples of both genders.....	40
Figure 2.16	Average ratios of epicardial to endocardial expression of repolarization targets.....	41
Figure 3.1	OCT of the atria.....	55
Figure 3.2	OCT of the ventricles.....	56
Figure 3.3	OCT of an isolated coronary artery.....	57
Figure 3.4	Transmural OCT of the infarcted right ventricle.....	58
Figure 3.5	Endocardial OCT of the sinoatrial node.....	59
Figure 3.6	Transmural OCT of the sinoatrial node.....	60
Figure 3.7	Endocardial OCT of the atrioventricular junction.....	62
Figure 4.1	Identification of the atrial pacemaker complex.....	74
Figure 4.2	Correlation of histology and OCT.....	75
Figure 4.3	Identification of the crista terminalis and interatrial septum with OCT.....	76

Figure 4.4	Identification of the sinoatrial node with OCT.....	77
Figure 4.5	Fiber angle distribution in the crista terminalis, atrium, and sinoatrial node.....	78
Figure 4.6	Average fiber angle.....	79
Figure 4.7	Standard deviation of the average fiber angle.....	80
Figure 4.8	Identification of the block zone with OCT.....	81
Figure 5.1	Low-voltage multiple-shock experimental setup.....	94
Figure 5.2	Typical atrial flutter and fibrillation.....	95
Figure 5.3	Application of antitachycardia pacing to atrial flutter.....	96
Figure 5.4	Far field excitation.....	97
Figure 5.5	Defibrillation thresholds.....	99
Figure 5.6	Shock field strength as a function of number of shocks.....	99
Figure 5.7	Defibrillation threshold as a function of arrhythmia cycle length.....	100
Figure 5.8	Application of multiple shocks to atrial flutter.....	102
Figure 5.9	Application of multiple shocks to atrial fibrillation.....	103
Figure B.1	Schematic of the overall experimental setup for defibrillation study.....	120
Figure B.2	User interface for LabVIEW program used to coordinate pacing protocols, shock delivery, and optical data acquisition.....	121
Figure B.3	LabVIEW block diagram for application of dual prematurity and optical data acquisition.....	123
Figure B.4	LabVIEW block diagram for delivery of defibrillation therapy and optical data acquisition.....	123

## List of Tables

Table 2.1	Clinical data for nonfailing hearts.....	24
Table 2.2	Clinical data for failing hearts.....	25
Table 3.1	Clinical data.....	52

# 1 Introduction

Atrial fibrillation (AF) affects more than 2.2 million Americans (Lloyd-Jones, Adams et al. 2010), a number that continues to grow as the population ages. By the year 2050 it is estimated that between 12 and 16 million Americans may be affected by this condition (Miyasaka, Barnes et al. 2006). In addition to an increased mortality rate, AF also leads to more hospitalizations than any other cardiac arrhythmia, resulting in a significant socioeconomic burden (Coyne, Paramore et al. 2006; Crandall, Horne et al. 2009; Kannel and Benjamin 2009). Despite over a century of research, no single effective pharmacological treatment for AF has been developed (Tamargo, Caballero et al. 2004). In addition, surgical ablation procedures are fraught with risks, including, but not limited to, esophageal injury, phrenic nerve injury, and pulmonary vein stenosis (Doppalapudi, Yamada et al. 2009). Electrical cardioversion, on the other hand, is extremely effective in defibrillating AF (Koster, Dorian et al. 2004), but the high shock energies required for

termination can cause cardiac damage (Khan 2003; Fedorov, Kostecki et al. 2008) and substantial pain to the patient (Mitchell, Spurrell et al. 2004).

AF can be classified as a progressive disease and, if left untreated paroxysmal AF can degenerate into permanent AF (Cohen and Naccarelli 2008), for example, in a process personified as “AF begets AF” (Wijffels, Kirchhof et al. 1995). Understanding the electrical, structural, and molecular remodeling associated with this process is ongoing. Ultimately, the success of AF therapy depends on a thorough understanding of the global mechanisms of this complicated, confounding arrhythmia.

The work presented in this dissertation will seek to further understand the molecular and structural substrates of atrial fibrillation and then explore the application of a novel defibrillation therapy to a rabbit model of atrial tachyarrhythmias. A variety of experimental techniques, including high-throughput quantitative PCR, optical coherence tomography, and optical mapping will be applied in this investigation.

## **1.1 Historical Identification of Atrial Fibrillation**

The earliest record of atrial fibrillation is believed to be located in The Yellow Emperor’s Classic of Internal Medicine composed over two millennia ago (Lip and Beevers 1995).

The first description of auricular fibrillation, now more commonly known as AF, is, however, credited to Sir William Harvey in 1628 (McMichael 1982). After Harvey’s initial description of the arrhythmia, it was not until the late nineteenth century that the

first pulse tracings of patients in atrial fibrillation were recorded and identified as such (Silverman 1994; Khasnis and Thakur 2009). The first electrocardiographic identification followed shortly thereafter and was published in 1909 by Thomas Lewis. The arrhythmia was described as “pulsus inaequalis and irregularis” and the ECG, shown in Figure 1.1, showed a distinct lack of p-waves, which would have represented normal atrial activity, exhibiting instead a jagged series of fibrillatory waves termed f-waves (Lewis 1909).

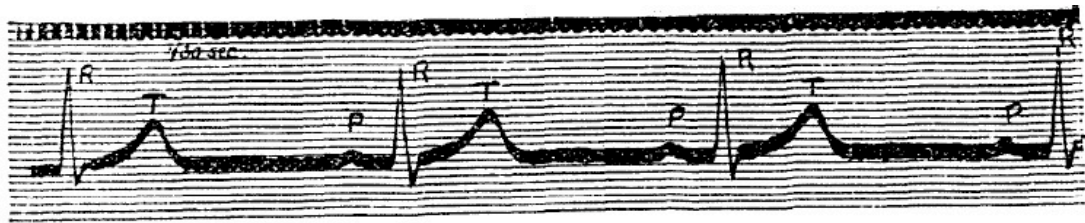
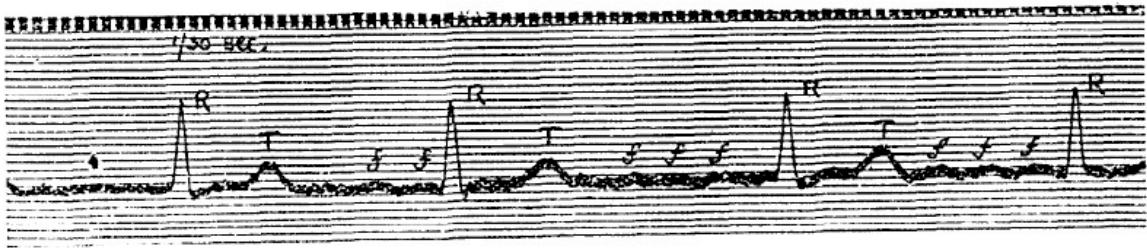


Fig. 2.—An electro-cardiogram from a normal subject, showing the usual electric variations, p, r, and t; p corresponds to auricular contraction, r and t correspond to ventricular systole. The time is in 1/50 second.



**Figure 1.1:** Electrocardiograms recorded by Thomas Lewis, 1912. Top, a patient in normal sinus rhythm. Bottom, a patient in atrial fibrillation displaying f-waves (Lewis 1912a).

## 1.2 Elucidating the Mechanisms of Atrial Fibrillation

Despite more than a century of research, the mechanisms of atrial fibrillation remain unclear. Initially, AF was thought to arise due to rapid focal activity in one (or more) atrial locations (Lewis 1912b). In 1913, however, George Mines proposed that

fibrillatory waves are caused by reentrant circuits in tissue with specific refractory characteristics (Mines 1913), as illustrated in Figure 1.2.

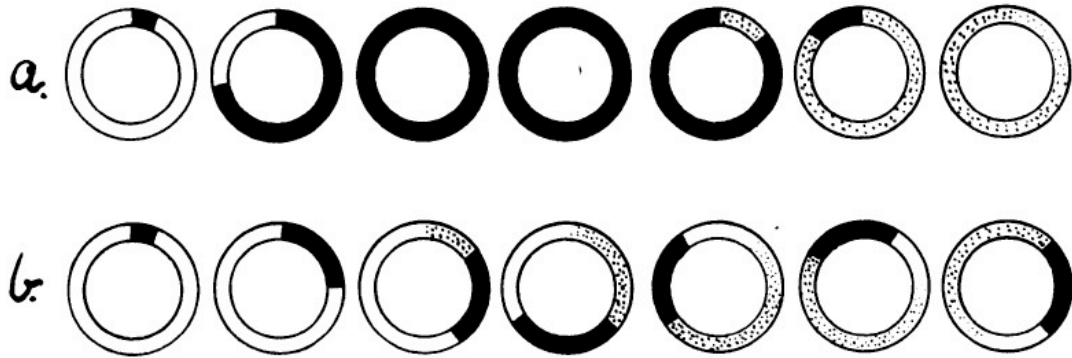


**Figure 1.2:** Concept of reentry proposed by George Mines, 1913. (a) Nonsustained reentry. (b) Sustained reentry (Mines 1913).

In 1921, Lewis and colleagues formulated a “mother ring” theory, which suggested that a single reentrant circuit is sufficient to maintain atrial fibrillation. This theory was later developed into the modern-day “mother rotor” hypothesis and has since been demonstrated experimentally (Mandapati, Skanes et al. 2000). In contrast to the “mother rotor” hypothesis, Walter Garrey and later Gordon Moe suggested that multiple reentrant waves, as opposed to one main rotor, are necessary for the maintenance of AF (Garrey 1924; Moe 1968). Maurits Allessie has since provided compelling experimental evidence supporting this latter theory (Allessie, Lammers et al. 1985). In addition, more recent clinical evidence in support of the original focal activation theory has been presented by Michel Haissaguerre and colleagues (Haissaguerre, Jais et al. 1998). Focal activity has since been shown to arise from the pulmonary veins (Haissaguerre, Jais et al. 1998), superior vena cava (Li and Wang 2006), coronary sinus (Haissaguerre, Hocini et al.



2006), and the vein of Marshall (Chen, Chou et al. 2006). In addition, the autonomic basis of atrial fibrillation has also been explored (Coumel 1994a).

### **1.2.1 Critical Mass Hypothesis**

The maintenance of a reentrant arrhythmia also relies upon a critical mass of tissue required for fibrillation. This theory was first proposed by William Garrey in 1914, during his tenure at Washington University. In that study, Garrey found that by progressively diminishing the size of cardiac tissue, fibrillation could eventually no longer be sustained (Garrey 1914). The subsequent development of the maze procedure for surgical treatment of atrial fibrillation, also developed at Washington University, was based on this concept (Cox and Sundt 1997). By dividing the fibrillating atrium into smaller units while still allowing for normal sinus node activation, this procedure eliminates the minimum path length needed to sustain reentry in fibrillation (Weiner and Rosenbluth 1946).

### **1.2.2 Atrial Remodeling in Fibrillation**

Atrial fibrillation is accompanied by both short- and long-term remodeling processes (Brundel, Henning et al. 2002), which makes it increasingly difficult to convert to and maintain normal sinus rhythm with either pharmacological agents or cardioversion, the longer the arrhythmia persists (Van Gelder, Crijns et al. 1991; Coro, Delise et al. 2001). Experimental and clinical studies point to both electrical and structural remodeling as the cause of this maladaptation (Wijffels, Kirchhof et al. 1995; Ausma, Wijffels et al. 1997).

Immediate short-term changes in the atrial substrate include functional changes in the L-type calcium channel ( $I_{Ca,L}$ ) (Yue, Feng et al. 1997) accompanied by concurrent changes in protein-level expression of the channel subunits (Van Wagoner, Pond et al. 1999; Brundel, Van Gelder et al. 2001a). This reduction in  $I_{Ca,L}$  results in a marked decrease of the atrial effective refractory period (ERP) and detrimental changes in action potential rate adaptation (Wijffels, Kirchhof et al. 1995). Longer-term changes associated with AF include, in addition to persistently reduced levels of  $I_{Ca,L}$ , marked reductions in the expression of repolarizing potassium channels (Brundel, Van Gelder et al. 2001a; Brundel, Van Gelder et al. 2001b). Although it has been shown that the primary electrophysiological changes during AF are due to the reduction in  $I_{Ca,L}$  (Yue, Feng et al. 1997; Brundel, Van Gelder et al. 2001a), the concomitant reductions in potassium currents are thought to be an adaptation of the atrial cells to these overall detrimental changes (Brundel, Van Gelder et al. 2001a). The long-term, persistent alterations in these (and other) ion channels, which directly affect the atrial electrophysiological properties, play an important role in the continued susceptibility to the reinduction of AF even after restoration of normal sinus rhythm.

In addition to molecular-level remodeling of ion channels and their resulting effects on basic electrophysiological parameters, AF is also accompanied by the development of structural abnormalities. For instance, in a goat model of rapid atrial pacing-induced AF up to 92% of atrial myocytes exhibited mitochondrial enlargement, glycogen accumulation, and loss of myofibrils (Ausma, Wijffels et al. 1997). A similar study in human atrial myocytes showed that patients with persistent AF exhibited the most

pronounced structural changes (Mary-Rabine, Albert et al. 1983). In addition, increased atrial fibrosis can lead to the continued generation and maintenance of AF (Pellman, Lyon et al. 2010). Taken together, these electrophysiological, molecular, and structural changes create overall tissue heterogeneities, which can further effect atrial ERPs and continue the promotion of AF in the cycle termed “AF begets AF” (Wijffels, Kirchhof et al. 1995).

### **1.3 Atrial Fibrillation and Atrial Flutter**

AF typically involves multiple reentrant circuits defined by both local tissue heterogeneities and electrophysiological properties. Classic atrial flutter (AFl), on the other hand, is typically defined by a macro-reentrant circuit rotating around an anatomical and/or functional line of block. Major anatomical structures, including the region between the vena cavae and pulmonary veins, are usually involved in defining reentry (Fedorov, Chang et al. 2010). It is also well-known from the seminal studies in atrial tachyarrhythmias that AF can revert to AFl and vice versa (Garrey 1924). More recent investigations have defined the inter-relationships between these two arrhythmias and have shown that in most cases AF, of variable durations, precedes most instances of AFl and is instrumental in creating the functional line of block between the vena cavae responsible for the subsequent maintenance of AFl (Waldo 2003). Although molecular remodeling associated with AFl has not been investigated in detail, a recent study has shown that patients with occasional episodes of AFl did indeed exhibit structural and

functional atrial abnormalities that may also predispose them to the eventual development of permanent AF (Stiles, Wong et al. 2010).

Treatment options for AFI are similar to those for AF specifically with respect to both rhythm and rate control (Dhar, Lidhoo et al. 2009). Pharmacological treatments are often utilized to maintain normal sinus rhythm and control fast and/or irregular ventricular rates (Van Gelder, Tuinenburg et al. 1999). Electrocardioversion of AFI has success rates close to 100% and rapid pacing protocols, also known as antitachycardia pacing, can also be used to interrupt the reentrant circuits maintaining the arrhythmia, although its published success rates are variable (Van Gelder, Tuinenburg et al. 1999; Koster, Dorian et al. 2004). Finally, ablation is also an option for severely symptomatic patients whose rate and rhythm cannot be controlled by other means (Dhar, Lidhoo et al. 2009).

## **1.4 Atrial Fibrillation and Heart Failure**

Congestive heart failure (CHF) affects 5.8 millions Americans (Lloyd-Jones, Adams et al. 2010) and is associated with any number of comorbidities, including AF. In fact, 25% of heart failure patients will develop AF within five years of their initial diagnosis (Wang, Larson et al. 2003) and its prevalence increases with increasing severity of CHF (Maisel and Stevenson 2003). In addition, within five years of being diagnosed with AF, 15% of all patients will develop heart failure (Wang, Larson et al. 2003). Not only does the development of one condition increase the risk of developing the other, but there is also an increased mortality risk with the development of both AF and CHF (Wang,

Larson et al. 2003). Consequently, there is a complex interplay of factors predisposing patients with AF to CHF and vice versa.

In CHF, atrial pressure and volume overload contribute to the development of atrial enlargement which can directly effect atrial electrophysiological parameters, including dispersion of refractory properties (Maisel and Stevenson 2003). In addition, neurohormonal activation can affect the synthesis and degradation of the extracellular matrix thus creating the substrate necessary for the generation and maintenance of AF (Tomaselli and Marban 1999). Conversely, in AF the loss of atrio-ventricular synchrony and development of an irregular ventricular response eventually lead to the long-term remodeling processes associated with CHF (Boyle and Shivkumar 2009).

## **1.5 Tools for Understanding the Structure-Function Relationship of Atrial Flutter and Fibrillation**

The investigations presented in this dissertation were completed through the use of various experimental models and techniques. We used human and canine models to elucidate the molecular and structural mechanisms of atrial tachyarrhythmias, as well as a rabbit model to explore a novel method for low-voltage termination of AF and AFL. To accomplish these tasks we applied several experimental techniques, including high throughput quantitative PCR, optical coherence tomography, and optical mapping.

## 1.5.1 Experimental Models

### 1.5.1.1 Human

Over the last four and a half years, we have developed the infrastructure necessary to collect human hearts for both functional- and structural-level analyses. For the projects contained within this dissertation, we have received hearts from two sources: (1) nonfailing donor hearts rejected for cardiac transplantation from Mid-America Transplant Services (St. Louis, Missouri) and (2) failing hearts from transplant recipients at Barnes-Jewish Hospital (St. Louis, Missouri). The wide spectrum of clinical characteristics, as shown in Figure 1.3, in the hearts we have collected provides the basis for investigating the structural and molecular components important in both normal and abnormal cardiac conduction.

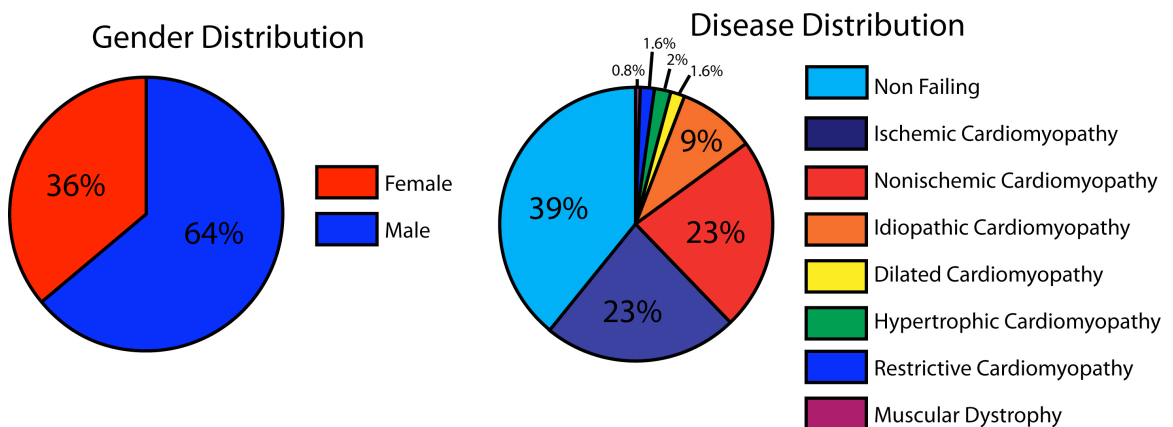


*Figure 1.3: Summary of human heart clinical characteristics (n=128).*

### **1.5.1.2 Dog**

Canine cardiac models, on the other hand, have the distinct advantages of being more readily available, as well as similar in size to the human heart. Recent studies from our group have also demonstrated the functional similarity of the human and dog sinoatrial nodal conduction patterns (Fedorov, Schuessler et al. 2009; Fedorov, Glukhov et al. 2010). Since canine hearts are more reliably available than human hearts, we have consequently used a canine model in our investigation of the structure of the atrial pacemaker complex.

### **1.5.1.3 Rabbit**

The Langendorff-perfused rabbit heart as an experimental model for the defibrillation of AF and AFl offers several unique advantages to our study. First and foremost, this species has been proven to be the most suitable model for *in vitro* research of defibrillation due to its ability to sustain clinically-relevant arrhythmias, which are not typically observed in smaller species (Panfilov 2006). In addition, the size of the rabbit atria allows for thorough reconstruction of electrical activity throughout the thickness of the intact heart using optical techniques. Finally, its atrial tachyarrhythmias are similar to clinically-observed paroxysmal forms of vagal-related “lone-AF” (Coumel 1994b).

## 1.5.2 Experimental Techniques

### 1.5.2.1 Quantitative PCR

Polymerase chain reaction (PCR), developed in 1983, is a commonly-used technique for the amplification and detection of DNA (Bartlett and Stirling 2003). Real-time PCR, also known as quantitative PCR (qPCR), is used to simultaneously amplify and quantify target DNA sequences based on the use of fluorescent probes (VanGuilder, Vrana et al. 2008). Probes can either be non-specific, in which case they will bind to any double stranded DNA molecule, or specific, in which case they bind directly to a desired DNA sequence. In this investigation, we have used Taqman probes, which consist of a reporter and quencher molecule attached to each end of a specific oligonucleotide sequence (Holland, Abramson et al. 1991). When the reporter and quencher are in close proximity (i.e., attached to the 5' and 3' ends of the probe), fluorescence is quenched. When the reporter and quencher are separated (i.e., during primer extension by the Taq polymerase), fluorescence is emitted. Consequently, at each stage of the amplification process, product can be quantified based on the increasing amount of fluorescence in the system. This process is illustrated in Figure 1.4.

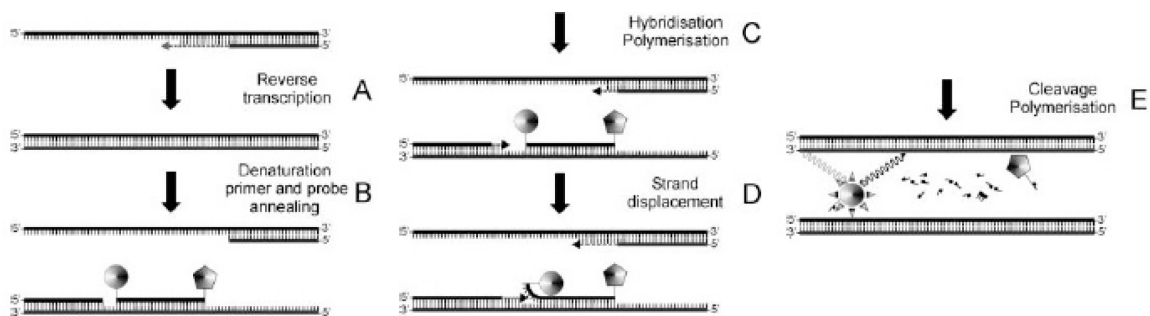


**Figure 1.4:** Mechanism of qPCR using the Taqman probe (Bustin 2000).



The amplification process proceeds in three phases: (1) the exponential phase during which PCR product doubles after each cycle, (2) the linear phase during which reagents begin to run out and the process slows, and (3) the plateau phase during which reagents are depleted and the reaction stops. The exponential phase consequently yields the most useful information for subsequent analysis. As shown in Figure 1.5, during the exponential phase of amplification a threshold is established (as shown by the green line), which represents a level for detection above the background fluorescence. A threshold cycle, more commonly referred to as the  $C_t$ , is then automatically specified. Analysis proceeds using the  $C_t$  relative quantification method (Livak and Schmittgen 2001) with a chosen endogenously-expressed control gene.

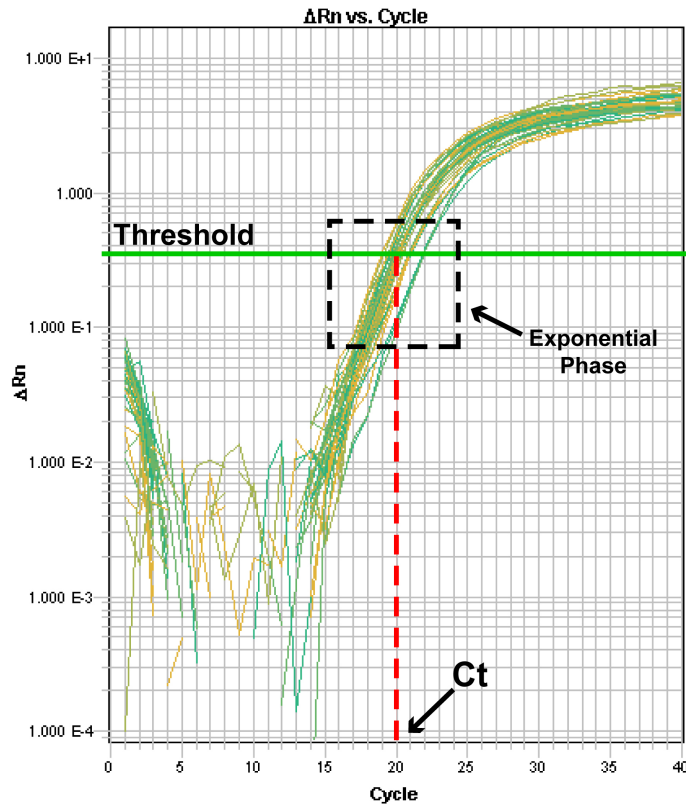


**Figure 1.5:** Example qPCR amplification plot.

### 1.5.2.2 Optical Coherence Tomography

Optical coherence tomography (OCT) was first introduced in 1991 and used to visualize the retina and coronary arteries (Huang, Swanson et al. 1991). Since then it has gained prominence as a diagnostic imaging modality in the fields of ophthalmology (Costa, Skaf et al. 2006; Chang and Budenz 2008; Drexler and Fujimoto 2008), vascular cardiology (Pinto and Waksman 2006; Tearney, Jang et al. 2006; Brezinski 2007; Guagliumi and Sirbu 2008), and dermatology (Welzel 2001; Gambichler, Moussa et al. 2005). In biological specimens, OCT boasts resolutions of submicrometer through 15  $\mu\text{m}$ , which can be 10 to 100 times greater than other modalities, such as MRI and ultrasound (Povazay, Bizheva et al. 2002; Fujimoto 2003). OCT is, however, limited by its depth penetration, estimated to be 2 to 3 mm in nontransparent biological tissues (Fujimoto 2003).

OCT, based on the principle of low-coherence interferometry, measures the backscatter of light reflected from within the depth of nontransparent tissues, as shown in Figure 1.6. Signal intensity is determined by the amplitude and coherence of the reflected waves in comparison with light reflected along a reference arm of known length. Resulting scans consequently create high resolution, non-invasive tissue biopsies. We have termed this technique “virtual histology”.

A typical OCT data set is shown in Figure 1.7. In this example, a trabeculation from the human right atrial endocardium is being imaged (Figure 1.7A). Figure 1.7B shows an example A-scan, or virtual slice, taken perpendicular to the tissue surface. In total, 400

two-dimensional virtual slices are recorded and then reconstructed into a three-dimensional virtual piece of tissue as shown in Figure 1.7C. Subsequently, the virtual tissue can be sliced in any desired direction. In this dissertation, we are most interested in visualizing and quantifying fiber orientation. Consequently, we can virtually slice the tissue parallel to the surface and visualize the underlying cardiac fibers, as shown in Figure 1.7D.

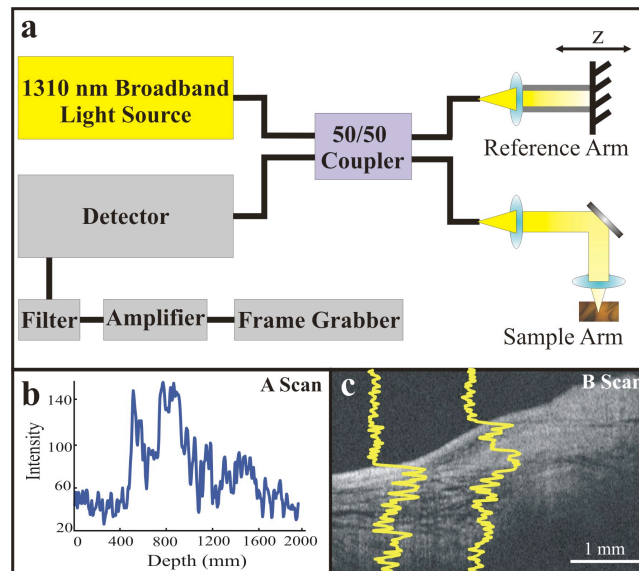


**Figure 1.6:** Principles of OCT. (a) The setup for our bench top OCT system includes a light source feeding directly into a 50/50 coupler splitting light between the reference and sample arms. The reflected light is then sensed by the detector, filtered, and amplified before advancing to the frame grabber. (b) An example A-scan describing the intensity of the reflected light at various depths in the tissue. (c) Multiple A-scans create the final image slices, or 2-D tomogram (B-scan).

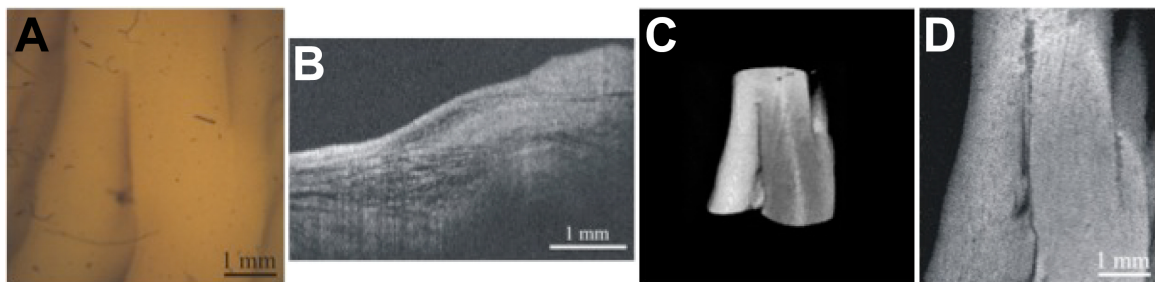


**Figure 1.7:** Typical OCT data set. (A) Atrial trabeculations of the RA appendage as viewed from the endocardium. (B) 2-D virtual slice of tissue. (C) 3-D OCT rendering of the trabeculations. (D) Fiber architecture located 0.44 mm below the surface.

### 1.5.2.3 Optical Mapping

Optical mapping, first used to record cardiac electrical activity in 1976 (Salama and Morad 1976), has provided a wealth of information regarding cardiac conduction. This technique, first applied in earlier studies with the squid axon (Davila, Salzberg et al. 1973; Cohen, Salzberg et al. 1974), is based on the use of voltage-dependent fluorescent molecules and allows one to record electrical activity from hundreds to thousands of sites simultaneously in a single preparation. In short, a voltage-sensitive fluorophore is inserted into the excitable cell membrane and, upon excitation by an appropriate wavelength of light, exhibits changes in its emission spectra proportional to changes in the cell transmembrane potential (Ross, Salzberg et al. 1977; Morad and Salama 1979). Consequently, these changes in fluorescence mimic the cardiac action potential and experimentally are known as the optical action potential. The most commonly used voltage-sensitive dye for cardiac applications is di-4-ANEPPS, a member of the styryl family of dyes (Fluhler, Burnham et al. 1985).

A typical optical mapping setup as used in this dissertation is shown in Figure 1.8. It consists of a Langendorff- or coronary-perfused cardiac preparation stained with a voltage-sensitive dye, in this case di-4-ANEPPS. The heart is then illuminated by light-emitting diodes (LEDs) at 520 nm and fluorescence emitted by the preparation is long-pass filtered at 610 nm before being recorded by a 100x100 MiCAM Ultima-L CMOS camera. Optical action potentials are then digitized, normalized, and filtered before being reconstructed as cardiac electrical activity.

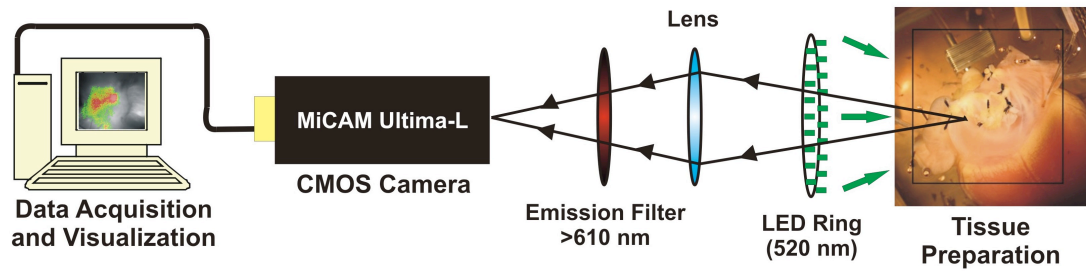


*Figure 1.8: Typical optical mapping setup.*

During cardiac optical mapping, one must also consider the confounding contribution of motion artifacts to the optical signals. Consequently, both pharmacological agents (Cheng, Mowrey et al. 1997; Biermann, Rubart et al. 1998) and mechanical strategies (Salama and Choi 2000) have been employed to remove these effects. Unfortunately, such agents as 2,3-butanedione monoxime (BDM) and cytochalasin-D, have been shown to have nonspecific effects that can further distort the interpretation of physiological experiments (Cheng, Li et al. 2004; Kettlewell, Walker et al. 2004). More recently, a specific inhibitor of the ATPases associated with myosin II isoforms, was characterized by our group and has since been shown to have no significantly detrimental effects on cardiac parameters in a variety of species, including mouse, rabbit, dog, and human (Fedorov, Lozinsky et al. 2007).

## 1.6 Scope and Procedure of the Dissertation

In this dissertation, we first explore the molecular and structural mechanisms associated with atrial flutter and fibrillation and then test a novel method for terminating these atrial tachyarrhythmias. We employ a variety of experimental techniques and models as

discussed in this Introduction. Chapter 2 will present a study in which we explore gender-dependent molecular remodeling that occurs in the setting of both atrial fibrillation and congestive heart failure using human tissues and high-throughput quantitative PCR techniques. In addition to probing gene targets in atrial tissues, we also investigate remodeling in the ventricle in the setting of ventricular tachyarrhythmias and heart failure. Chapters 3 and 4 will present our evaluation of optical coherence tomography in high-resolution imaging of the cardiac conduction system and other structures in the explanted human and canine hearts. Chapter 3 focuses on imaging various elements of the human heart, whereas Chapter 4 focuses specifically on imaging and quantifying fiber structure in the canine atrial pacemaker complex, which is an active participant in the generation and maintenance of both atrial flutter and fibrillation. Finally, Chapter 5 will explore a novel method for low-voltage defibrillation of atrial flutter and fibrillation. Chapter 6 will then present final conclusions and future directions of the larger investigation.

## **2 Gender Dependent Differences in Molecular Electrophysiological Targets in Failing and Nonfailing Human Hearts**

### **2.1 Abstract**

Previous epidemiological studies have shown that males tend to have an increased overall lifetime risk of developing atrial fibrillation, whereas females tend to be more susceptible to the development of ventricular tachyarrhythmias resulting from long-QT syndrome and drug-induced Torsades de Pointes. In this study, we compare transcript-level expression of 89 ion channel subunits, calcium handling proteins, and other transcription factors important in cardiac conduction and arrhythmogenesis in the left atria (LA) and ventricles (LV) of human hearts of both genders. Total RNA from failing male (n=9), failing female (n=7), nonfailing male (n=9), and nonfailing female (n=9) hearts was probed using a custom-designed gene array. Analyses were performed to explore the

relationships between gender, failure state, and compartmental expression. Hierarchical cluster analysis revealed expression patterns with chamber specificity, but not overall disease or gender dependent clustering. Gender-specific analysis of the LA showed that females exhibited significant reductions in  $K_{v4.3}$ ,  $K_{ChIP2}$ ,  $K_{v1.5}$ , and  $K_{ir3.1}$ , as compared with males. On the other hand, gender specific analysis of LV targets associated with repolarization did not reveal significant differences or patterns based on gender. Overall, our data highlight the differential expression and transcriptional remodeling of ion channel subunits in the human heart as a function of gender and cardiac disease. Continued access to and analysis of human cardiac tissues, such as those studied here, is consequently critically important in increasing our understanding of gender dependent differences in the pathogenesis of disease and susceptibility to arrhythmias.

## 2.2 Introduction

Epidemiologically, there are well-established differences in the manifestations of cardiac arrhythmias across gender. Men are typically more susceptible to the development of atrial fibrillation (AF) (Kannel, Wolf et al. 1998; Wolbrette, Naccarelli et al. 2002), whereas women have higher incidences of long-QT syndrome (LQTS) and drug-induced Torsades de Pointes (Locati, Zareba et al. 1998; Abi-Gerges, Philp et al. 2004). In addition, men and women also exhibit differences in basic electrophysiological parameters during normal sinus rhythm. Women tend to have increased resting heart rates (Burke, Goldberger et al. 1996) and longer rate-corrected QT (QTc) intervals



(Kligfield, Lax et al. 1996), and men have been reported to have longer P-waves suggesting differences in atrial electrophysiology (Dhala, Underwood et al. 2002). Interestingly, autonomic blockade does not mask the gender difference in resting heart rate, suggesting that intrinsic sinus node differences as opposed to gender dependent autonomic tone are responsible for this variability (Burke, Goldberger et al. 1996).

Not as much is known about the molecular mechanisms underlying these gender differences in arrhythmia susceptibility and basic electrophysiological parameters in the human heart. Insight has been gained, however, from various animal models, including the rabbit, dog, and mouse (James, Choisy et al. 2007). The rabbit heart has been shown to be a relevant model for the study of human arrhythmias (Panfilov 2006) and female rabbits also exhibit the same gender dependent QTc prolongation (Ebert, Liu et al. 1998; Lu, Remeysen et al. 2001) as is present in the human heart (Kligfield, Lax et al. 1996). Mice, although useful from a genetic manipulation standpoint, manifest profound differences in their action potential as compared to the human (Nerbonne 2004; Ahrens-Nicklas and Christini 2009) and must be carefully considered when extending conclusions to human pathologies (Glukhov, Flagg et al. 2010; Fedorov, Glukhov et al. 2011).

Since cardiac conduction and arrhythmia susceptibility are determined by characteristic expression profiles of ion channels and other transporters, several studies to date have begun to explore gene expression patterns in the human heart (Borlak and Thum 2003; Gaborit, Le Bouter et al. 2007; Chandler, Greener et al. 2009; Nattel, Frelin et al. 2009;

Gaborit, Varro et al. 2010; Gronich, Kumar et al. 2010). The ever-present limitation to these studies, however, is the availability of human tissues for analysis. We have consequently developed the infrastructure necessary to collect tissues from a wide variety of both failing and nonfailing human hearts for use in this study.

We focused on probing tissues of the LA and LV as left-sided heart failure is the most common manifestation of this disease (McKee, Castelli et al. 1971). We subsequently explored the expression of 89 target genes in the LA and LV of failing and nonfailing human hearts of both genders. We also have probed tissues from the epicardium and endocardium of the LV since we have previously shown that heart failure may result in a heterogeneous dispersion of repolarization across the ventricular wall (Glukhov, Fedorov et al. 2010), which may also be pro-arrhythmic (Antzelevitch 2007).

## **2.3 Materials and Methods**

### **2.3.1 Human Tissue Samples**

The use of human hearts for research was approved by the Institutional Review Board at Washington University in St. Louis.

For this study, a total of 34 explanted human hearts of both genders (n=16 women, 52±10 years old; n=18 men, 52±14 years old) were acquired from two sources (Figure 2.1).

Failing human hearts (n=16; 9 men, 7 women) were obtained at the time of cardiac

transplantation at Barnes-Jewish Hospital (St. Louis, Missouri) and nonfailing hearts (n=18; 9 men, 9 women) were provided by Mid-America Transplant Services (St. Louis, Missouri) after they were deemed unsuitable for cardiac transplantation. Each heart was immediately perfused with and stored in cardioplegic solution (4°C) for preservation during the 15-20 minute delivery from the operating room to the research laboratory. Upon arrival, tissue samples from the LA (n=22) and LV (n=22) free walls (Figure 2.2A) were immediately harvested. Epicardial and endocardial samples were also harvested from the LV free wall (n=12) as shown in Figure 2.2B. All tissue samples were stored in RNAlater (Sigma-Aldrich, St. Louis, Missouri) at -80°C. Relevant clinical characteristics of the patients are shown in Table 2.1 for nonfailing hearts and Table 2.2 for failing hearts.

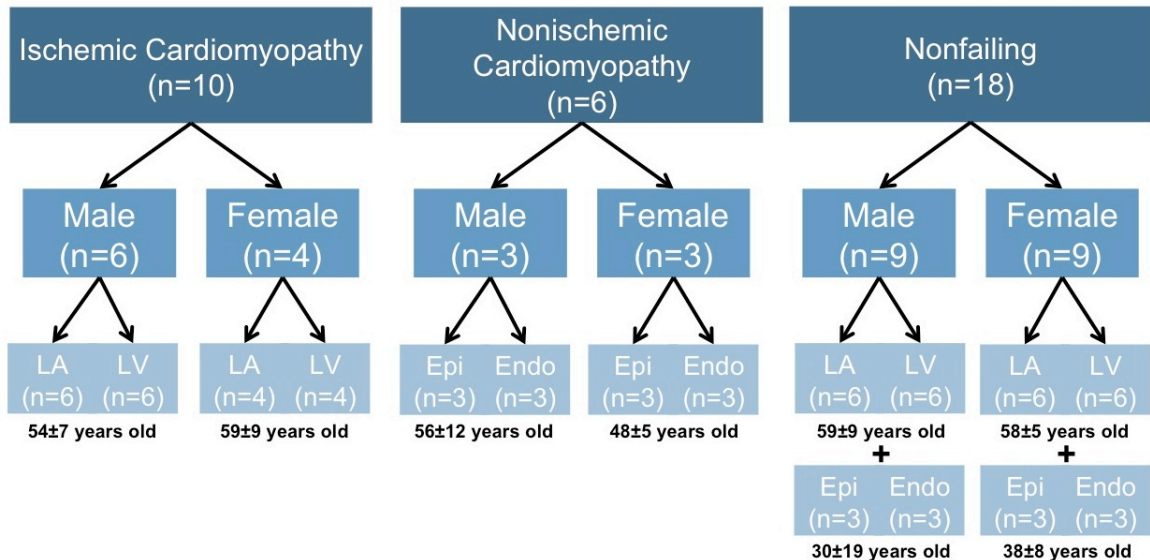


**Figure 2.1:** Study population (n=34).

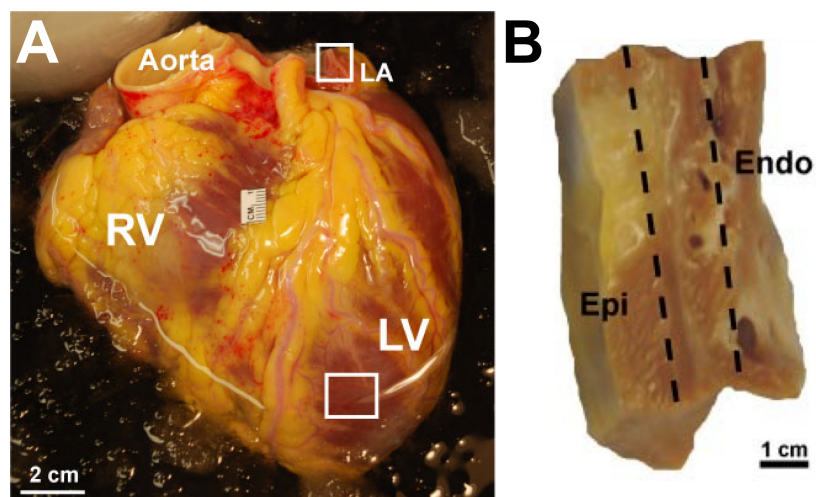


**Figure 2.2:** Tissue sample locations in the human heart. (A) Anterior view of a typical heart after harvest with the locations for the LA and LV samples marked by the white squares. (B) Left ventricular wedge preparation from which the epicardial and endocardial samples were taken as indicated.

**Table 2.1:** Clinical characteristics of the nonfailing human hearts.

Heart Number	Gender	Age	Cause of Death	Echo Parameters	
				LVEDD (cm)	EF (%)
1	F	55	Intercranial Hemorrhage/ Stroke	unknown	<20
2	F	33	Head Trauma/ Brain Death	unknown	unknown
3	F	59	Anoxic Brain Injury	unknown	unknown
4	F	66	Intercranial Hemorrhage/ Stroke	unknown	unknown
5	F	34	Brain Death	4.8	20
6	F	58	Intercranial Hemorrhage/ Stroke	unknown	30
7	F	47	Anoxia	4.1	65
8	F	59	Unknown	unknown	unknown
9	F	50	Anoxia	unknown	60-65
10	M	19	Anoxia	4.1	45
11	M	60	Head Trauma/ Brain Death	3.3	65
12	M	55	Intercranial Hemorrhage/ Stroke	4.7	35
13	M	50	Cerebrovascular Accident	unknown	unknown
14	M	52	Head Trauma/ Brain Death	4.3	60-70
15	M	65	Intercranial Hemorrhage/ Stroke	unknown	unknown
16	M	58	Intercranial Hemorrhage/ Stroke	unknown	60-70
17	M	20	Overdose	unknown	unknown
18	M	59	Brain Death	unknown	unknown

**Table 2.2: Clinical characteristics of the failing human hearts.**

Heart Number	Gender	Age	Diagnosis	Devices	Other Cardiac Surgery	Echo Parameters		Medications	Arrhythmia History
						LVEDD (cm)	EF (%)		
1	F	65	Ischemic Cardiomyopathy	ICD	CABG	6.4	15	ASA, Statins, Amio, $\beta$ -blockers, Inotropes, ACE-I	NSVT, VF
2	F	49	Ischemic Cardiomyopathy	ICD	Stents	5.9	25-30	ASA, Statins, Amio, $\beta$ -blockers, Inotropes, ACE-I, Coumadin	VT
3	F	53	Ischemic Cardiomyopathy	ICD	Stents	6.5	20	ASA, Statins, $\beta$ -blockers	No arrhythmias
4	F	67	Ischemic Cardiomyopathy	ICD	Mitral valve replacement	7	10	$\beta$ -blockers, Inotropes, ACE-I, Coumadin	No arrhythmias
5	M	50	Ischemic Cardiomyopathy	PPM, ICD, BIV	Stents	7	<15	Statins, Amio, $\beta$ -blockers, Coumadin	Refractory VT
6	M	44	Ischemic Cardiomyopathy	ICD, LVAD	Stents	7	<15	ASA, ACE-I, Coumadin	No arrhythmias
7	M	69	Ischemic Cardiomyopathy	PPM, ICD, BIV	CABG	7.13	39	Statins, Amio, $\beta$ -blockers, Inotropes, ACE-I, Coumadin	AF, VT
8	M	63	Ischemic Cardiomyopathy	PPM, ICD, BIV	CABG	7.6	15	ASA, Statins, Amio, $\beta$ -blockers, Inotropes, ACE-I	No arrhythmias
9	M	50	Ischemic Cardiomyopathy	ICD	Stents	6.6	30	ASA, Statins, $\beta$ -blockers, Inotropes	NSVT, VF
10	M	67	Ischemic Cardiomyopathy	ICD, LVAD	Stents	7.9	10	ASA, Statins, Inotropes, ACE-I	No arrhythmias
11	F	44	Nonischemic Cardiomyopathy	ICD, LVAD	None	5.5	20-25	ASA, Inotropes, ACE-I, Coumadin	AF
12	F	54	Nonischemic Cardiomyopathy	ICD	None	6.1	<20	Amio, $\beta$ -blockers, ACE-I, Coumadin	AF, VT
13	F	46	Nonischemic Cardiomyopathy	ICD, LVAD	None	7.8	16	Amio, $\beta$ -blockers, Coumadin	AF, VT
14	M	70	Nonischemic Cardiomyopathy	ICD	Aortic valve replacement	>6.6	16	Amio, $\beta$ -blockers, Inotropes, Coumadin	AF
15	M	47	Nonischemic Cardiomyopathy	LVAD	WPW ablation	6.4	25	ASA, Statins, Amio, $\beta$ -blockers, Inotropes, ACE-I	VT
16	M	53	Nonischemic Cardiomyopathy	ICD	None	8.2	16	Statins, $\beta$ -blockers, Inotropes, ACE-I, Coumadin	VT

### 2.3.2 RNA Extraction and Preparation

Total RNA was extracted from 68 samples using the RNEasy Fibrous Tissue Mini Kit (Qiagen, Valencia, California) according to the manufacturer's instructions. RNA yield was measured using a Nanodrop 1000 (Thermo Scientific) and quality was assessed by verifying the presence of the 18S and 28S bands as run on a 1% agarose gel (Figure 2.3).

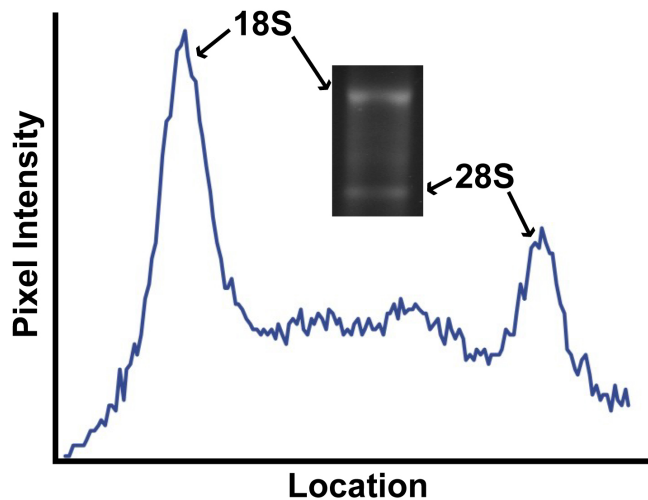


**Figure 2.3: RNA quality assessment.**

### **2.3.3 Low-Density Taqman Gene Arrays**

Custom-designed low-density Taqman gene arrays (Applied Biosystems, Foster City, California) were then used to probe for the presence of 96 targets in a two-step process as described previously (Marionneau, Couette et al. 2005; Gaborit, Le Bouter et al. 2007; Gaborit, Varro et al. 2010). In short, total RNA (1-2 µg) was first converted to cDNA using the High Capacity cDNA Reverse Transcription Kit (Applied Biosystems, Foster City, California). Subsequent reactions were performed, using 100 ng of cDNA loaded into each well of our custom-designed gene arrays, with the ABI PRISM 7900HT Sequence Detection System (Applied Biosystems, Foster City, California). Genes selected for analysis included 56 ion channels and accessory proteins, 14 calcium-handling proteins, 9 autonomic receptors, 6 transcription factors, 3 signaling proteins, and 8 controls/marker genes and are listed in Appendix A.

### **2.3.4 Statistics and Data Analysis**

Data were collected and analyzed by the Applied Biosystems SDS 2.3 software using the threshold cycle ( $C_t$ ) relative quantification method (Livak and Schmittgen 2001) with GAPDH as an endogenous control. Quantitative data are expressed as mean  $\pm$  standard deviation. Statistically significant differences were identified using a one-way analysis of variance followed by Tukey-Kramer's test with a significance level of  $p < 0.05$ . All quantitative results are listed in Appendix A.

In addition, two-way hierarchical agglomerative cluster analysis was performed using the  $\Delta\Delta C_t$  of each target. We applied average linkage clustering with calculation of the Euclidean distances. Clusters were analyzed and visualized using Cluster 3.0 and Treeview software (Eisen, Spellman et al. 1998).

## 2.4 Results

### 2.4.1 Hierarchical Cluster Analysis

Hierarchical cluster analysis is an unsupervised algorithm used to both visualize and explore relationships within large sets of data. In this study, this technique was used to determine if there existed strong enough overall trends across gender, disease, and compartmental expression to create distinct clusters of highly related samples. As is shown in Figure 2.4A, LA and LV samples from ischemic and nonfailing hearts of both genders show distinct clustering based on their chamber location. These samples did not cluster, however, based on either gender or disease state. We also explored cluster analysis of ischemic, nonischemic, and nonfailing LV samples of both genders, as well as nonischemic and nonfailing samples from the epicardium and endocardium of the LV. As is evident in Figure 2.4B-C, we did not see clustering of these latter samples based on gender, disease, or cardiac location.

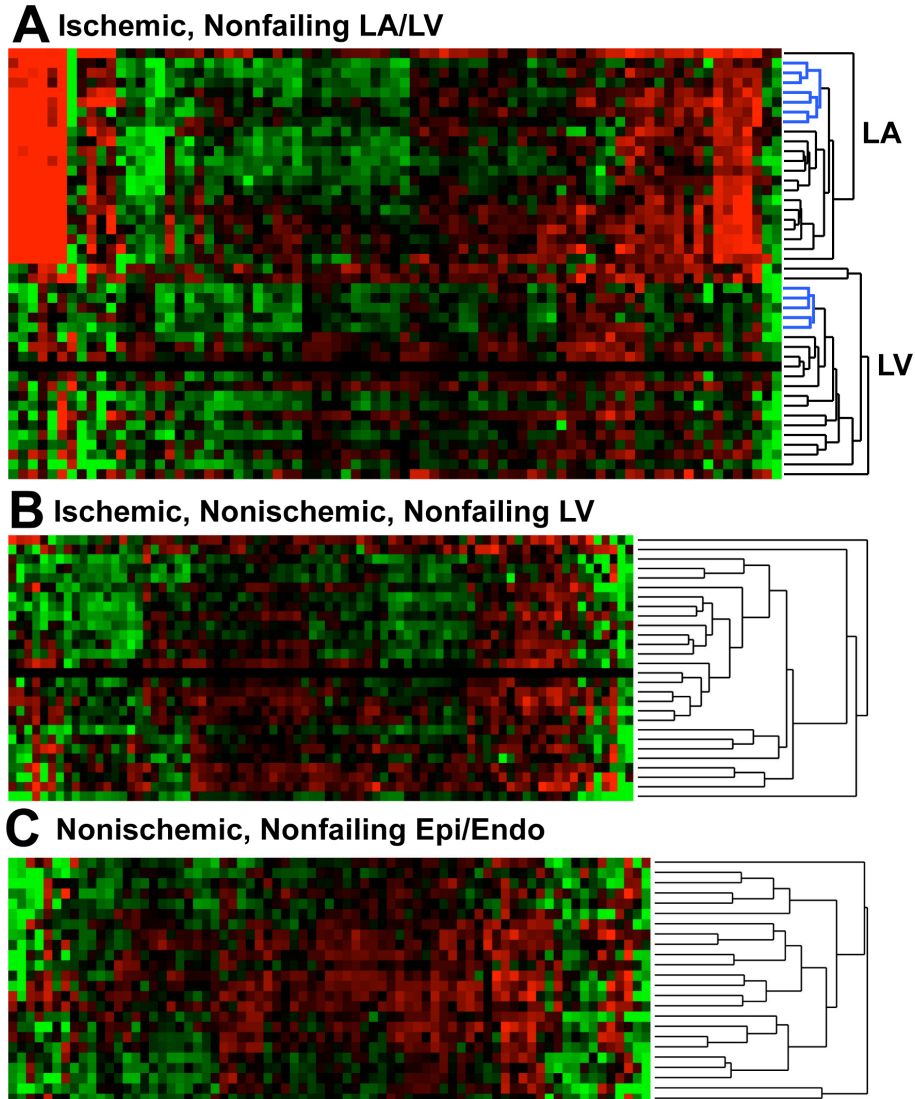


**Figure 2.4:** Hierarchical cluster analysis. (A) Cluster analysis of ischemic and nonfailing LA/LV samples of both genders showing distinct separation based on cardiac location. (B) Cluster analysis of ischemic, nonischemic, and nonfailing LV samples showing no clustering. (C) Cluster analysis of nonischemic and nonfailing epicardial/ endocardial samples also showing no clustering.

## 2.4.2 Ventricular Remodeling in Heart Failure

Studies have revealed that during the heart failure remodeling process, the cardiac action potential is significantly prolonged and conduction is slowed due to pathological changes in the expression and function of ion channels (Janse 2004; Aiba and Tomaselli 2010).



As shown in Figure 2.5, we observe significant reductions and trends for reduction in the transcript-level expression of ion channel subunits important in cardiac conduction and repolarization, as well as changes in key calcium handling proteins. As confirmed in previous studies, we observe significant downregulation of subunits encoding for  $I_{KATP}$  (Flagg and Nichols 2005) and  $I_{to}$  (Kaab, Dixon et al. 1998; Zicha, Xiao et al. 2004).  $I_{to}$ , in particular, encoded by the pore-forming subunit  $K_v4.3$  and the accessory protein KChIP2, is one of the most consistently altered ion channels during the heart failure remodeling process across species (Zicha, Xiao et al. 2004). In addition, it has been reported that reduction of  $I_{to}$  is linked to protein-level downregulation of  $K_v4.3$  and transcript-level downregulation of KChIP2 (Soltysinska, Olesen et al. 2009), which is also reflected in our transcript-level expression data. We observe no significant changes in  $I_{K1}$ ,  $I_{Na}$ , and  $I_{Ca,L}$ , although their function and patterns of expression during heart failure are still controversial (Aiba and Tomaselli 2010). We also observe a trend for reduction of  $K_v11.1/HERG$ , the subunit encoding for the repolarization current  $I_{Kr}$ , and trends with respect to the calcium handling proteins, SERCA2a and NCX1, consistent with recent findings (Soltysinska, Olesen et al. 2009). Finally, we observe a significant downregulation of connexin 43 in nonischemic, but not ischemic, cardiomyopathy. In addition to global downregulation of connexin 43, impaired conduction in heart failure may also be due to an altered distribution of the protein in the cell membrane (Akar, Nass et al. 2007).

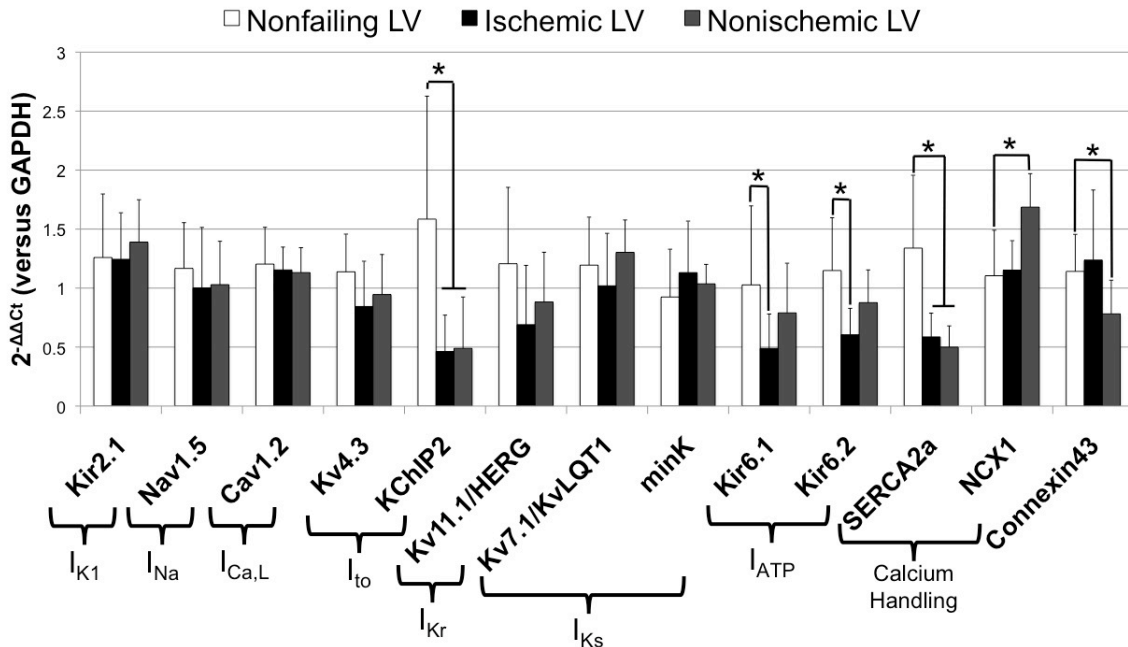


**Figure 2.5:** Ventricular remodeling in heart failure. The asterisks (\*) indicate  $p < 0.05$ .

The general agreement of our findings, regarding ventricular remodeling during heart failure, with previous studies both supports the validity of our findings and allows for the exploration of other novel gene expression patterns with regards to gender and arrhythmia susceptibility.

### 2.4.3 Regional Specificity of Target Expression

Major atrial-ventricular expression differences are shown in Figure 2.6. We confirm known predominantly atrial transcripts, such as connexin 40, TASK-1, TWIK-1,  $K_{ir}2.1$ ,  $K_v1.5$ ,  $K_{ir}3.1$ ,  $Ca_v3.1$ , and sarcolipin (Ellinghaus, Scheubel et al. 2005; Nattel, Frelin et al. 2009; Shanmugam, Molina et al. 2011). In addition, with the exception of atrial connexin 40, we show relatively consistent transcript-level expression of connexin 40, 45, and 43 in the both the LA and LV. Because this is not reflective of protein-level

expression patterns (Vozzi, Dupont et al. 1999; Severs, Bruce et al. 2008), it is important to note that within the realm of this study and other transcript-level investigations, post-translational modifications may play an important role in final functional expression and specificity.

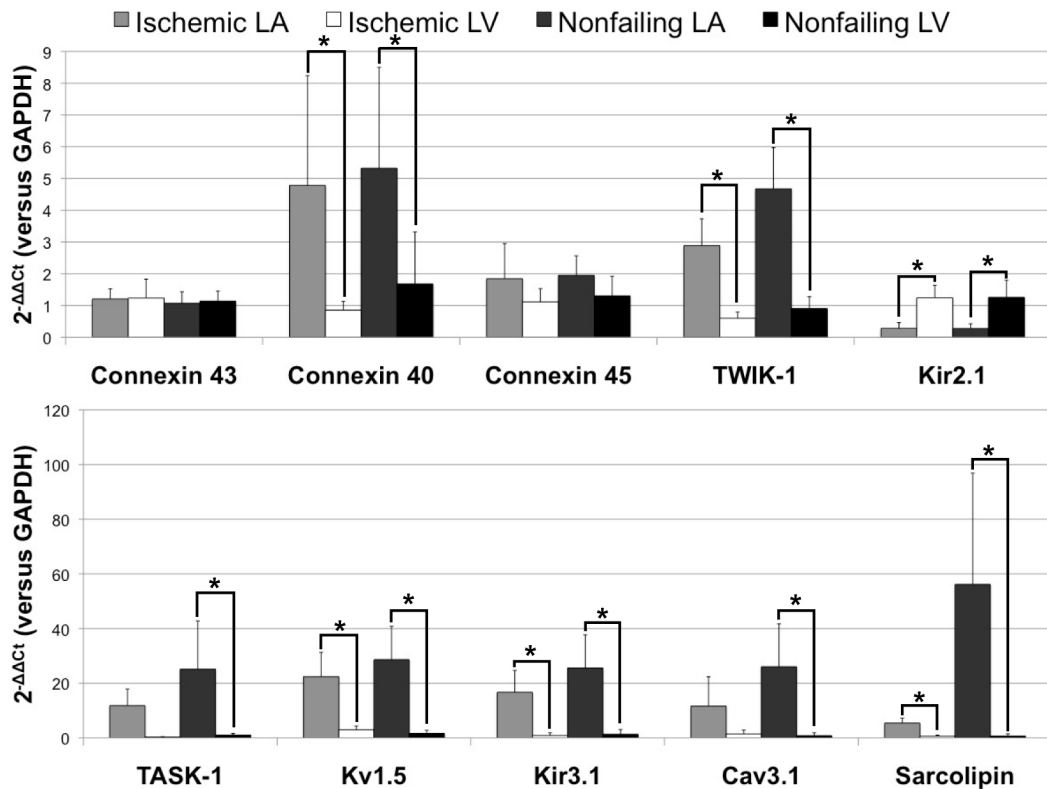


**Figure 2.6:** Regional specificity in failing and nonfailing hearts. The asterisks (\*) indicate  $p < 0.05$ .

#### 2.4.3.1 Regional Specificity of $I_{K_{ATP}}$ Subunits

ATP-sensitive potassium ( $K_{ATP}$ ) channels are prominent in cardiac sarcolemmal membranes and their activation during myocardial ischemia and hypoxia results in an enhanced potassium efflux, reduction in action potential duration, and reduced refractoriness (Noma 1983; Wilde, Escande et al. 1990; Zhang, Flagg et al. 2010).

Consequently, their activation during an ischemic insult plays an important role in cardioprotection, but also may promote ventricular fibrillation (Padrini, Bova et al. 1992). Sarcolemmal  $K_{ATP}$  channels are composed of a pore-forming subunit ( $K_{ir}6.1$  or  $K_{ir}6.2$ ) and a sulfonylurea receptor (SUR1, SUR2A, or SUR2B) (Pountney, Sun et al. 2001; Chan, Wheeler et al. 2008). The SUR subunit determines the specificity and selectivity against  $K_{ATP}$  agonists and antagonists (Liu, Ren et al. 2001). In mouse isolated cells (Flagg, Kurata et al. 2008) and whole hearts (Glukhov, Flagg et al. 2010), it has been shown that atrial  $K_{ATP}$  is only sensitive to the  $K_{ATP}$  channel opener diazoxide, which is specific to SUR1 and not to pinacidil, which is specific to SUR2A. On the other hand, ventricular  $K_{ATP}$  channels were shown to have the opposite sensitivity to these channel openers. The few published studies on human  $K_{ATP}$  channels have focused either on isolated single cells (Koumi, Martin et al. 1997; Pelzmann, Schaffer et al. 2001; Balana, Dobrev et al. 2003; Wu, Huang et al. 2005; Raeis, Philip-Couderc et al. 2010) or fibers (Gautier, Bertrand et al. 1991) and to date there has been little information regarding the chamber specificity of  $K_{ATP}$  channel openers in the human heart.

In our recently published study, we functionally assessed the effects of the  $K_{ATP}$  channel openers, diazoxide and pinacidil, in coronary-perfused human atrio-ventricular preparations (Fedorov, Glukhov et al. 2011). In short, we found that both pinacidil and diazoxide affected the action potential duration (APD) in all chambers of both failing and nonfailing human hearts as shown in Figure 2.7.

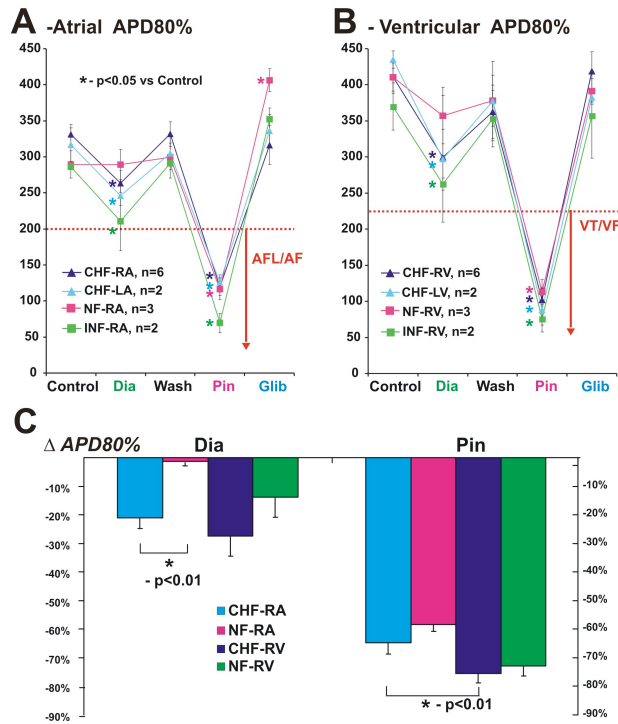


**Figure 2.7:** Effect of  $K_{ATP}$  channel openers on the action potential duration in isolated human hearts. From Fedorov, Glukhov, Ambrosi, et al. *JMCC*. 2011.

As a complement to the functional data collected using optical mapping in this study, we also analyzed transcript-level expression of the  $K_{ATP}$  channel subunits ( $K_{ir}6.1$ ,  $K_{ir}6.2$ , SUR1, and SUR2), which were part of our larger molecular electrophysiological investigation. In choosing primers, we did not distinguish between SUR2A and 2B. As shown in Figure 2.8, all targets were expressed in both chambers with no obvious chamber specificity of either the channels or their subunits, which had been previously found in the mouse heart (Glukhov, Flagg et al. 2010). In comparing transcript-level expression with functional observations from the application of diazoxide and pinacidil, we observed the following: (1) no significantly increased expression level of SUR1 in failing hearts, even though diazoxide significantly shortened APDs in the failing hearts in both chambers as compared to nonfailing hearts; (2) a statistically higher level of SUR2

expression in the ventricles of nonfailing hearts, consistent with our functional observation that pinacidil tends to have a greater effect on APD shortening in the ventricles as compared to the atria; (3) significantly higher overall expression of SUR2 ( $1.08 \pm 0.37$ ) than SUR1 ( $0.73 \pm 0.35$ ,  $p=0.002$ ) across all chambers, consistent with our observation that overall pinacidil has a greater effect on APDs than diazoxide; and (4) heterogeneous expression of Kir6.1 and Kir6.2 in both the LA and LV. Since we were unable to obtain working antibodies for immunohistochemistry, we are unable to confirm these findings at the protein level.

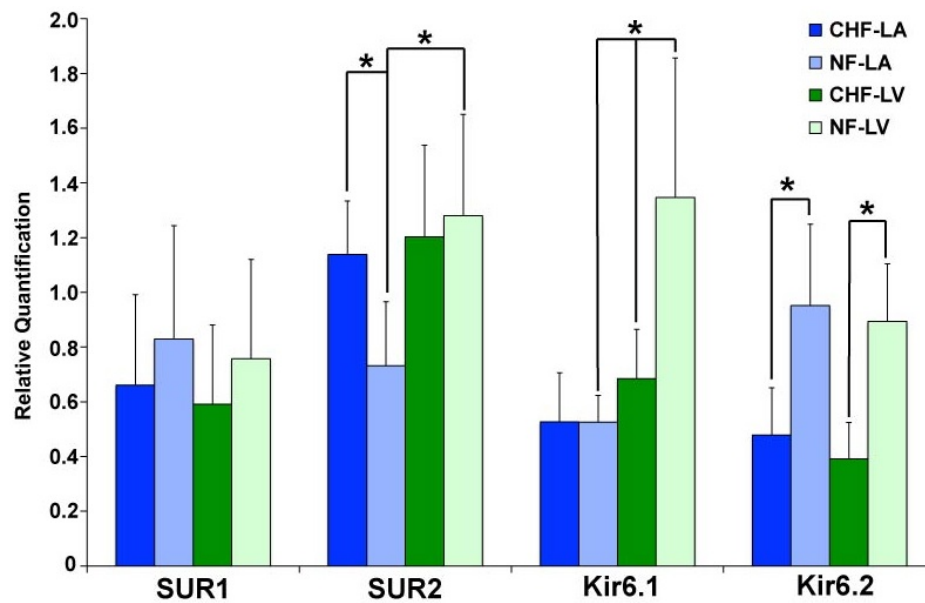


**Figure 2.8:** Transcript-level expression of  $K_{ATP}$  channel subunits in the failing and nonfailing human heart. The asterisks (\*) indicate  $p < 0.05$ .

#### 2.4.4 Gender Dependent Atrial/Ventricular Bias

A gender based comparison of overall relative expression levels for all targets in both failing and nonfailing hearts is shown in Figure 2.9. As is evident in Figure 2.9B, there is

a distinct atrial gender bias, with males exhibiting overall higher expression of almost all genes tested in this study as compared to their female counterparts. In the ventricles, we again observed a male bias of overall relative expression levels (Figure 2.9C), however this time the pattern emerges in nonfailing hearts, as opposed to failing hearts. A similar gender comparison was completed in a study of the wild-type mouse heart and found a similar male gender bias in overall atrial gene expression (Iacobas, Iacobas et al. 2010).

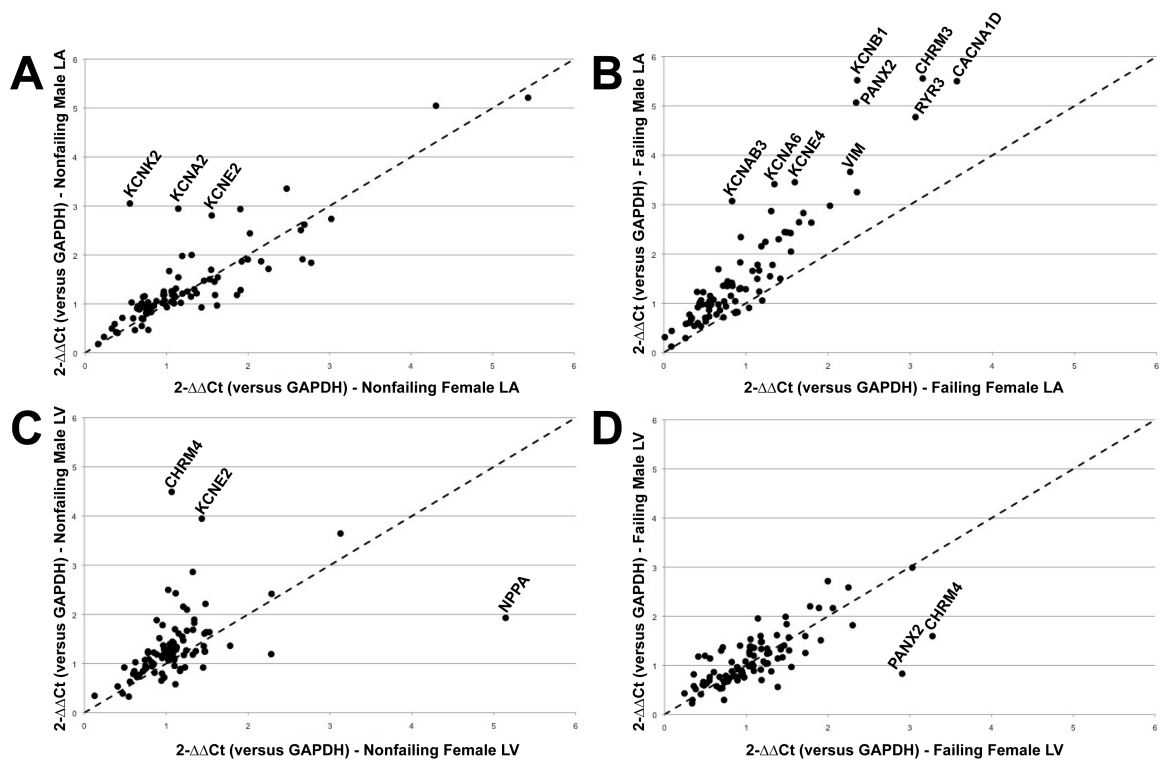


**Figure 2.9:** Gender dependent comparison of relative expression levels of all genes. (A) Nonfailing male versus female LA. (B) Failing male versus female LA showing a distinct male bias. (C) Nonfailing male versus female LV. (D) Failing female versus male LV. The dotted diagonal line represents equal expression levels between genders.

## 2.4.5 Gender Dependent Atrial Remodeling

Since epidemiologically males have an increased overall lifetime risk of developing atrial fibrillation (Kannel, Wolf et al. 1998; Wolbrette, Naccarelli et al. 2002), we focused our

analysis on a specific group of major ion channel transcripts known to be altered during the pathological electrophysiological remodeling process (Van Wagoner 2003; Gaborit, Steenman et al. 2005; Workman, Kane et al. 2008). The gender dependent relative expression levels of these targets are shown in Figure 2.10.

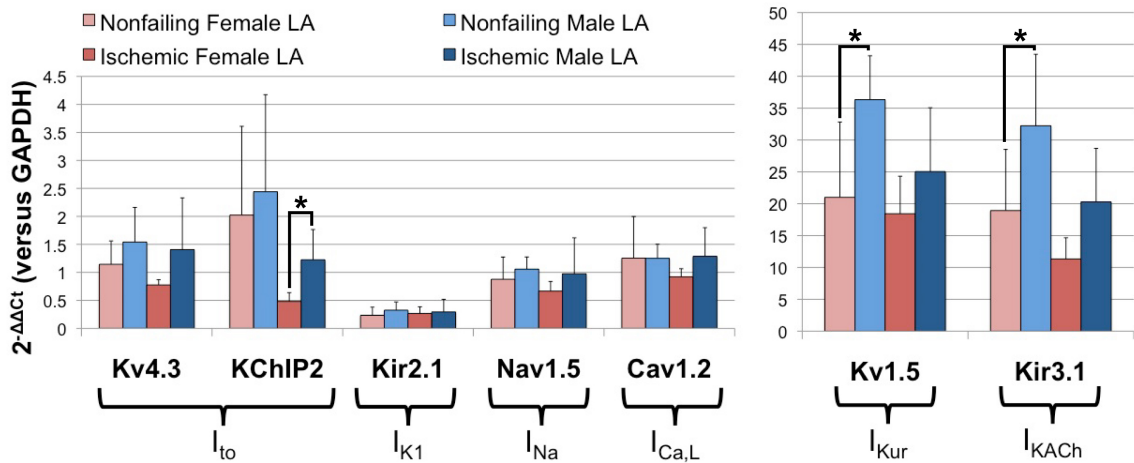


**Figure 2.10:** Gender dependent atrial remodeling in failing and nonfailing hearts. The asterisks (\*) indicate  $p < 0.05$ .

Atrial fibrillation remodeling processes have revealed significant reductions in  $I_{to}$  (Van Wagoner, Pond et al. 1997),  $I_{Kur}$  (Brandt, Priebe et al. 2000),  $I_{KACH}$  (Dobrev, Wettwer et al. 2002), and  $I_{Ca,L}$  (Yue, Feng et al. 1997; Van Wagoner, Pond et al. 1999).  $I_{K1}$  current tends to be increased in AF patients (Dobrev, Wettwer et al. 2002) and  $I_{Na}$  has been shown to not be significantly altered (Bosch, Zeng et al. 1999). Surprisingly, when we assess the gender dependence of these targets in our overall patient population, we observe patterns reflective of the potential propensity of our female population being more susceptible to the development of atrial fibrillation. As seen in Figure 2.10, our female subjects (in red) exhibit significant reductions in  $K_v4.3$ ,  $KCHIP2$ ,  $K_v1.5$ , and



$K_{ir}3.1$ , as compared with our male subjects (in blue). We also see trends for reductions in  $Na_v1.5$  and  $Ca_v1.2$ , with no significant changes or trends regarding  $K_{ir}2.1$ .

Based on the known clinical characteristics of our patient population (Tables 2.1 and 2.2), we identified one failing human heart (no. 7) with a documented history of atrial fibrillation from which we analyzed an LA specimen. Contrary to our expectations, as shown in Figure 2.11, this particular sample (shown in red) had the highest relative expression levels of  $K_v4.3$ ,  $KChIP2$ ,  $K_{ir}2.1$ ,  $Na_v1.5$ , and  $K_v1.5$  when displayed with all failing LA specimens of both genders. This sample does, however, have a lower relative expression level of  $Ca_v1.2$  than other specimens in this group.

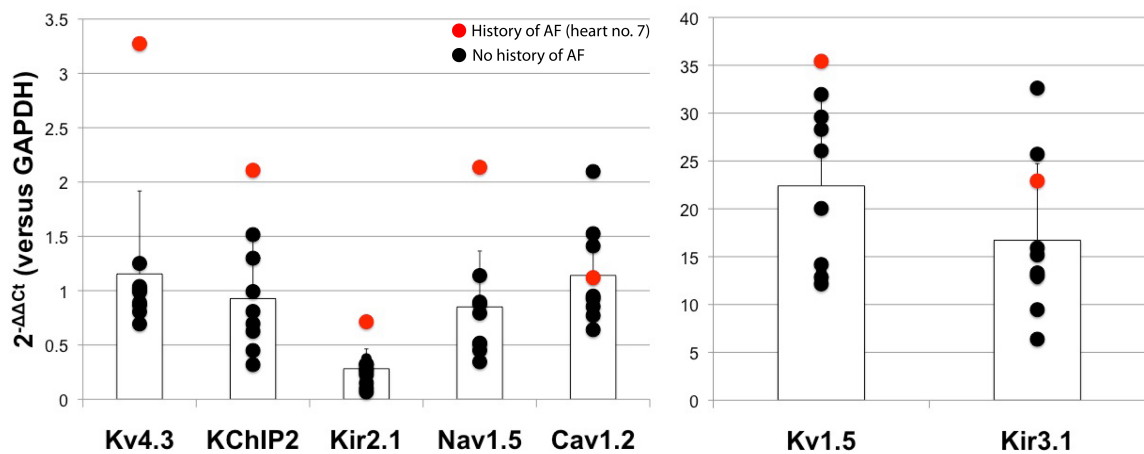


**Figure 2.11:** Relative expression levels of failing left atrial samples of both genders. The red data points indicate the patient with a documented history of atrial fibrillation.

We also explored the gender dependence of relative expression levels for adrenergic receptors as an increased level of adrenergic activity can be associated with the onset of atrial fibrillation (Workman 2010). As seen in Figure 2.12, we do not observe any significant differences in adrenergic receptor expression in the LA of failing and

nonfailing hearts. There is an apparent trend that males tend to exhibit higher overall relative expression levels of  $\alpha 1b$ ,  $\alpha 1d$ ,  $\beta 1$ , and  $\beta 2$  adrenergic receptors. This finding, however, may be due to an intrinsically increased sympathetic tone in men as compared to women (Ramaekers, Ector et al. 1998). Interestingly, as shown in Figure 2.13, the one failing heart with a history of atrial fibrillation (shown in red) displays the highest relative expression levels of all adrenergic receptors analyzed in this study.

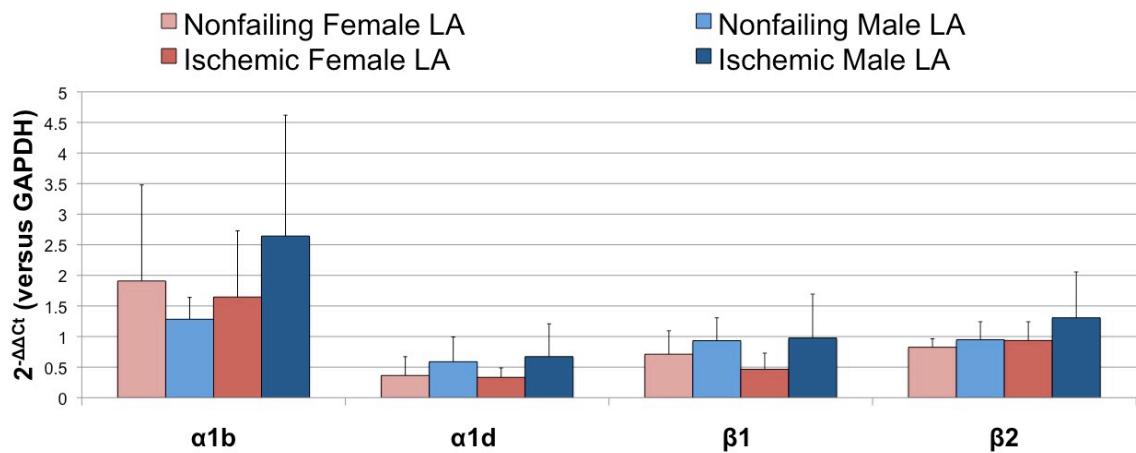


**Figure 2.12:** Gender dependent adrenergic receptor remodeling in failing and nonfailing hearts.

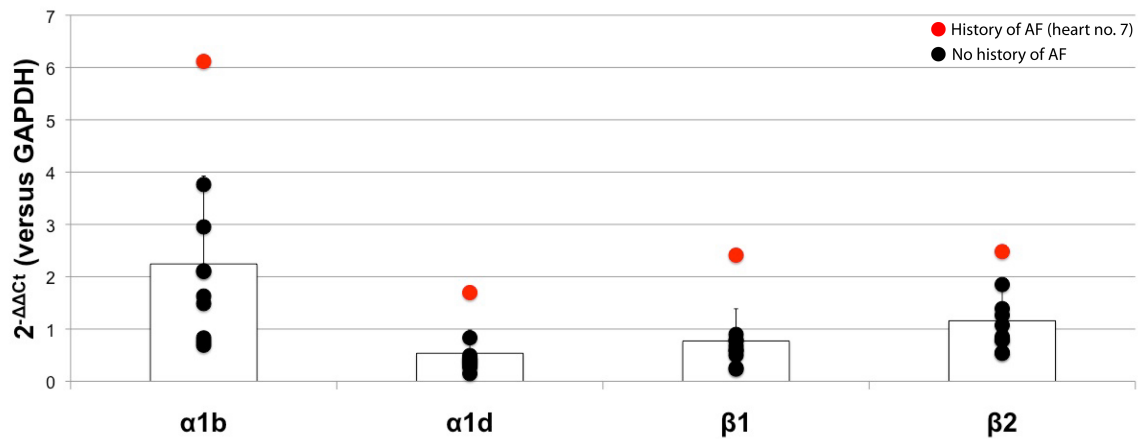


**Figure 2.13:** Relative expression levels of adrenergic receptors in failing left atrial samples of both genders. The red data points indicate the patient with a documented history of atrial fibrillation.

## 2.4.6 Gender Dependent Ventricular Remodeling

Since epidemiologically, females tend to have a higher incidence of long-QT syndrome (LQTS) and drug-induced Torsades de Pointes (Locati, Zareba et al. 1998; Abi-Gerges, Philp et al. 2004), we focused our analysis on a subset of ion channels known to be important in cardiac repolarization (Nerbonne and Kass 2005; James, Choisy et al. 2007). As shown in Figure 2.14, the relative expression levels of these targets reveal no significant differences or patterns based on gender.

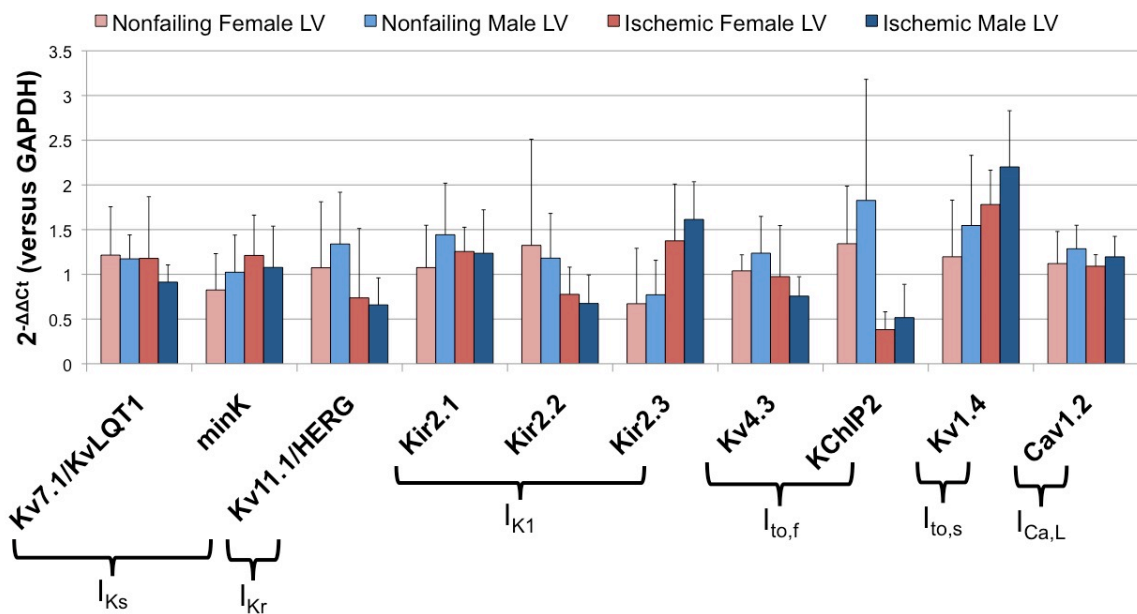


**Figure 2.14:** Gender dependent ventricular remodeling in failing and nonfailing human hearts.

In addition, we identified five failing hearts with known histories of ventricular tachyarrhythmias (Table 2.2). Their expression of these key repolarization targets in comparison with other failing LV samples also do not reveal any striking patterns as shown in Figure 2.15.

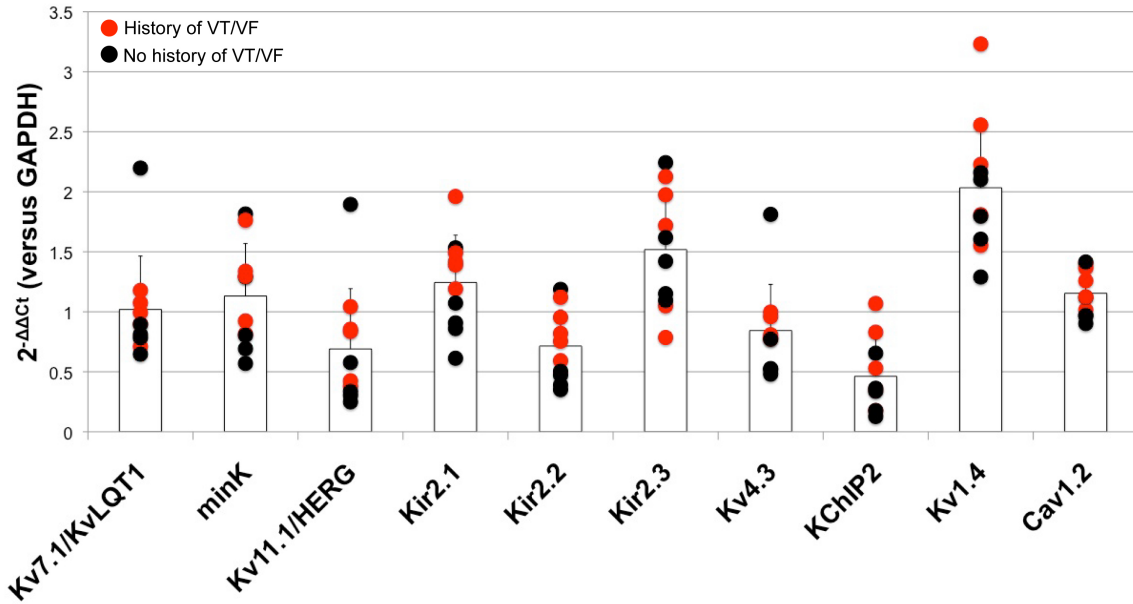


**Figure 2.15:** Relative expression levels of failing left ventricular samples of both genders. The red data points indicate patients with a documented history of ventricular tachyarrhythmias.

## 2.4.7 Gender Dependent Transmural Heterogeneity

Action potential heterogeneity across the transmural ventricular wall directly alters electrophysiological properties during heart failure (Glukhov, Fedorov et al. 2010) and can be a major determinant of arrhythmias (Antzelevitch and Fish 2001). Figure 2.16 shows the ratios of epicardial to endocardial expression for key repolarization targets in both failing and nonfailing hearts of both genders. Ratios of around one represent those targets, such as  $K_v7.1/K_vLQT1$ , minK,  $K_{ir}2.1$ ,  $K_{ir}2.2$ ,  $K_{ir}2.3$ ,  $K_v4.3$ , and  $Ca_v1.2$ , that are uniformly expressed across the transmural wall of the LV in both failing and nonfailing hearts. On the other hand, ratios of either greater or less than one represent targets that are more heterogeneously expressed across the LV transmural wall. For example, KCHIP2, the accessory protein for  $I_{to}$  current, exhibits a significantly larger ratio than any

of the other targets shown in Figure 2.16. This heterogeneity, however, is lost in the failing male heart.  $K_v1.4$ , an additional pore-forming subunit for  $I_{to}$ , displays a reduced ratio in nonfailing hearts, but again the heterogeneity is lost in the failing heart.

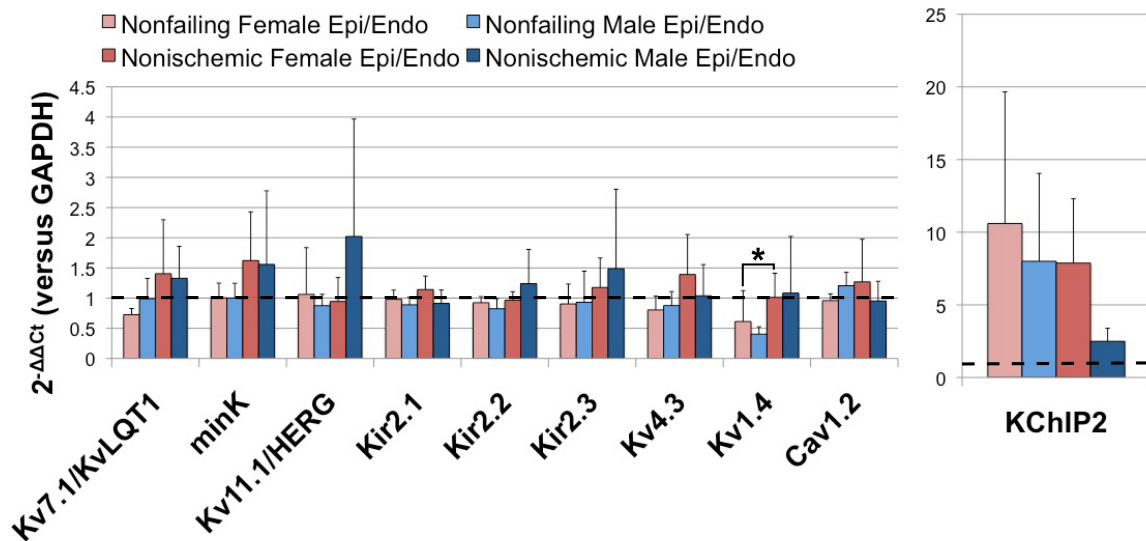


**Figure 2.16:** Average ratios of epicardial to endocardial expression of repolarization targets in failing and nonfailing hearts of both genders. The dotted black line represents a ratio of one. The asterisks (\*) indicate  $p < 0.05$ .

## 2.5 Discussion

In the present study, we explored gender dependent differences in major cardiac ion channels, calcium handling proteins, and other transcription factors in the failing and nonfailing human heart. We found significant gender-specific differences in relative expression levels of LA targets, such as  $K_v4.3$ , KChIP2,  $K_v1.5$ , and  $K_{ir}3.1$ , but no clear gender specific differences or patterns in relative expression levels in the LV. Analyses of transmural heterogeneity in the LV, however, revealed significant differences in the

epicardial and endocardial expression of  $I_{to}$  subunits and accessory proteins, such as  $K_v1.4$  and  $KChIP2$ .

Until recently, there has been very limited data available regarding global gender dependent cardiac ion channel gene expression in the human heart. A 2010 study by Gaborit, et al explored gender dependent differences in the nonfailing human ventricle (left and right) and, unlike in our investigation, found significantly reduced expression levels in the female LV of key ion channels and accessory proteins important in cardiac repolarization (Gaborit, Varro et al. 2010). Their patient population consisted of 10 men and 10 women with average ages of  $38\pm12$  years and  $43\pm13$  years, respectively. Our patient population, on the other hand, consisted of both failing and nonfailing human hearts with significantly older average ages (failing females,  $54\pm9$  years; failing males,  $56\pm9$  years; nonfailing females,  $51\pm11$  years; failing males,  $50\pm18$  years). The variability of qPCR data has been shown to be significantly increased in aged animals (Tellez, Maczewski et al. 2011) and humans (Boheler, Volkova et al. 2003), which in our case may mask any intrinsic gender dependent expression differences in the LV in our study.

The use of an older patient population may, however, be advantageous with respect to the gender dependent analysis of LA targets important in the generation and maintenance of atrial fibrillation as AF is uncommon before the age of 60 and 10% of the overall population develops AF by 80 years of age (Go, Hylek et al. 2001). In addition, 1 in 4 heart failure patients develop AF within five years of diagnosis (Wang, Larson et al. 2003), so it is highly likely that relevant atrial remodeling processes (Nattel, Burstein et

al. 2008) are well underway in our patient population. Interestingly, although overall men are more likely to develop heart failure (Bui, Horwich et al. 2011), women diagnosed with heart failure are approximately 1.5 times more likely to develop atrial fibrillation than their male counterparts (Benjamin, Levy et al. 1994) which may, in part, explain why our female population tends to display LA molecular characteristics with a greater potential propensity for the generation and maintenance of atrial fibrillation. Additionally, the overall higher atrial expression levels of almost all transcripts analyzed in this study, as shown in Figure 2.9B, in the failing male hearts, as compared to failing female hearts, may mask any intrinsic gender based differences.

Interpretation of these results, however, with respect to both the LA and LV must be considered in light of the available clinical information, as shown in Tables 2.1 and 2.2. We identified one patient (failing heart no. 7) with a history of AF. Contrary to our expectations with regards to atrial remodeling in AF, this patient exhibited high expression levels of  $K_v4.3$ ,  $KChIP2$ ,  $K_{ir}2.1$ ,  $Na_v1.5$ , and  $K_v1.5$  when compared with all other failing LA specimens of both genders, as shown in Figure 2.11. This sample did, however display a relatively lower expression level of  $Ca_v1.2$  as compared with other specimens in the group, indicative of the patient's four month history of permanent AF prior to transplantation. It should also be noted that, prior to diagnosis of AF, this patient had been previously diagnosed with ventricular arrhythmias which concurrently played a role in the progression of heart failure and overall arrhythmia history. As previously reported, in human AF the primarily physiological remodeling results from changes in  $I_{Ca,L}$  and significant reductions of current density have only been reported after 18 months

of persistent AF (Brundel, Henning et al. 2002). In addition, as shown in Figure 2.15, we observed no remarkable expression patterns in key repolarization targets in the LV of failing hearts with and without a history of ventricular tachyarrhythmias.

The etiology of heart failure is thought to play an important role in the remodeling of specific ion channels (Koumi, Backer et al. 1995; Cerbai, Sartiani et al. 2001). However, relative action potential prolongations among investigations, for example, between dilated and ischemic cardiomyopathy, are not always consistent (Koumi, Backer et al. 1995; Sipido, Stankovicova et al. 1998; Verkerk, Veldkamp et al. 2000). A recent study in cardiomyopathic rabbits found that the degree of hypertrophy in heart failure, as opposed to the general disease etiology, is the key underlying determinant of molecular remodeling and, consequently, action potential duration (Verkerk, Baartscheer et al. 2011). In particular, etiologies of heart failure with higher degrees of hypertrophy, such as dilated (or nonischemic) cardiomyopathy (Markus, Freitas et al. 2004), exhibit increased action potential prolongation as compared to other heart failure etiologies, such as ischemic cardiomyopathy, with lesser degrees of hypertrophy (Verkerk, Baartscheer et al. 2011). In our study, we analyzed tissues from patients diagnosed with either ischemic or nonischemic cardiomyopathy. Since we did not observe dramatic differences in gene expression between the two etiologies as shown in Figure 2.5, we assessed the left ventricular end diastolic dimension (LVEDD, Table 2.2) as an indicator of the degree of hypertrophy (Lauschke and Maisch 2009). We did not, however, find significant differences in our patient population in the LVEDD ( $6.9 \pm 0.58$  cm, ischemic cardiomyopathy versus  $6.8 \pm 1$  cm, nonischemic cardiomyopathy;  $p=0.74$ ), between the



two heart failure etiologies. This finding subsequently supports the lack of discernable overall gene expression differences between ischemic and nonischemic cardiomyopathy in this study.

Regardless of disease etiology, prolongation of the cardiac action potential is a hallmark of heart failure (Tomaselli and Marban 1999). Furthermore, heterogeneous dispersion of repolarization transmurally across the ventricular wall manifests as a larger-scale prolongation in the QT interval of the electrocardiogram. This prolongation, which is also present in heritable conditions, such as long-QT and Brugada syndromes, may also be proarrhythmic (Antzelevitch and Fish 2001). In our recent study, we provide direct functional experimental evidence of transmural, heterogeneous action potentials in the human LV wedge preparation (Glukhov, Fedorov et al. 2010). In this study, as shown in Figure 2.16, we explored the potential molecular mechanisms of that heterogeneity. We confirm that epicardial cells exhibit a prominent transient outward current ( $I_{to}$ ) manifested as significant differences in KChIP2 across the transmural wall (Antzelevitch and Fish 2001). We are unable, however, to pinpoint other targets potentially responsible for this heterogeneity as other ion channels prominent in repolarization are more homogeneously expressed across the transmural surface in our specimens. In addition, we do not find transcript-level expression of connexin 43 to be heterogeneous, despite its significant reduction in the epicardium at the protein level in both failing and nonfailing hearts in our previous study (Glukhov, Fedorov et al. 2010). Consequently, patterns of molecular heterogeneity directly affecting action potential durations may either be due to the presence of smaller “islands” of differential gene expression and function (Antzelevitch,

Shimizu et al. 1999; Glukhov, Fedorov et al. 2010) not captured in this study or post-translational protein modifications (Roden and Kupersmidt 1999) not assessed in our transcript-level investigation.

This study was conducted without assessing the potential contribution of sex steroid hormones (James, Choisy et al. 2007; Luczak and Leinwand 2009; Yang, Kurokawa et al. 2010). It has been shown that these hormones effect the expression of various ion channels though both genomic and non-genomic mechanisms and consequently alter cardiac conduction, repolarization, and susceptibility to arrhythmias (Furukawa and Kurokawa 2007). Therefore, in assessing the gender dependency of cardiac ion channels, it will be important to consider the presence and effect of these hormones in the patient population in future studies.

The wealth of information gathered from large-scale gene expression studies such as this and others (Chandler, Greener et al. 2009; Gaborit, Varro et al. 2010), not only provides insight into the gender dependent, pathological, or regional changes in ion channel expression, but also provides solid physiological data that can be incorporated into computational models. Constructing useful models of human electromechanical activity requires a thorough understanding of the distribution of ion channels, calcium handling proteins, and other ion transporters in various regions of the heart, as well as their modifications due to disease and gender as we have investigated in this study of the human heart.

## 2.6 Conclusion

Epidemiologically, it is clear there is a gender disparity in arrhythmia incidence. To attempt to elucidate the underlying molecular mechanisms of these differences, we have explored the gender dependent expression of various ion channels, calcium handling proteins, and other transcription factors in the failing and nonfailing human heart in this study. While we observed significant gender dependent differences in atrial tissues, we did not however observe clear patterns of gender dependent expression in the ventricles. Our data do, however, emphasize the importance of addressing such confounding factors as gender, age, and disease progression when exploring ionic remodeling processes in the human heart.

## **3 Virtual Histology of the Human Heart Using Optical Coherence Tomography**

### **3.1 Abstract**

Optical coherence tomography (OCT) allows for the visualization of micron-scale structures within nontransparent biological tissues. For the first time, we demonstrate the use of OCT in identifying components of the cardiac conduction system and other structures in the explanted human heart. Reconstructions of cardiac structures up to 2 mm below the tissue surface were achieved and validated with Masson Trichrome histology in atrial, ventricular, sinoatrial nodal, and atrioventricular nodal preparations. The high spatial resolution of OCT provides visualization of cardiac fibers within the myocardium, as well as elements of the cardiac conduction system; however, a limiting factor remains its depth penetration, demonstrated to be ~2mm in cardiac tissues. Despite its currently limited imaging depth, the use of OCT to identify the structural

determinants of both normal and abnormal function in the intact human heart is critical in its development as a potential aid to intracardiac arrhythmia diagnosis and therapy.

## 3.2 Introduction

In the 17 years since its initial introduction (Huang, Swanson et al. 1991), optical coherence tomography (OCT) has gained prominence as a diagnostic imaging modality in the fields of ophthalmology (Costa, Skaf et al. 2006; Chang and Budenz 2008; Drexler and Fujimoto 2008), vascular cardiology (Pinto and Waksman 2006; Tearney, Jang et al. 2006; Brezinski 2007; Guagliumi and Sirbu 2008), and dermatology (Welzel 2001; Gambichler, Moussa et al. 2005). Major clinical applications of cardiac OCT currently focus on the visualization of the coronary vasculature – for example, identifying unstable plaques and guiding interventional techniques such as stent placement (Brezinski 2007). However, within the realms of cardiac research, the applications of OCT have been steadily increasing. Recently, OCT has been used to study developing murine and avian hearts (Luo, Marks et al. 2006; Jenkins, Chughtai et al. 2007), as well as the morphogenesis and myocardial strains of the embryonic chick heart (Filas, Efimov et al. 2007). Additional studies have shown the utility of OCT in recognizing the components of the cardiac conduction system of the rabbit, specifically the atrioventricular (AV) node (Gupta, Rollins et al. 2002) and the Purkinje network (Jenkins, Wade et al. 2005). Our recent study extended these findings by exploring the relationship in the rabbit heart between function, visualized through optical mapping, and structure, imaged through OCT (Hucker, Ripplinger et al. 2008). Concurrently, tools are also under development to

analyze OCT data, including 3-D cardiac fiber structure (Fleming, Ripplinger et al. 2008). In this study, we aimed to explore the utility of OCT in identifying components of the conduction system and other structures in the explanted human heart.

Clinical cardiac anatomical visualization and reconstruction techniques, including magnetic resonance imaging (MRI), computed tomography (CT), and ultrasound, have a variety of diagnostic capabilities, including localization of arterial plaques, evaluation of bypass grafts and stents, and quantification of wall properties. Although these modalities provide better depth of penetration than OCT, they deliver relatively low resolution images. In biological specimens, OCT, on the other hand, boasts spatial image resolutions ranging from submicrometer though 15  $\mu\text{m}$ , which can be 10 to 100 times greater than other modalities and comparable to conventional histological analyses (Povazay, Bizheva et al. 2002; Fujimoto 2003).

In addition to its high spatial resolution, OCT also has other advantages pertaining to diagnostics and surgical guidance. First, OCT can be performed in real time and *in situ*, allowing for convenient online guidance and evaluation of treatment. Second, OCT technology can be miniaturized into a catheter-based imaging system (Tearney, Brezinski et al. 1996; Tearney, Brezinski et al. 1997) and threaded through the vasculature into the cardiac chambers. Last, OCT can be used for Doppler blood flow and the quantification of blood oxygenation (Chen, Milner et al. 1997; Rollins, Yazdanfar et al. 2002).

Despite its high spatial resolution, OCT is limited by its depth penetration, estimated to be 2 to 3 mm in nontransparent biological tissues (Fujimoto 2003). Although there are techniques in development to enhance both its depth penetration and resolution (Schenk and Brezinski 2002; Fujimoto 2003; Huang, Liu et al. 2008), currently standard OCT does not achieve the typical depths of MRI, CT, and ultrasound, which can acquire images of internal structures noninvasively. The advantage of OCT, however, lies in its superior spatial resolution, which enables the visualization of complex fiber architecture, as explored in this study of the human heart.

### **3.3 Materials and Methods**

#### **3.3.1 Experimental Preparations**

The use of human hearts for research was approved by the Institutional Review Boards at both Washington University and the University of Minnesota.

Explanted failing human hearts (n=12) were obtained at the time of cardiac transplantation (Barnes-Jewish Hospital, St. Louis, Missouri) and immediately perfused with cardioplegic solution (4°C). Tissue preparations from the right atria (RA), left ventricle (LV), infarcted right ventricle (RV), and atrioventricular junction (AVJ) were isolated from the rest of the heart. An additional sinoatrial nodal (SAN) specimen was obtained through the Upper Midwest Organ Procurement Organization (Life Source, St. Paul, Minnesota) and the University of Minnesota and shipped frozen to St. Louis. The

tissues were perfused and fixed with 3.7% formaldehyde overnight and then transferred to 20% sucrose for 2 days. The tissues were photographed and clearly marked with pins to precisely correlate the OCT images with histology. OCT was performed 3 to 4 days later. Table 3.1 shows the clinical data regarding each specimen.

Heart Number	Gender	Age	Diagnosis
1	Male	58	Intercerebral Injury
2	Male	46	Ischemic cardiomyopathy
3	Female	37	Idiopathic cardiomyopathy
4	Female	52	Nonischemic cardiomyopathy
5	Female	45	Hypertrophic obstructive cardiomyopathy
6	Male	55	Ischemic cardiomyopathy
7	Male	51	Ischemic cardiomyopathy
8	Male	60	Ischemic cardiomyopathy
9	Female	59	Idiopathic cardiomyopathy
10	Male	64	Nonischemic cardiomyopathy
11	Male	50	Ischemic cardiomyopathy
12	Male	48	Dilated cardiomyopathy
13	Male	28	Idiopathic cardiomyopathy

**Figure 3.1:** Clinical data. Relevant clinical information regarding each specimen. The mean age of the patients was  $50 \pm 10$  years.

### 3.3.2 OCT Imaging

OCT, based on the principle of low-coherence interferometry, measures the backscatter of light. The coherence of the backscattered light from the sample arm (or tissue) and reference arm result in the generation of multiple A-scans (axial scans), which are then converted to pixel intensity and combined to form a tomogram (B-scan), or slice of tissue (Brezinski 2006), as described in Section 1.5.2.2 and shown in Figure 1.6. The basics of our OCT system have been described previously (Hu and Rollins 2005; Hucker, Ripplinger et al. 2008). We imaged all cardiac tissues in 1x1, 2x2, or 4.5x4.5 mm



overlapping segments from the epicardial, endocardial, or transmural surfaces, with final axial and lateral resolutions of 10  $\mu\text{m}$  (in air).

### **3.3.3 Histology**

After imaging, the tissue specimens were embedded and frozen in Tissue-Tek OCT compound (Electron Microscopy Sciences, Hatfield, Pennsylvania) and stored at  $-80^{\circ}\text{C}$ . The tissues were then cryosectioned at 16  $\mu\text{m}$  and mounted on Superfrost Plus glass slides (Fisher Scientific). Sections were then stained using Masson Trichrome (IMEB, San Marcos, California), imaged on a Nikon C1/80i confocal microscope with an attached AxioCam MRc5 brightfield camera (Carl Zeiss), and visually compared with the corresponding OCT images.

### **3.3.4 Computational Analysis and Statistics**

Images were processed using MATLAB (Mathworks) and Volocity (Improvision). Initially, each 2-D slice was acquired six times, and the six frames were then averaged together to reduce background noise. Subsequently, during post acquisition data analysis, median filtering was performed with a 3x3 smoothing kernel to further reduce speckle noise (Tearney, Yabushita et al. 2003). Three-dimensional (3-D) tissue reconstructions were created using both Volocity and custom-written MATLAB programs. Additional analysis programs were developed in MATLAB for optical tissue slicing, to determine fiber orientation in relation to the tissue surface (Hucker, Ripplinger et al. 2008), and for determination of the depth of OCT penetration. Depth penetration of each 4.5x4.5 mm

field of view acquired across all tissue preparations was assessed via a global thresholding approach (Brezinski 2006). Quantitative data are expressed as mean  $\pm$  standard deviation. A Student's *t*-test was used to determine statistical significance. A *p* value of  $<0.05$  was considered statistically significant.

## 3.4 Results

### 3.4.1 OCT of the Atria and Ventricles

Atrial (n=6) and ventricular (n=8) preparations were imaged from both the endocardial and epicardial surfaces. Atrial depth penetration ( $0.94\pm 0.14$  mm) significantly differed ( $p=1.74\times 10^{-8}$ ) from that of the ventricles ( $1.29\pm 0.46$  mm).

In atrial tissues, we created 3-D reconstructions of the trabeculations and distinguished fiber structures up to 1 mm below the endocardial surface (Figure 3.1). In the ventricle, we were able to distinguish changes in fiber orientation in areas located within 4.5 mm of each other and 0.4 mm below the epicardial tissue surface (Figure 3.2a-c). Although our current means of imaging does not achieve the depth required to reconstruct fiber architecture throughout the entire thickness of the human myocardium, we do have evidence that this can be accomplished in animal models, in which our current OCT system is able to penetrate through a larger percentage of the myocardium (Hucker, Ripplinger et al. 2008).

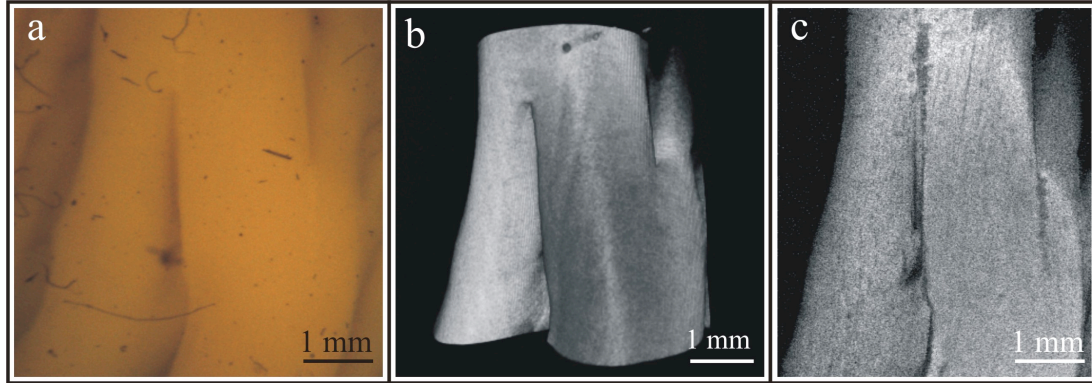


**Figure 3.1:** OCT of the Atria. (a) Atrial trabeculations of the RA appendage as viewed from the endocardium. (b) 3-D OCT rendering of the trabeculations. (c) Fiber architecture located 0.44 mm below the surface.

Epicardial OCT can also afford us a view of the coronary vessels. Figure 3.2d shows a histological cross section through an intact coronary vein, with the corresponding OCT cross section shown in Figure 3.2e. Figure 3.3 shows the resultant 2-D and 3-D OCT images from a coronary artery, isolated from the RV epicardial surface, with a main branch diameter of 2 mm. In particular, note that in Figure 3.3c, we are able to distinguish arterial branches less than 1 mm in diameter, as indicated by the red arrowhead.

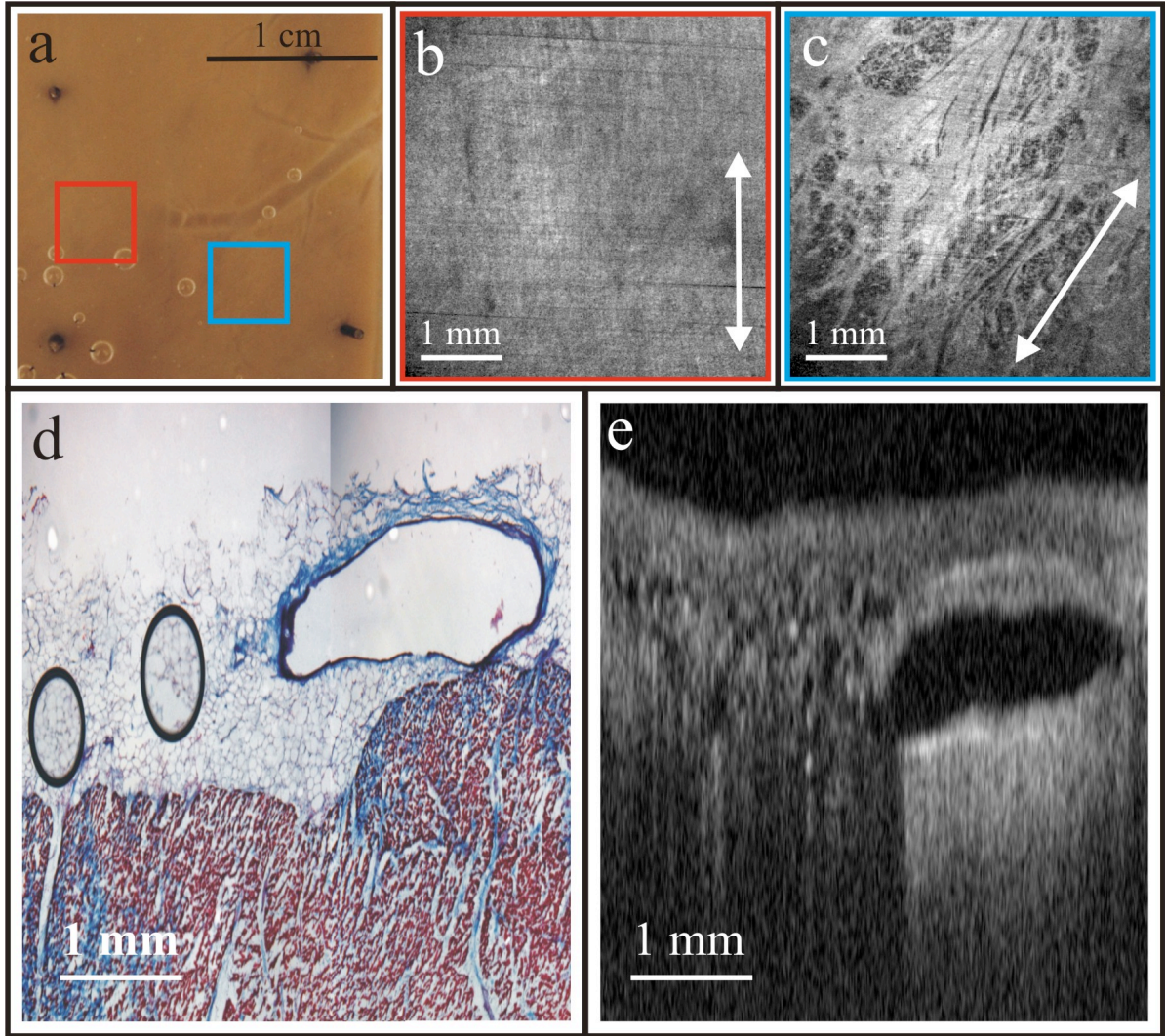


**Figure 3.2:** OCT of the Ventricles. (a) Photograph of an LV preparation as viewed from the epicardium. (b) Fiber architecture in the area indicated by the red box, 0.4 mm below the epicardial surface. (c) Fiber architecture 0.4 mm below the epicardial surface located 4.5 mm to the right of (b) as indicated by the blue box. The average angle of the fibers shifted by  $30^\circ$ . (d) Histological cross section of the LV, affording a view of a coronary vein. (e) 2-D OCT image corresponding to (d).

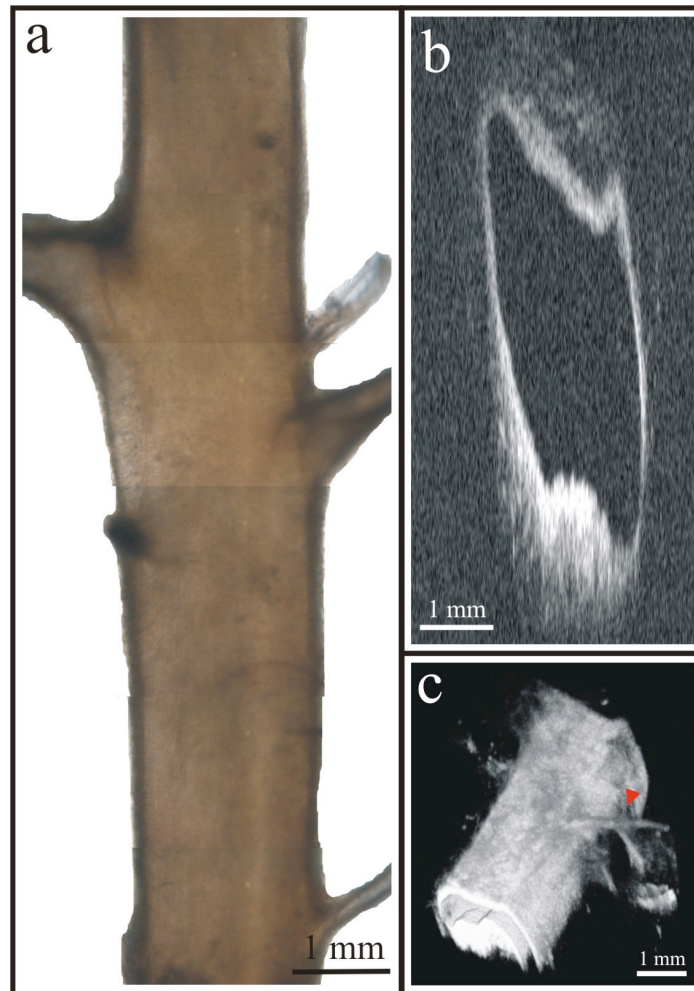


**Figure 3.3:** OCT of an isolated coronary artery. (a) Photograph of an isolated coronary artery. (b) 2-D cross section of the artery. (c) 3-D OCT rendering of the artery. The red arrowhead indicates an arterial branch less than 1 mm in diameter.

In addition, we imaged RV infarcts (n=3) from the epicardial, endocardial, and transmural surfaces. Although we were able to detect significant ( $p=3.16 \times 10^{-7}$ ) changes in depth penetration as compared with adjacent noninfarcted ventricles, as measured from the epicardium and endocardium, we could not visually identify the fibroses from these surfaces with our OCT system. In contrast, when we imaged from the dissected transmural surface, as shown in Figure 3.4, the fibrotic tissue of the infarct is clearly visible using OCT and correlates well with histology.

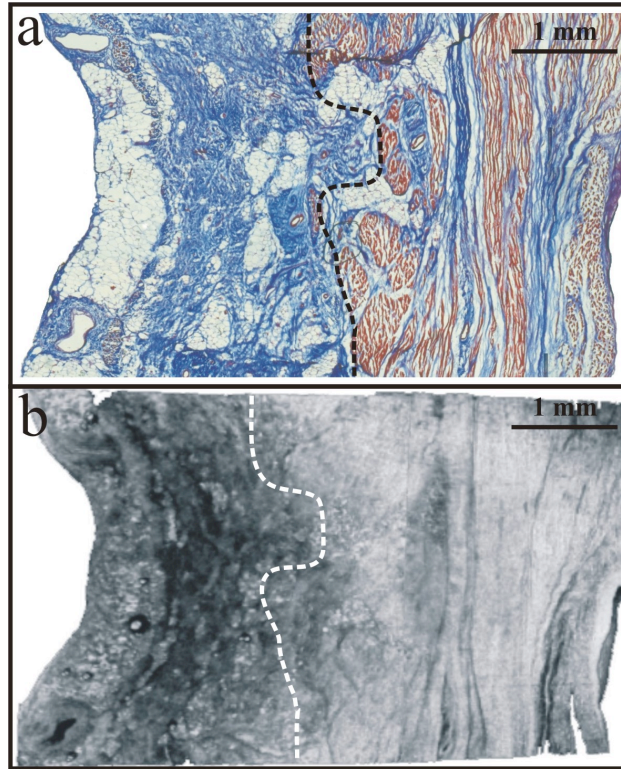


**Figure 3.4:** *Transmural OCT of the infarcted right ventricle. (a) Histology of an epicardial RV infarct and its underlying tissue. (b) Corresponding OCT cross section of the infarct. The dotted line represents the approximate border between the infarct and viable myocardium.*

### 3.4.2 OCT of the Sinoatrial Node

OCT of the SAN was initially attempted from the endocardial surface, the primary point of access during intracardiac procedures. The SAN specimen was dissected to include the RA appendage, crista terminalis (CT), and approximately 2 cm of atrium beyond the CT (Figure 3.5a). The specimen was then imaged in overlapping 4.5x4.5 mm segments, beginning along the CT and extending to the border of dissection. Figure 3.5b shows 3-D reconstructions of the tissue recreated from scans along the CT/RA border, as indicated by the dashed line in Figure 3.5a. Compared with the 2-D tomogram in Figure 3.5c, Figure 3.5d exhibits an increased number of tissue layers as the transitional area closer to

the SAN is approached. As the OCT field of view begins to incorporate the tissue layers above the SAN (Figure 3.5e,f), it is readily apparent that the primary pacemaker of the heart, defined as a subepicardial structure (Ho, Anderson et al. 2002), is located too deep within the myocardium (at 1.75 mm) for imaging from the endocardial surface. The average depth penetration for this specimen from the endocardial surface was  $1.06 \pm 0.21$  mm. Imaging from the epicardial surface was hindered by a layer of fat along the sulcus terminalis. Although fat intrinsically has a lower backscattered reflectance than normal cardiac tissue (Brezinski, Tearney et al. 1996), the loss in depth penetration was such that we could not visualize the SAN. In addition, the thin layer of epicardial fibrous tissue, indicated by the arrow in Figure 3.6a, may contribute to the loss of depth when the SAN is imaged from the epicardium.

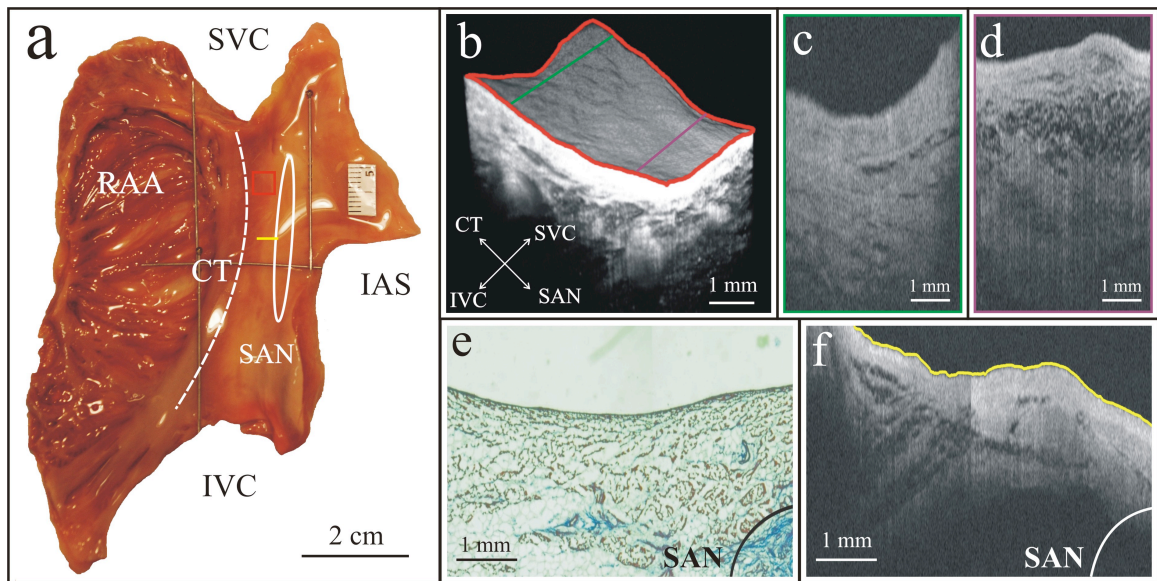


**Figure 3.5:** Endocardial OCT of the sinoatrial node. (a) Dissected SAN preparation. (b) 3-D reconstruction of the tissue area as indicated by the red box. (c,d) 2-D tomograms from (b) as indicated by the green and purple lines. (e) Histology with the SAN indicated by the solid line in the lower-right corner. (f) OCT cross section corresponding to (e) showing a strong relationship between the transitional area as defined histologically and via OCT; however the SAN is unable to be imaged endocardially using this method. Abbreviations – RAA: RA appendage; SVC: superior vena cava; IVC: inferior vena cava; CT: crista terminalis; IAS: interatrial septum; SAN: sinoatrial node.

We also imaged the SAN specimen transmurally (i.e., in dissected tissue), which allowed us to consistently locate the SAN throughout its entire length and its proximity to the SAN artery. In this way, we were also able to compare the OCT image to a sister histology section. Due to the prominence of fibroblasts and connective tissue, which serve to isolate the SAN myocytes from the surrounding atrial tissue (Boyett, Honjo et al. 2000), the SAN is readily identifiable as a unique structure with transmural OCT (Figure 3.6), without the need for histological staining.

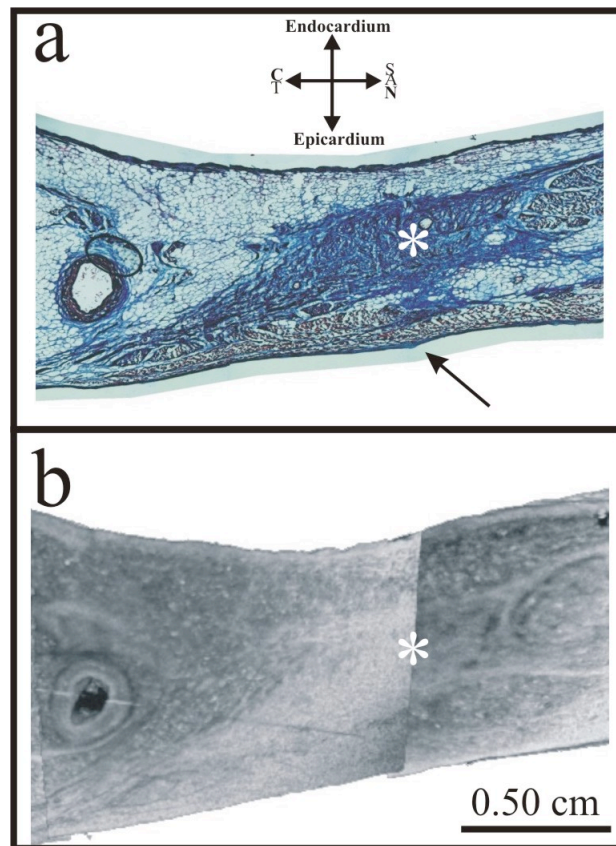


**Figure 3.6:** Transmural OCT of the sinoatrial node. (a) Histological section of the SAN and surrounding tissues. (b) Transmural OCT of the same area. The asterisk (\*) identifies the SAN, and the black arrow in (a) points to a thin layer of epicardial fibrous tissue that may have prevented OCT imaging of the SAN from the epicardium. Abbreviations – CT: crista terminalis; SAN: sinoatrial node.



### 3.4.3 OCT of the Atrioventricular Junction

OCT of the AVJ was achieved endocardially in five of nine preparations (56%). In the five preparations whose AVJ was imaged, those junctional elements, including the His bundle and AVN, were located within 2 mm of the endocardial surface. As the average depth penetration in this region across all specimens was  $0.96 \pm 0.25$  mm, those elements located deeper than 2 mm, as confirmed via histology, were unable to be identified in this manner.

All AVJ specimens were dissected for imaging of the entire Triangle of Koch, including a 1 to 2 cm border incorporating additional atrial and ventricular tissues (Figure 3.7a). The specimens were then optically mapped in overlapping 4.5x4.5 mm segments, with higher magnification images acquired in regions of interest, particularly the His bundle and AVN. In Figure 3.7, 3-D reconstructions revealed discrete structures located approximately 1 mm below the tissue surface (Figure 3.7b), corresponding to the locations of the His bundle and AVN as identified with traditional histology. In addition, 2-D tomograms showed this discrete structure encased in fibrous tissue, which manifests as a black envelope surrounding the brighter tissue of the bundle itself (Figure 3.7c,d). As our field of view progresses proximal to the His bundle, approaching the rightward extension (RE), also known as the inferior nodal extension (INE), we have a clear view of the AVN/RE (Figure 3.7e,f). The clarity is such that we can resolve the blood vessels (ranging from 320 to 750  $\mu\text{m}$  in diameter) located within the AVN itself. The location of the blood vessels are confirmed with both histology and OCT.

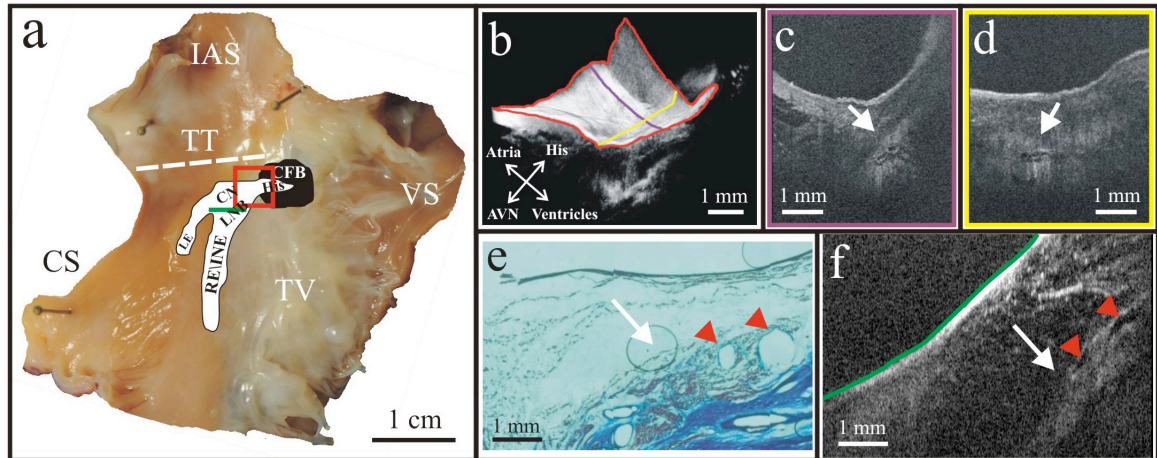


**Figure 3.7:** Endocardial OCT of the atrioventricular junction. (a) Dissected AVJ preparation. (b) 3-D reconstruction of the tissue area as indicated by the red box. (c,d) 2-D tomograms from (b) as indicated by the purple and yellow lines. (e) Histology of the AVN as indicated by the green line in (a). (f) Corresponding 2-D OCT image of (e) showing a strong relationship between the AV node as defined histologically and via OCT. Red arrowheads indicate blood vessels within the node, visible with both histology and OCT. Abbreviations- IAS: interatrial septum; TT: tendon of Todaro; CS: coronary sinus; LE: leftward extension; CN: compact node; LNB: lower nodal bundle; CFB: central fibrous body; RE: rightward extension; INE: inferior nodal extension; VS: ventricular septum; TV: tricuspid valve; AVN: atrioventricular node.

### 3.5 Discussion

Since its inception, OCT has undergone technical advances, including, but not limited to, the establishment of ultrahigh-resolution OCT (Drexler, Morgner et al. 1999; Drexler 2004), spectral/Fourier domain OCT (Fercher, Hitzenberger et al. 1995; Wojtkowski, Leitgeb et al. 2002; Yun, Tearney et al. 2003; Nassif, Cense et al. 2004; Oh, Yun et al. 2008), numerous improvements in light sources (Bouma, Tearney et al. 1995; Bouma, Tearney et al. 1996; Unterhuber, Povazay et al. 2004), development of a catheter-based imaging probe (Tearney, Brezinski et al. 1996; Tearney, Brezinski et al. 1997), and ultrasound-enhanced OCT, delivering greater spatial resolution and depth penetration (Schenk and Brezinski 2002; Huang, Liu et al. 2008). However, as OCT technology

continues to advance, there still exist technical challenges that remain to be addressed, such as the removal of blood from the imaging field to avoid substantial signal attenuation due to a refractive index mismatch between the cytoplasm of red blood cells (RBCs) and blood plasma. Current intravascular OCT systems incorporate a balloon catheter occlusion system (Guagliumi and Sirbu 2008); however, this technique cannot be easily applied to imaging the intact heart. In addition, Dextran, a biocompatible agent, has been shown to substantially improve the resolution and depth of OCT imaging through blood by increasing the refractive index of plasma to a value near that of the RBC cytoplasm (Brezinski, Saunders et al. 2001; Xu, Yu et al. 2008). This technique, known as index matching, has been shown to significantly diminish signal attenuation; however, additional *in vivo* testing is necessary.

The use of OCT to image the cardiac conduction system and other structures in the explanted human heart has many potential applications in cardiology. For example, cardiac fibers in the trabeculated endocardial structures of the atria and ventricles, as well as surviving fibers in the infarct border zone, often may contribute to the propensity to develop reentrant arrhythmias (Valderrabano, Lee et al. 2001; Valderrabano 2007). Our data indicates that OCT may prove of value in identifying these structures (Figures 3.1, 3.2, and 3.4), and thus potentially arrhythmic areas of the heart.

Although OCT catheters, with diameters as small as 0.3 mm, are commercially available for intravascular imaging of vulnerable plaques (Guagliumi and Sirbu 2008), the size of the target artery and/or tortuosity of the approach may preclude imaging in this manner.

In a recent review of the clinical use of intravascular OCT, Guagliumi and Sirbu state that cardiac vessels suitable for intravascular OCT are between 2.5 and 3.75 mm in diameter and have tortuosity angles less than 90 degrees (Guagliumi and Sirbu 2008). However, for vessels not exhibiting these characteristics, epicardial imaging may be a viable alternative to intravascular imaging (Figures 3.2 and 3.3).

We have also demonstrated OCT imaging of the conduction system, specifically the SAN and AVJ. These components are vital in the normal function of the heart; therefore, the ability to target them with a high-resolution imaging modality, such as OCT, has any number of potential applications. As the precise location of both the SAN and AVJ within the atrial myocardium is difficult to pinpoint with currently used imaging modalities, their structure can be uniquely identified due to the varying absorption properties present both in the nodal structures, which contain a prominence of fibroblasts and connective tissue, and in the surrounding tissues, as is shown in Figures 3.5-3.7, using OCT.

### **3.6 Conclusion**

Although traditional cardiac imaging modalities, including MRI, CT, and ultrasound, continue to provide physicians with vital information in the diagnosis of cardiac conditions, we have shown the potential of OCT in providing high-resolution, *in situ* images of the cardiac conduction system and other structures in the intact, explanted human heart. However, despite its ability to distinguish cardiac microstructures as shown

in this study, the technique is currently hampered by its depth penetration in cardiac tissues. Based on the presented data, we conclude that OCT is emerging as an important imaging modality with the potential to facilitate and guide electrophysiology studies, ablation therapy, implantation of pacing leads, and future cell and tissue engineering therapies subsequent to additional development.

## **4 Quantification of Fiber Orientation in the Canine Atrial Pacemaker Complex Using Optical Coherence Tomography**

### **4.1 Abstract**

The atrial pacemaker complex is responsible for the initiation and early propagation of cardiac impulses. It can also participate in such arrhythmias as atrial fibrillation and flutter. Optical coherence tomography (OCT), a nondestructive imaging modality, with spatial resolutions  $\sim 1-15 \mu\text{m}$  can be used to identify unique fiber orientation patterns in this region of the heart. In this study, functionally characterized canine sinoatrial nodes (SAN,  $n=7$ ) were imaged using OCT up to  $\sim 1$  mm below the endocardial tissue surface. OCT images were directly compared to their corresponding histological sections. Fiber orientation patterns unique to the crista terminalis (CT), SAN, and surrounding atrial myocardium were identified with dominant average fiber angles of  $89 \pm 12^\circ$ ,  $110 \pm 16^\circ$ , and

95±35°, respectively. Both the CT and surrounding atrial myocardium displayed predominantly unidirectional fiber orientation patterns within each specimen, whereas the SAN displayed an increased amount of fiber disarray manifested quantitatively as a significantly greater standard deviation in fiber angle distribution within specimens (33±7° versus 23±5°, atrium (p=0.02); 18±3°, CT (p=0.0003)). We also identified unique, local patterns of fiber orientation specific to the functionally characterized block zone. In addition, we demonstrate the ability of OCT to detect components of the atrial pacemaker complex, which are involved in both normal and abnormal cardiac conduction.

## 4.2 Introduction

The sinoatrial node (SAN) is a complex, heterogeneous structure located in the upper, posterior region of the right atrium (RA) responsible for initiating cardiac impulses during normal conduction. Structural investigations of the SAN have revealed it to be a diffuse, cigar-shaped structure extending between the superior and inferior vena cavae (Dobrzynski, Li et al. 2005), and electrically isolated from the remaining bulk of atrial tissue (Sanchez-Quintana, Cabrera et al. 2005; Boyett, Inada et al. 2006; Oren and Clancy 2010). The location of the leading pacemaker within the larger SAN is highly variable and can be affected by both vagal tone and changes in extracellular ion concentrations (Fedorov, Huckler et al. 2006; Monfredi, Dobrzynski et al. 2010). Early experiments investigating the mechanism of impulse formation and propagation through the SAN have pointed to the presence of discrete exit pathways (Bromberg, Hand et al. 1995;

Schuessler 2003), which have more recently been functionally and anatomically identified in both the canine and human SAN (Fedorov, Schuessler et al. 2009; Fedorov, Glukhov et al. 2010).

Atrial arrhythmias, such as flutter and fibrillation, have been shown to involve both the SAN and its exit pathways (Fedorov, Chang et al. 2010). These arrhythmias can be diagnosed during routine electrophysiology studies and potentially eradicated by catheter ablation procedures. Successful procedural outcomes oftentimes depend on the precise *in situ* identification of the atrial pacemaker complex, as well as normal/abnormal atrial myocardium. Current clinical anatomical visualization techniques, including magnetic resonance imaging (MRI), computed tomography (CT), and ultrasound, deliver relatively low spatial resolutions and cannot be performed in real time during electrophysiology procedures. Optical coherence tomography (OCT), on the other hand, is an imaging technique allowing for the visualization of micron-scale structures within nontransparent biological tissues, with resolutions ranging from submicrometer through 15  $\mu\text{m}$  (Povazay, Bizheva et al. 2002; Fujimoto 2003).

The use of OCT in visualizing components of the human heart vital to both normal and abnormal conduction, including high-resolution identification of the SAN, was evaluated in our recent study as described in Chapter 3 of this dissertation. Additional previous studies have shown the utility of OCT in imaging components of the conduction system in both rabbit (Gupta, Rollins et al. 2002; Jenkins, Wade et al. 2005) and human hearts as described in Chapter 3. We have also explored the relationship between structure,



imaged using OCT, and function, visualized using optical mapping, in the rabbit SAN (Hucker, Ripplinger et al. 2008). The rabbit SAN, however, is essentially a two-dimensional structure (Bleeker, Mackaay et al. 1980), as opposed to the three-dimensional canine (Bromberg, Hand et al. 1995; Fedorov, Schuessler et al. 2009) and human (Boineau, Canavan et al. 1988; Fedorov, Glukhov et al. 2010) SANs. In this study, we aimed to apply *ex vivo* OCT imaging to canine SANs, which have been functionally characterized using optical mapping as published in our previous study (Fedorov, Schuessler et al. 2009). Furthermore, we aimed to structurally identify elements of the atrial pacemaker complex, including nodal tissue and exit pathways, in addition to quantifying local fiber orientation in these areas important in the generation and maintenance of both normal and abnormal cardiac conduction.

## **4.3 Materials and Methods**

### **4.3.1 Experimental Preparation**

The experimental protocol was approved by the Institutional Animal Care and Use Committee of Washington University.

Canine right atrial preparations (n=7) were initially isolated and functionally-characterized using optical mapping with a voltage-sensitive dye, as described in our previous study (Fedorov, Schuessler et al. 2009). Immediately after the optical mapping experiment, the tissue preparations were perfused and fixed with 3.7% formaldehyde

overnight and then transferred to 20% sucrose for two days. Specimens were dissected to include the right atrial appendage (RAA), crista terminalis (CT), and 2-3 cm of tissue beyond the CT where the SAN is located (James 1962; Monfredi, Dobrzynski et al. 2010). The tissues were then photographed and clearly marked with pins to correlate OCT images with corresponding structural and functional data sets.

### **4.3.2 OCT Imaging**

The basics of our OCT system have been described previously (Hu and Rollins 2005; Hucker, Ripplinger et al. 2008). In short, we imaged each specimen in overlapping segments from the endocardial surface, with final axial and lateral resolutions of 10  $\mu\text{m}$  (in air).

### **4.3.3 Histology and Immunohistochemistry**

After imaging, tissue specimens (n=5) were embedded and frozen in Tissue-Tek OCT compound (Electron Microscopy Sciences, Hatfield, Pennsylvania) and stored at  $-80^{\circ}\text{C}$ . The tissues were then cryosectioned at 16  $\mu\text{m}$  (n=4, parallel to endocardium; n=1, perpendicular to endocardium) and mounted on Superfrost Plus glass slides (Fisher Scientific). Sister sections were then stained using either Masson Trichrome (IMEB, San Marcos, California) or antibodies for the gap junctional protein- connexin 43 (Sigma-Aldrich, St. Louis, Missouri), the cardiac myocyte marker-  $\alpha$ -actinin (Sigma-Aldrich, St. Louis, Missouri), and the fibroblast marker- vimentin (Progen Biotechnik, Heidelberg, Germany), as described previously (Hucker, McCain et al. 2008; Fedorov, Schuessler et

al. 2009). Imaging of both histology and immunohistochemistry was performed on a Nikon C1/80i confocal microscope with an attached AxioCam MRc5 brightfield camera (Carl Zeiss).

#### **4.3.4 OCT Image Processing and Analysis**

OCT images were processed using MATLAB (Mathworks), as described previously in Chapter 3. Individual OCT images were acquired six times, and then averaged to reduce background noise. Median filtering was also performed with a 3x3 smoothing kernel to further diminish speckle noise (Tearney, Yabushita et al. 2003). Custom-designed analysis programs were developed in MATLAB for virtual tissue slicing in order to visualize fiber orientation in relation to the tissue surface (Hucker, Ripplinger et al. 2008), as well as to quantify the depth of OCT imaging as described in Chapter 3. Quantification of 2-D fiber orientation was performed using an automated gradient based algorithm developed and validated in cardiac tissue (Fleming, Ripplinger et al. 2008). Areas of interest from which fiber orientation was assessed included the CT, atrial myocardium, SAN, block zone, and exit pathway(s). These areas were identified using a combination of histology, immunohistochemistry, and functional data sets.

Quantitative data are expressed as mean  $\pm$  standard deviation. A Student's *t*-test was used to determine statistical significance. A *p*-value of  $<0.05$  was considered statistically significant.

## 4.4 Results

### 4.4.1 Identification of the Atrial Pacemaker Complex

OCT imaging of the canine atrial pacemaker complex achieved an average depth penetration of  $1.28 \pm 0.23$  mm from the endocardial surface across all specimens. The approximate thickness of tissue incorporating and surrounding the atrial pacemaker complex was 2-3 mm. Although the SAN is defined as a primarily subepicardial structure (Sanchez-Quintana, Cabrera et al. 2005), inferior portions of the node are located closer to the endocardial surface bringing them within range for OCT (Fedorov, Glukhov et al. 2010). Consequently, although OCT could not consistently image throughout the entire thickness of tissue in the area of the SAN, the depth penetration was such that key components of the atrial pacemaker complex could be visualized. OCT failed, however, at identifying nodal tissue in one heart out of seven total imaged.

The initial functional and structural identification of the atrial pacemaker complex was achieved through the merging of several data sets, as shown in Figure 4.1. The primary field of view for all imaging modalities encompassed tissue ranging from the crista terminalis (CT) to the interatrial septum (IAS) (Figure 4.1A), which incorporated both nodal tissue and normal atrial myocardium into each data set. Optical mapping revealed the location of the primary pacemaker (Figure 4.1B), the block zone, and two (or more) exit pathways from the SAN (Fedorov, Schuessler et al. 2009). In addition, both histology (Figure 4.1C) and immunofluorescent labeling for connexin 43 (Figure 4.1D)

pinpointed the location of the SAN, as distinguished from surrounding normal atrial myocardium.

Resolution-wise OCT is comparable to conventional histological analyses (Povazay, Bizheva et al. 2002; Fujimoto 2003), which allows for the direct comparison of both techniques in identifying structures within the myocardium. Figure 4.2 illustrates this concept from two overlying fields of view. The images shown in Figure 4.2A-B are located approximately 0.44 mm below the endocardial surface, whereas those images shown in Figure 4.2C-D are located at a depth of approximately 0.69 mm. Major identifying structures, such as the sinus node artery and a pinhole (as indicated by the red arrowheads), are apparent using both conventional and virtual histology. In addition, abrupt changes in fiber orientation and organization can be identified and confirmed with OCT, as indicated by the arrows in Figure 4.2.

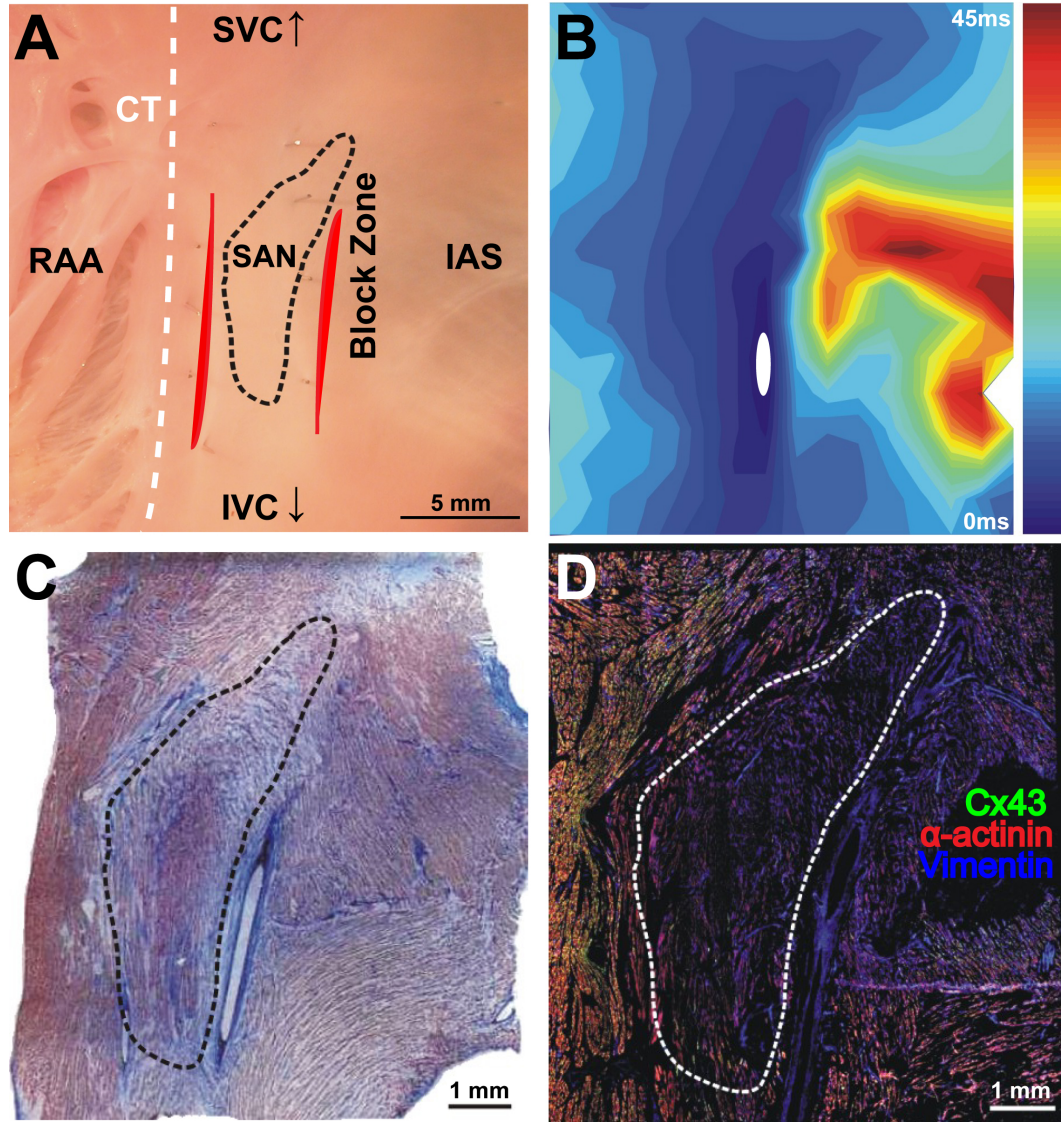


**Figure 4.1:** Identification of the atrial pacemaker complex. (A) Photograph of a typical SA nodal preparation as viewed from the endocardium with relevant structures labeled. (B) Typical activation map of normal sinus rhythm from the same field of view as in panel A. The white ellipsoid represents the area of earliest activation within the node. (C) Typical histology slide of the SAN with its approximate borders outlined by the dotted black line. (D) Typical immunofluorescent slide of the SAN with its approximate border outlined by the dotted white line. Connexin 43 is absent within the borders of the SAN. Abbreviations – SAN: sinoatrial node; SVC: superior vena cava; IVC: inferior vena cava; RAA: right atrial appendage; IAS: interatrial septum; Cx43: connexin 43.

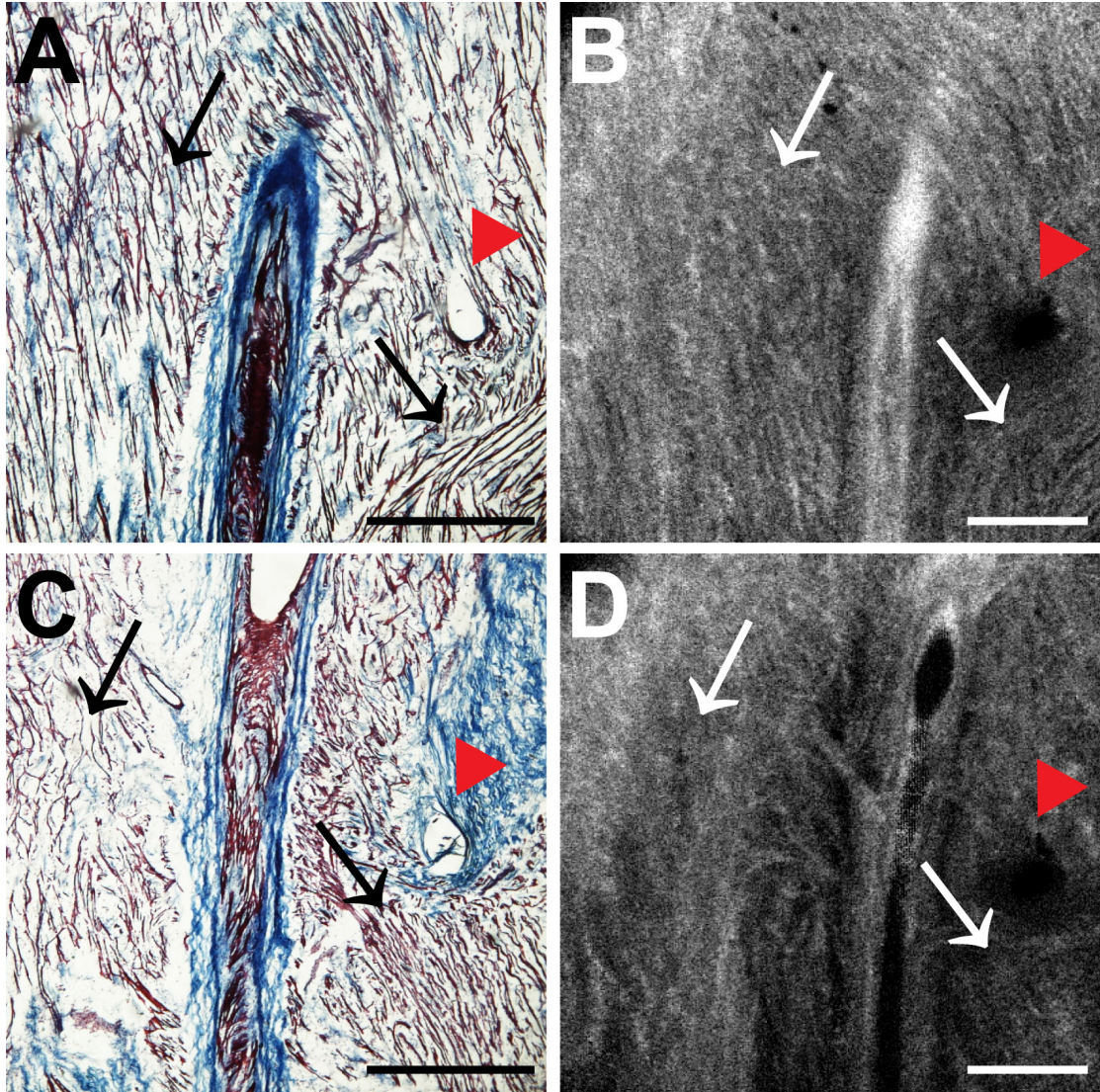


**Figure 4.2:** Correlation of histology and OCT. Corresponding histology and OCT slices taken from approximately 0.44 mm (A,B) and 0.69 mm (C,D) below the endocardial surface. Red arrowheads indicate pinholes used as reference points and arrows indicate abrupt changes in fiber orientation.

#### 4.4.2 Quantification of Fiber Orientation

Fiber orientation, as related to impulse propagation in the atrial pacemaker complex, was assessed from three fields of view in each heart. Figure 4.3 shows typical fiber orientation patterns from areas identified as the crista terminalis, as indicated by the green

boxes in Figure 4.3B-C, and the interatrial septum, as indicated by the blue boxes in Figure 3D-E, at two depths (0.17 and 0.49 mm) below the endocardial tissue surface. As is evident in the OCT images, these areas of tissue exhibit strong unidirectional fiber orientation with dominant fiber angles of  $70\pm 20^\circ$  and  $137\pm 16^\circ$  as measured in the crista terminalis and interatrial septum, respectively.

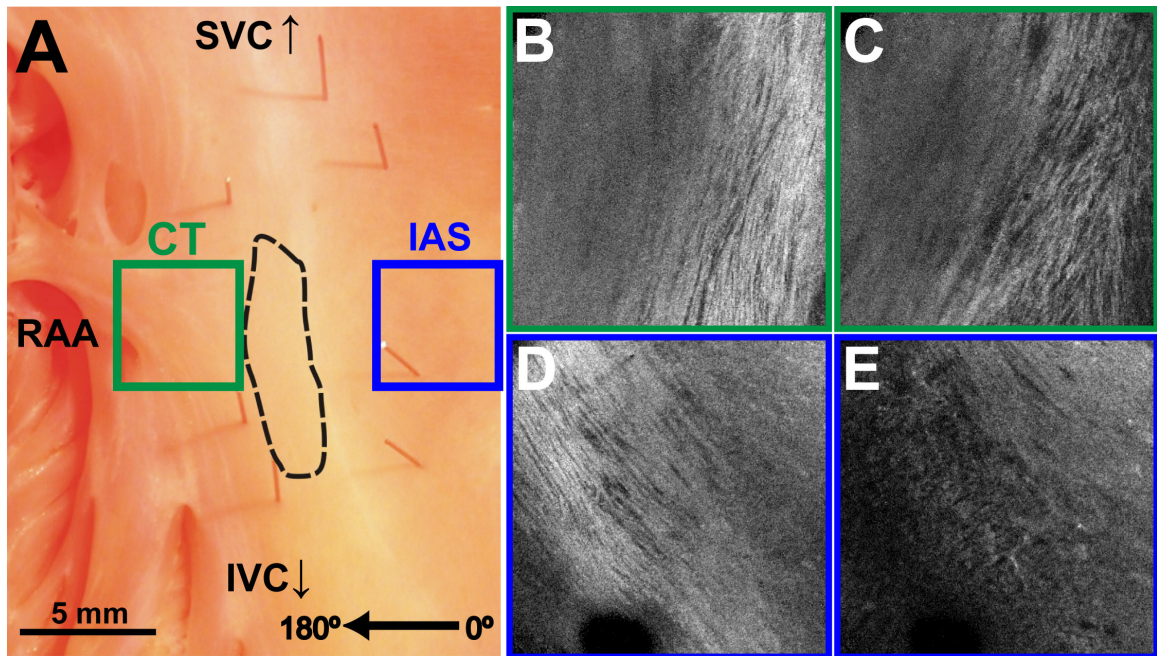


**Figure 4.3:** Identification of the crista terminalis and interatrial septum with OCT. (A) Photograph of an SA nodal preparation as viewed from the endocardium with the OCT fields of view for the CT and IAS identified by the green and blue boxes, respectively. OCT images of the unidirectional fiber orientation of the CT and IAS 0.17 mm (B,D) and 0.49 mm (C,E) below the endocardium. Abbreviations – SVC: superior vena cava; IVC: inferior vena cava; RAA: right atrial appendage; CT: crista terminalis; IAS: interatrial septum.

OCT fields of view encompassing nodal tissue, on the other hand, exhibit very different orientation patterns as shown in Figure 4.4. Initially, immediately under the endocardial tissue surface (Figure 4.4B, depth = 0.17 mm), there is a tendency for a strong unidirectional fiber orientation with a dominant angle of  $130\pm 14^\circ$ , similar to the interatrial septum. As the field of view progresses from the endocardium towards the



epicardium and through nodal tissue, the cardiac fibers display an increased amount of disarray, as shown in Figure 4.4E-G. This fiber disarray is representative of SA nodal tissue, which propagates impulses at slower conduction velocities than normal atrial myocardium (Boyett, Inada et al. 2006; Fedorov, Schuessler et al. 2009).

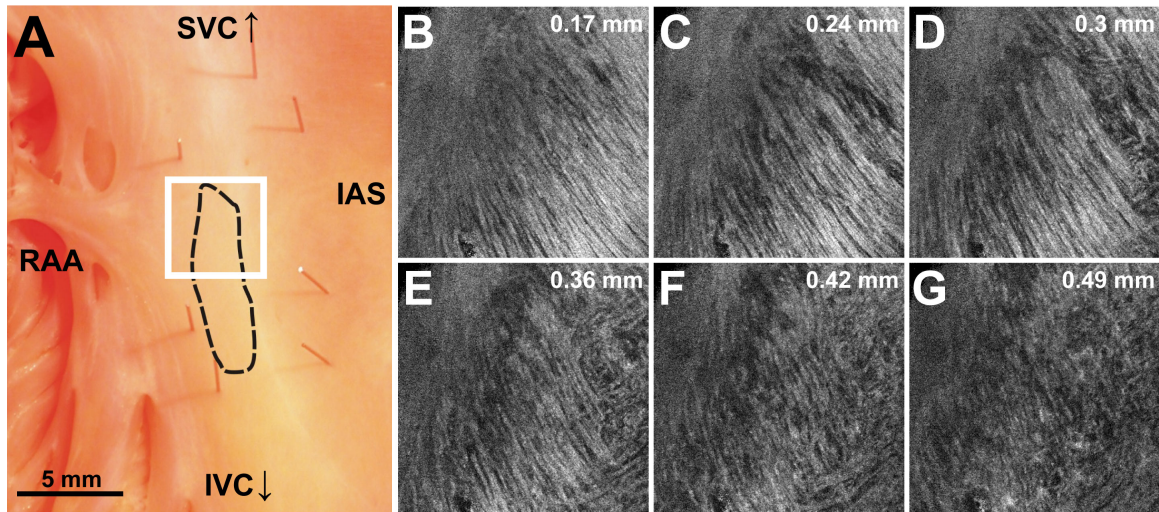


**Figure 4.4:** Identification of the sinoatrial node with OCT. (A) Photograph of an SA nodal preparation as viewed from the endocardium with the OCT field of view for the SAN identified by the white box. OCT images of the fiber orientation are shown at (B) 0.17 mm, (C) 0.24 mm, (D) 0.3 mm, (E) 0.36 mm, (F) 0.42 mm, and (G) 0.49 mm below the endocardium.

Specific fiber angle analyses, as shown in Figure 4.5, illustrate the changing orientation and fiber angle distributions in the CT, endocardial atrial layer above the SAN, and the SAN itself. Both the CT and endocardial atrial tissue layers exhibit strong unidirectional fiber orientations with dominant angles centered around  $69^\circ$  and  $130^\circ$  as shown in Figure 4.5A-F. Nodal tissue, as verified with standard histology and immunohistochemistry, exhibits a higher degree of fiber disarray as reflected in a wider range of fiber angles ( $112 \pm 34^\circ$ ), as shown in Figure 5G-I. All fiber orientation distributions in this specimen are significantly different from each other ( $p < 0.0001$ ).

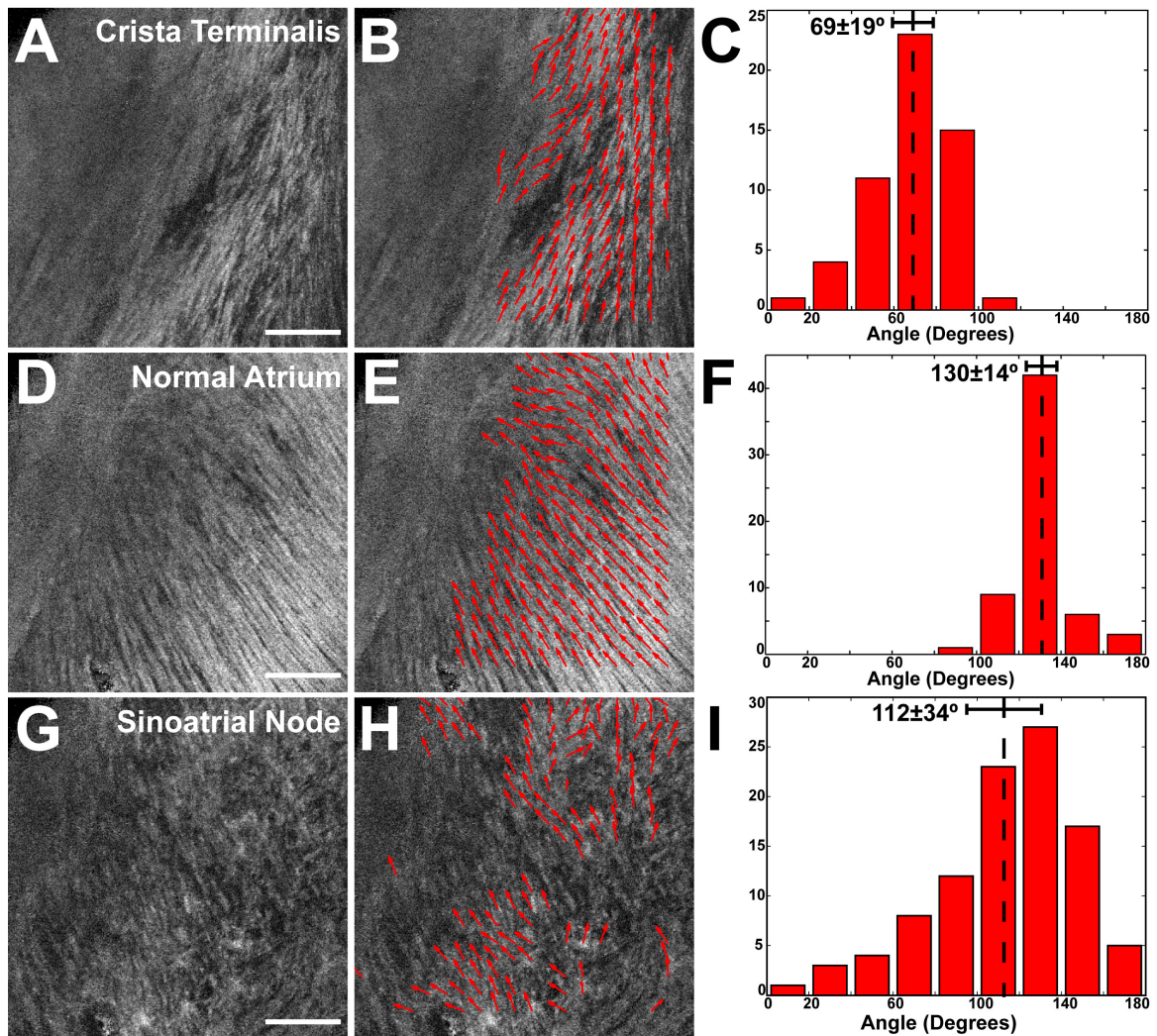


**Figure 4.5:** Fiber angle distribution in the crista terminalis, atrium, and sinoatrial node. (A) OCT image of cardiac fibers in the CT. (B) Distribution of fiber angles in the CT with an average dominant angle of  $69\pm 19^\circ$ . (D) OCT image of cardiac fibers in normal atrial myocardium located endocardial to the SAN. (E) Assigned fiber angle vectors in normal atrial myocardium. (F) Distribution of fiber angles in the atrium with an average dominant angle of  $130\pm 14^\circ$ . (G) OCT image of cardiac fibers in the SAN. (H) Assigned fiber angle vectors in the SAN. (I) Distribution of fiber angles in the SAN with an average dominant angle of  $112\pm 34^\circ$ .

Overall fiber angle orientation, as summarized in Figure 4.6, was consistent across samples within the CT ( $89\pm 12^\circ$ ), however, the endocardial atrial layer located above the SAN exhibited a wide range of dominant fiber angles ( $36-128^\circ$ ) between specimens.

Within each specimen, there was still a strong tendency for the endocardial atrial layer

above the SAN to exhibit unidirectional fiber orientation as in Figure 4.5D-F. The overall average angle of the SAN itself was relatively consistent among the specimens at  $110 \pm 16^\circ$ , however each individual specimen did exhibit a high degree of fiber disarray within the node, such as that illustrated in Figure 4.5G-I. The amount of fiber disarray was evaluated based on the standard deviation of angles within each structure (CT, endocardial atrial layer, and SAN) as shown in Figure 4.7. Overall, the SAN demonstrated significantly higher standard deviations ( $33 \pm 7^\circ$ ) than both the endocardial atrial layer ( $23 \pm 5^\circ$ ,  $p=0.02$ ) and the CT ( $18 \pm 3^\circ$ ,  $p=0.0003$ ) indicative of its higher degree of fiber disarray.

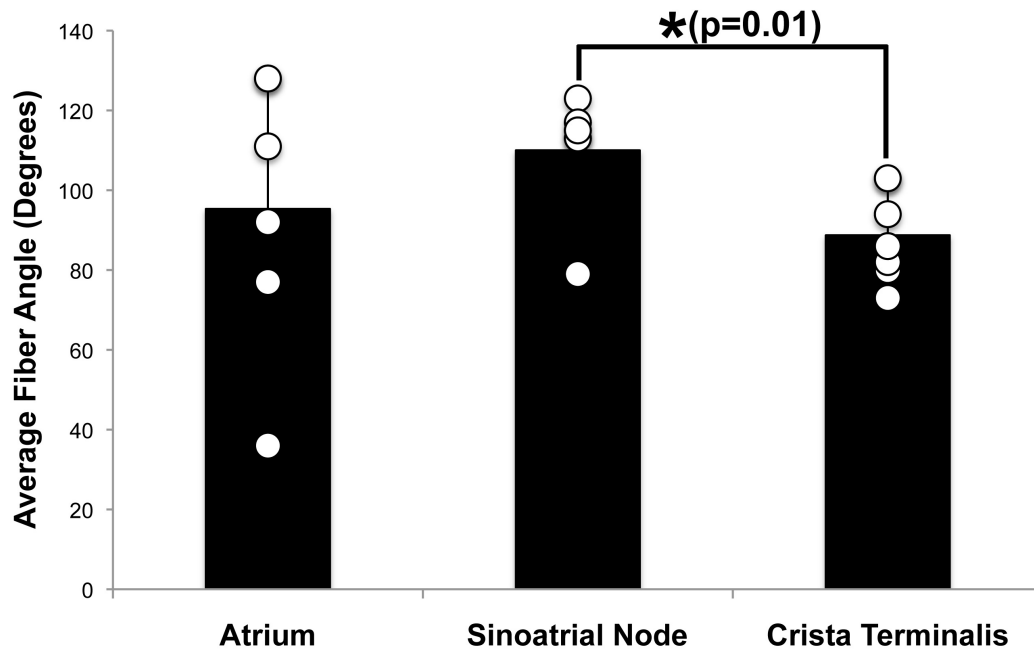


**Figure 4.6:** Average fiber angle. Average fiber angles across all hearts in three locations: the atrium (endocardial to the SAN), SAN, and CT.

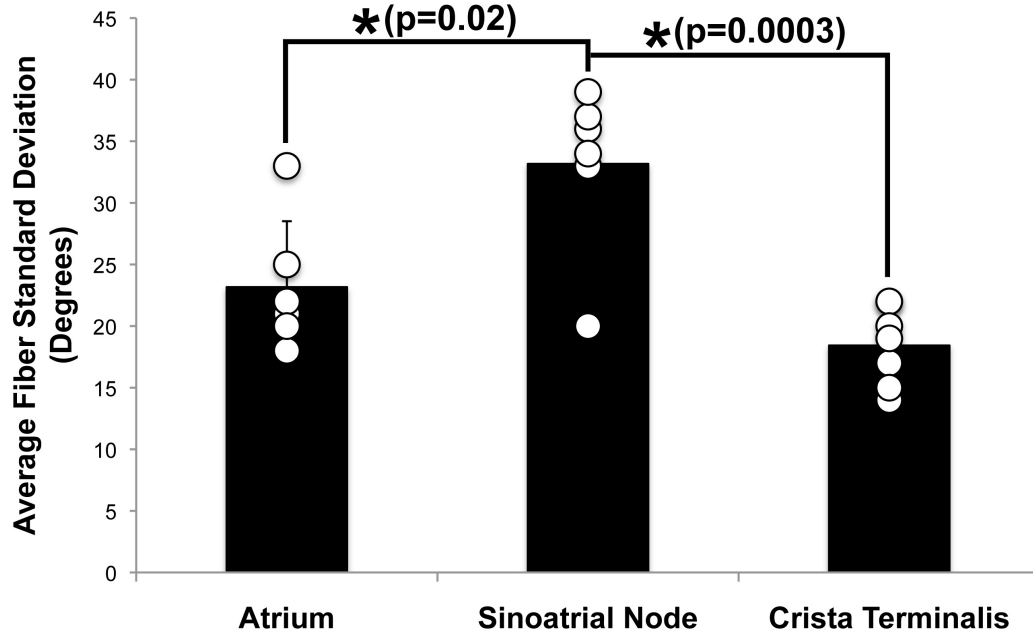


**Figure 4.7:** Standard deviation of the average fiber angle. Standard deviation of the average fiber angle as an indicator of fiber disarray across all hearts in three locations: the atrium (endocardial to the SAN), SAN, and CT.

#### 4.4.3 Fiber Orientation in the Block Zone

In addition to evaluating fiber orientation in the CT, endocardial atrium, and SAN, fibers were also identified with unique orientation patterns in the block zone (Boyett, Honjo et al. 2000) as shown in Figure 4.8. The bright white area, as indicated by the white arrow in Figure 4.8C, most likely contributes to the functional block zone, as shown in Figure 4.8A. The pattern of fibers indicated by the red arrow in Figure 4.8E appear to “dead-end” in the block zone. Consequently, an impulse originating from the SAN would not be able to traverse these fibers and would instead have to bypass the block zone, as indicated by the dotted white line in Figure 4.8E, in order to excite the remaining bulk of atrial tissue.

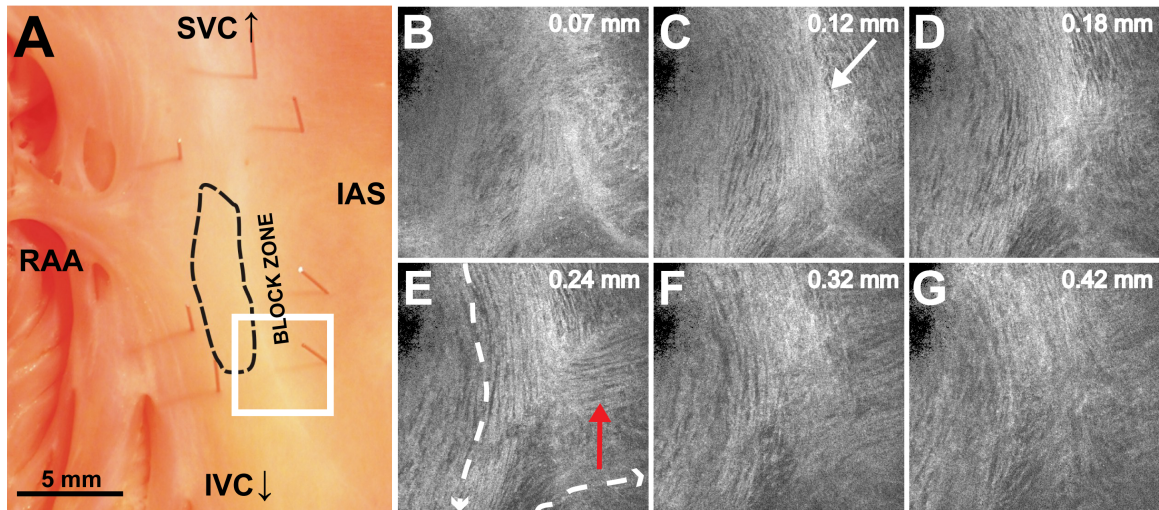


**Figure 4.8:** (A) Photograph of an SA nodal preparation as viewed from the endocardium with the OCT field of view for the functional SA nodal block zone identified by the white box. OCT images of fiber orientation are shown at (B) 0.07 mm, (C) 0.12 mm, (D) 0.18 mm, (E) 0.24 mm, (F) 0.32 mm, and (G) 0.42 mm below the endocardium. The white arrow in (C) indicates the probable anatomic correlate of the functional block zone. The dotted white lines indicate the pathways for impulse propagation around the block zone. The red arrow indicates fibers that “dead-end” in the functional block zone. Abbreviations – SVC: superior vena cava; IVC: inferior vena cava; RAA: right atrial appendage; IAS: interatrial septum.

## 4.5 Discussion

It is well known that cardiac function is intimately linked to underlying tissue structure. In this study, we had the distinct advantage of performing structurally-based imaging on electrophysiologically-characterized preparations. We focused specifically on the structure-function relationship in the canine SAN with particular emphasis on fiber orientation patterns as they relate to SA nodal conduction. Our previous study functionally identified the block zone, nodal tissue, and discrete exit pathways in the canine heart (Fedorov, Schuessler et al. 2009). In addition, these structures were also identified using more traditional histological and immunohistochemical techniques. Now

for the first time, we have demonstrated the existence of these structures using a nondestructive imaging modality.

We have identified unique fiber orientation patterns specific to the CT (Figure 4.3), SAN (Figure 4.4), atrial myocardium (Figures 4.3 and 4.4), and block zone (Figure 4.8). In addition, we quantified fiber orientation distributions, using an automated gradient-based algorithm (Fleming, Ripplinger et al. 2008), in these areas (Figure 4.5). We found that the CT and atrial myocardium tended to display unidirectional fiber orientations, whereas the SAN exhibited an increased amount of fiber disarray manifested as a significantly greater standard deviation in fiber angle distributions (Figure 4.7). Although we were unsuccessful in concretely identifying the exit pathways using OCT, we believe their presence may be masked by surrounding fibers with similar orientation patterns. We were, most importantly, able to distinguish SA nodal tissue from the surrounding atrial myocardium (Figures 4.4, 4.5, and 4.7).

In addition to being a key component of normal cardiac conduction, the atrial pacemaker complex, consisting of the SAN, block zone, exit pathway(s), and surrounding atrial myocardium, has also been shown to be involved in arrhythmias, such as atrial flutter and fibrillation (Fedorov, Schuessler et al. 2009; Fedorov, Chang et al. 2010). These arrhythmias are oftentimes associated with SA nodal dysfunction (Schuessler 2003) and, more importantly, are accompanied by both functional and structural changes in the SAN (Sanders, Morton et al. 2004). Structural changes, such as alterations in interstitial fibrosis (Ausma, Wijffels et al. 1997), within the SAN could potentially be monitored

over time with high spatial resolution OCT, as an indicator of disease progression. In addition, an increased amount of fibrosis or abrupt changes in fiber orientation patterns may result in a higher propensity for reentrant arrhythmias (Valderrabano, Lee et al. 2001).

Recently, it has been suggested that there is a unique structure running parallel to the human SAN termed the paranodal area (Chandler, Greener et al. 2009; Chandler, Aslanidi et al. 2011). This region was shown to have unique molecular and histological characteristics in the human heart, with properties intermediate between the SAN and normal right atrial myocardium. In our study, we were unable to identify this area in the canine heart using both traditional histology and OCT, despite the functional similarities we have found between the human and canine SANs (Fedorov, Schuessler et al. 2009; Fedorov, Glukhov et al. 2010). The identification of the paranodal area in the human heart with OCT still remains to be explored.

OCT is a nondestructive imaging technique with superior spatial resolution as compared to other anatomical visualization and reconstruction techniques (Povazay, Bizheva et al. 2002; Fujimoto 2003). Most importantly, OCT can be miniaturized into a catheter-based imaging system (Tearney, Brezinski et al. 1996; Fleming, Wang et al. 2010) to be threaded through the vasculature and into the cardiac chambers. In this way, physicians can directly relate, in real time and *in situ*, cardiac function to its underlying structure during electrophysiology studies and ablation procedures. In addition, the continued development of automated visualization and analysis tools (Fleming, Ripplinger et al.

2008; Hucker, Ripplinger et al. 2008) for OCT will only serve to power its movement into mainstream cardiology.

## 4.6 Conclusion

We have demonstrated the ability of OCT in detecting components of the atrial pacemaker complex, which are intimately involved in both normal and abnormal cardiac conduction. We identified and quantified fiber orientation patterns specific to the CT, SAN, atrial myocardium, and block zone using an automated gradient-based algorithm. Based on this study, we believe OCT is continuing to emerge as a key imaging modality with the potential to identify, in real time and *in situ*, structural substrates responsible for both normal and abnormal cardiac conduction.



## **5 Termination of Sustained Atrial Flutter and Fibrillation Using Low-Voltage Multiple-Shock Therapy**

### **5.1 Abstract**

Defibrillation therapy for atrial fibrillation (AF) and flutter (AFI) is currently limited by the pain induced by high-energy shocks. Thus, lowering the defibrillation energy for AFI/AF is highly desirable. In this study, we applied low-voltage multiple-shock therapy in a rabbit model of atrial tachyarrhythmias comparing its efficacy to single shocks and antitachycardia pacing (ATP). Optical mapping was performed in Langendorff-perfused rabbit hearts (n=18). Acetylcholine ( $7\pm 5$  to  $17\pm 16$   $\mu\text{M}$ ) was administered to promote sustained AFI and AF, respectively. Single and multiple (3-8) monophasic shocks were applied within 1 or 2 cycle lengths (CLs) of the arrhythmia. We observed AFI (CL =  $83\pm 15$  ms, n=17) and AF (CL =  $50\pm 8$  ms, n=11). ATP had a success rate of 66.7% in the case of AFI, but no success with AF (n=9). Low-voltage multiple shocks had 100%

success for both arrhythmias. Multiple low-voltage shocks terminated AF1 at  $0.86\pm 0.73$  V/cm (within 1 arrhythmia CL) and  $0.28\pm 0.13$  V/cm (within 2 arrhythmia CLs), as compared with single shocks at  $2.12\pm 1.31$  V/cm ( $p<0.001$ ) and AF at  $3.46\pm 3$  V/cm (within 1 arrhythmia CL), as compared with single shocks at  $6.83\pm 3.12$  V/cm ( $p=0.06$ ). For multiple shocks delivered within one CL, 4 shocks resulted in the lowest defibrillation threshold for both AF1 and AF ( $0.41\pm 0.22$  and  $1.97\pm 1.25$  V/cm, respectively). Additionally, despite the fact that multiple shocks delivered within 2 CLs resulted in the lowest defibrillation threshold for AF1 ( $0.28\pm 0.13$  V/cm), this therapy also resulted in an increased conversion rate of AF1 to sustained AF. No ventricular arrhythmias were induced. Optical mapping revealed that termination of AF1 was achieved by a properly timed, local shock-induced wave that collides with the arrhythmia wavefront, whereas AF required the majority of atrial tissue to be excited and reset for termination. Low-voltage multiple-shock therapy terminates AF1 and AF with different mechanisms and thresholds based on spatiotemporal characteristics of the arrhythmias.

## 5.2 Introduction

Atrial fibrillation (AF) is the most prevalent cardiac arrhythmia in the world, affecting over 2.2 million people in the United States (Lloyd-Jones, Adams et al. 2010). A recent population study estimates that by the year 2050, over 12 million Americans may be affected (Miyasaka, Barnes et al. 2006). Complications of AF include thromboembolic stroke, congestive heart failure, and increased mortality (Crandall, Horne et al. 2009; Seiler and Stevenson 2010). In addition, AF leads to more hospitalizations than any other

arrhythmia, resulting in a significant socioeconomic burden (Coyne, Paramore et al. 2006; Kannel and Benjamin 2009). Treatment strategies, including drug therapy, cardioversion, and ablation, are designed to reduce the frequency and duration of arrhythmia episodes as it is known that AF begets AF (Wijffels, Kirchhof et al. 1995). Furthermore, AF can be classified as a progressive disease and, if left untreated, paroxysmal AF can degenerate into permanent AF (Cohen and Naccarelli 2008), and atrial flutter (AFL) can degenerate into AF (Waldo and Feld 2008).

Options for drug therapy include quinidine and flecainide, however, these and other available antiarrhythmic drugs have potentially serious side effects and low efficacy (Nattel 1998; Dobrev and Nattel 2010). A newly-developed generation of anti-arrhythmic drug therapy could be effective, but still needs further clinical validation (Dobrev and Nattel 2010). There have also been many advances in ablative techniques (Lee, Melby et al. 2009); yet, these procedures are not without risks, including, but not limited to, esophageal injury, phrenic nerve injury, and pulmonary vein stenosis (Doppalapudi, Yamada et al. 2009). In addition, ablation of atrial tachyarrhythmias has yet to become a standardized procedure and, consequently, there is a wide variation in published success rates that can be both physician- and medical center-dependent (Calkins, Reynolds et al. 2009).

Antitachycardia pacing (ATP) delivers a train of stimuli coordinated with the arrhythmia cycle length (CL) that attempts to disrupt the aberrant circuit(s) maintaining AF or AFL; however, its success rates are often around, or significantly less than 60% (Gillis, Koehler

et al. 2005). Cardioversion delivers an electric shock designed to reset all cardiac electrical activity and clinical trials have shown its success to be higher when applied to shorter arrhythmia episodes (Van Gelder, Crijns et al. 1991; Coro, Delise et al. 2001). External cardioversion boasts success rates up to 97% (Koster, Dorian et al. 2004), but requires high-shock energies and sedation of the patient. In addition, high energy shocks can cause electroporation (Fedorov, Kostecki et al. 2008) and atrial stunning (Khan 2003), leading to an increased risk of thrombus formation and cardiac damage. On the other hand, the use of intracardiac shocks, by the implantable atrial defibrillator (IAD) (Doddall and Ideker 2007), requires less energy and patient sedation (Alt, Ammer et al. 1997). Although initial clinical trials have shown that the IAD has a high specificity and sensitivity to AF and delivers safe and effective shocks (Schoels, Swerdlow et al. 2001), it has not gained widespread acceptance because the energy for successful endocardial cardioversion still exceeds the pain threshold (Mitchell, Spurrell et al. 2004). Thus, lowering the defibrillation energy for atrial arrhythmias is highly desirable.

In a recent study, we applied a method for low-voltage termination of ventricular tachycardia in a rabbit whole heart model and found a significant reduction in the defibrillation threshold (Li, Ripplinger et al. 2009). In this study, we aim to apply this therapy to a rabbit model of AF1 and AF. Our technique of low-voltage multiple-shock therapy is based on the virtual electrode polarization (VEP) hypothesis (Efimov and Ripplinger 2006), and is a method of destabilizing and terminating anatomically-defined reentrant tachyarrhythmias (Ripplinger, Krinsky et al. 2006). This technique utilizes a lower voltage shock that serves to unpin the core of the arrhythmia's mother rotor, which

has anchored itself to a physical myocardial heterogeneity (Takagi, Pumar et al. 2004; Ripplinger, Krinsky et al. 2006). The core of reentry will experience a greater polarization in response to the applied electric field according to the VEP hypothesis. The depolarized region of the reentry core then becomes a secondary source of excitation, which can create a new wave. When timed correctly, the new wave can collide with and either terminate or unpin the anatomical reentry. If unpinned, the reentry will become unstable and self-terminate. In this study, we now aim to apply this technique to a rabbit model of cholinergically-induced AFI/AF and by applying multiple shocks within 1-2 arrhythmia CLs, we aim to increase the probability of a shock falling within the optimal time frame for successful termination.

In applying low-voltage multiple-shock therapy, important distinctions between AFI and AF must be considered. AFI is defined by a macro-reentrant circuit, which can rotate around an anatomic or functional line of block. Major anatomical structures, including the region between the vena cavae and pulmonary veins are usually involved in defining reentry (Fedorov, Chang et al. 2010). AF, on the other hand, involves multiple reentrant circuits defined primarily by local excitability and refractory periods. In this study, we hypothesize that low-voltage multiple-shock therapy will terminate anatomically-defined AFI with higher efficacy than functionally-defined AF because of its ability to efficiently penetrate the longer excitable gap associated with AFI and consequently, to unpin reentry.

## 5.3 Materials and Methods

### 5.3.1 Experimental Preparation

The experimental protocol was approved by the Institutional Animal Care and Use Committee of Washington University.

Experiments were performed *in vitro* on hearts obtained from New Zealand white rabbits (n=18) of both sexes. The isolation procedure has been described previously (Fedorov, Lozinsky et al. 2007). Briefly, rabbits were anesthetized intravenously with 50 mg/kg sodium pentobarbital and 1,000-2,000 U heparin. The heart was removed and placed onto a Langendorff apparatus, where it was coronary-perfused at 20 mL/min with oxygenated Tyrode's solution. Fat and connective tissue was carefully dissected from the posterior epicardium of the heart and all vena cavae and pulmonary veins were ligated. Perfusion fluid flowing out of the coronary sinus into the right ventricle exited the heart exclusively through a cannula in the pulmonary artery. In addition, the interatrial septum was perforated, allowing for equal pressures in both atria and a more uniform epicardial surface for optical mapping. The whole heart preparation was then placed posterior side up in a temperature-controlled bath (Radnoti, Monrovia, California) at 37°C and Langendorff-perfused under a constant pressure of 60 mmHg with oxygenated Tyrode's solution. The excitation-contraction uncoupler blebbistatin (Tocris Biosciences, Ellisville, Missouri) was added to the perfusate at 10  $\mu$ M to suppress motion artifacts in the optical recordings (Fedorov, Lozinsky et al. 2007). The heart was then stained with

the voltage-sensitive dye, di-4-ANEPPS (Molecular Probes, Eugene, Oregon), diluted in dimethylsulfoxide (Sigma-Aldrich, St. Louis, Missouri).

### **5.3.2 Optical Mapping and Defibrillation Setup**

During a 20-30 minute equilibration period, bipolar electrodes, which could be switched between pacing and sensing without disrupting their original positions, were placed on the left atrial appendage (LAA), right atrial appendage (RAA), and right atrial (RA) free wall. Two stainless steel mesh electrodes were placed vertically into the solution chamber approximately 10 cm apart parallel to the long axis of the heart. Shocks were delivered from two computer-controlled regulated power supplies (BOP 100-4M1; Kepko, Inc., Flushing, New York) connected in parallel to provide a maximum voltage of  $\pm 100\text{V}$  and a maximum current of 8A as described previously (Ripplinger, Lou et al. 2009).

Optical mapping was performed with a 100x100 pixel MiCAM Ultima-L CMOS camera (SciMedia, Costa Mesa, California). The preparation was illuminated by light-emitting diodes at 520 nm and fluorescence emitted from the preparation was long-pass filtered above 610 nm. Optical action potentials (OAPs) were recorded from a field of view of approximately  $30 \times 30 \text{mm}^2$ , which was sufficient to encompass both atrial appendages, with a spatial resolution of  $300 \mu\text{m}$  at a frame rate of 1000 frames/sec. The resultant fluorescent signals were amplified, digitized, and visualized during the experiment using specialized software (SciMedia, Costa Mesa, California).

### 5.3.3 Experimental Protocol

After optimization of the optical signals, the intrinsic activity of each preparation was recorded. Pacing thresholds and effective refractory periods (ERPs) were determined from all locations. All stimuli were subsequently delivered at 2-3x the pacing threshold. Far field stimulation thresholds as a result of shocks were also determined for both polarities (n=7).

After all control variables were obtained, programmed stimulation was applied to attempt to initiate an arrhythmia by a Master-8 programmable stimulator (A.M.P.I., Jerusalem) and a custom-written stimulation interface (see Appendix 2). Programmed stimulation consisted of either an S1-S2 protocol (10-20 basic stimuli at 300 ms followed by a premature beat at progressively shorter coupling intervals) or burst pacing. If arrhythmia initiation was unsuccessful, incremental concentrations of acetylcholine chloride (ACh, 1-100  $\mu$ M; Sigma-Aldrich, St. Louis, Missouri) were added until a sustained arrhythmia was induced (Sharifov, Fedorov et al. 2004). A sustained arrhythmia was defined as lasting at least 2-3 minutes, although if not terminated, the arrhythmias would persist on the order of one hour. Single or multiple (3-8) 5-10 ms monophasic shocks were applied equally spaced out within either one or two CLs of the arrhythmia (n=18). In addition, we also applied ATP consisting of 8 pulses at 50-100% of the arrhythmia CL from either the RAA or lower RA (n=9). If the arrhythmia was terminated by either the shock or ATP, a new arrhythmia was immediately reinitiated via the programmed stimulation described earlier. Success was defined as termination of the arrhythmias within three seconds of therapy applications.



### 5.3.4 Data Analysis

A custom-designed MATLAB-based computer program, described previously (Fedorov, Chang et al. 2010), was used to analyze experimental data offline. Activation maps were constructed from activation times calculated from the  $dV/dt_{\max}$  of each pixel.

Quantitative data are expressed as mean  $\pm$  standard deviation. The Student's *t*-test was used to determine statistical significance ( $p < 0.05$ ).

## 5.4 Results

### 5.4.1 Initiation of Arrhythmias

Figure 5.1a shows an optical mapping field of view encompassing the posterior side of the atria, including both the RAA and LAA. Figure 5.1b shows an example activation map while pacing the RAA (CL=300 ms), with the corresponding OAPs shown in Figure 5.1c. Upon addition of an ACh concentration needed for the induction of a sustained arrhythmia, the atrial ERP was reduced from  $67 \pm 11$  ms to  $40 \pm 8$  ms ( $p < 0.001$ ) (Figure 5.1d). Figure 5.1e illustrates the significant shortening of the action potential duration, establishing the functional substrate necessary for inducing and maintaining AFI/AF.

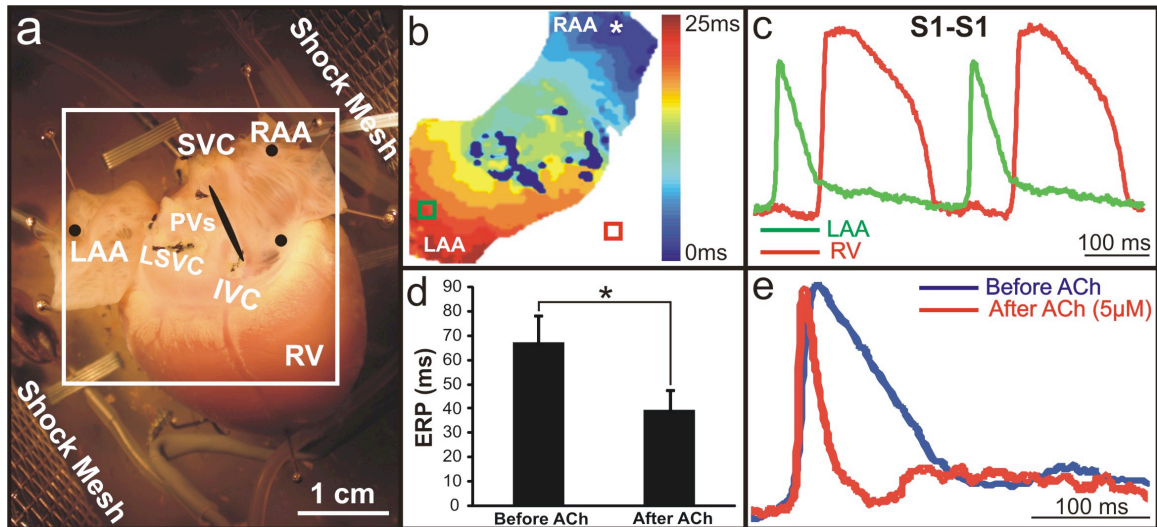


**Figure 5.1:** Low-voltage multiple-shock defibrillation experimental setup. (a) Photograph of a typical preparation with shock meshes labeled, located 10 cm apart. The black circles represent the locations of pacing/sensing electrodes. (b,c) Typical activation map and OAPs during pacing of the RAA (300 ms). The deep blue areas in the center represent pixels that have been excluded from analysis because of noise from sutures and connective tissue. (d) Average ERP before and after ACh. (e) Representative OAPs from the RAA before and after the addition of 5  $\mu\text{M}$  ACh, reflecting a 57% decrease in the action potential duration. Abbreviations – ACh: acetylcholine chloride; ERP: effective refractory period; IVC: inferior vena cava; LAA: left atrial appendage; LSVC: left superior vena cava; OAP: optical action potential; PV: pulmonary vein; RA: right atrium; RAA: right atrial appendage; RV: right ventricle; SVC: superior vena cava.

Upon addition of  $7 \pm 5 \mu\text{M}$  ACh, we induced AFI maintained by a single macro-reentrant circuit ( $\text{CL} = 83 \pm 15 \text{ ms}$ ,  $n=17$ ) rotating around the anatomic zone of conduction block between the superior and inferior vena cava (Figure 5.2a). Figure 5.2b shows that AF was maintained by multiple reentry circuits ( $\text{CL} = 50 \pm 8 \text{ ms}$ ,  $n=11$ ) with an average ACh concentration of  $17 \pm 16 \mu\text{M}$ . Dominant frequency analysis reflected the major rotors maintaining each arrhythmia as illustrated in Figure 5.2c,d. In only one heart out of 18 were we unable to induce any sustained arrhythmias even with the addition of  $500 \mu\text{M}$  ACh. Additionally, in three preparations we were able to initiate AFI before the addition

of ACh, although the arrhythmias were sustained enough in only two preparations in which we performed limited defibrillation testing.

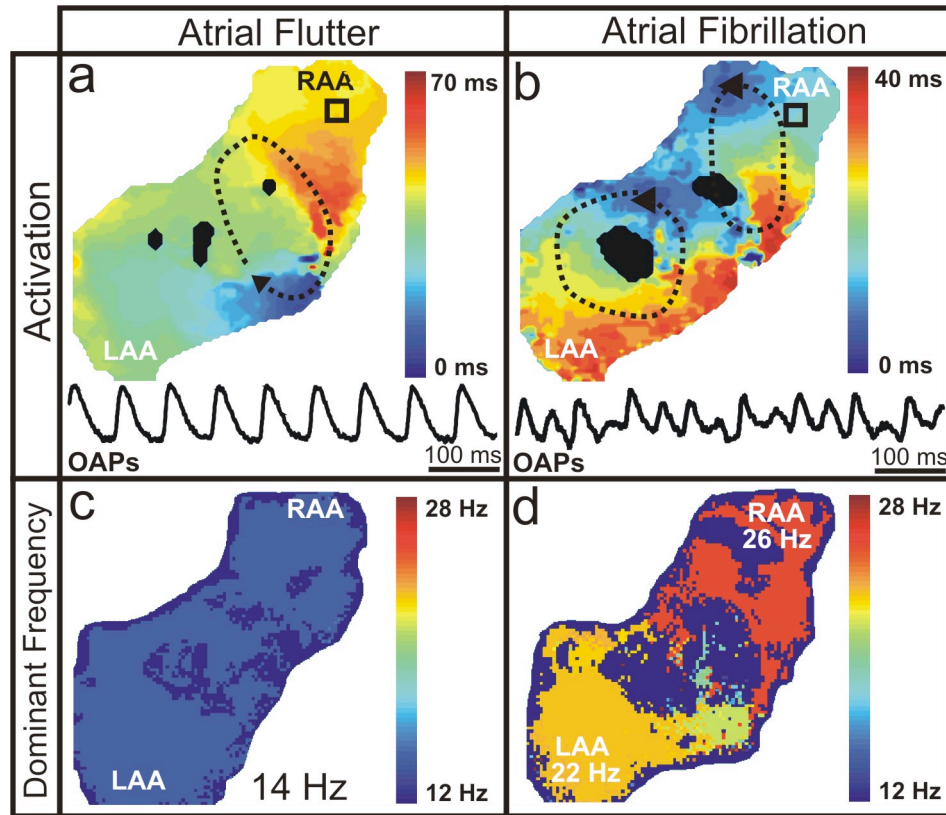


**Figure 5.2:** Typical atrial flutter and fibrillation. (a,b) Typical activation maps, representative of 1 arrhythmia cycle, and OAPs (as indicated by the black squares) of AF and AF, respectively. Dashed black lines with arrows show the location and direction of the reentrant circuits. (c,d) Frequency distribution for typical examples of AF and AF, respectively.

### 5.4.2 Application of Antitachycardia Pacing

ATP was applied in nine hearts from an electrode placed on either the RAA or lower RA, similar to clinical RA pacing leads. We applied 107 rounds of ATP from both locations consisting of 8 pulses at 50-100% of the arrhythmia CL (Figure 5.3). Figure 5.3b shows that 22.4% of ATP applications to AF were successful in terminating the arrhythmia.

However, 70.1% of applications had no effect on the arrhythmia and 7.5% of applications

converted AFL to AF. Therapy applied at 80% of the arrhythmia CL had the highest likelihood of success (13/34 applications resulted in termination,  $p=0.0006$ ), whereas ATP at 90% of the arrhythmia CL resulted in the highest incidence of failed termination (38/41 applications had no effect,  $p=0.0008$ ). As shown in Figure 5.3c, ATP was most successful in arrhythmias with longer average CLs (80-85 ms and 95-100 ms). Overall, ATP successfully terminated arrhythmias in 6 out of 9 preparations (66.7%). Furthermore, the outcome of ATP was not dependent on electrode location and, as expected, ATP did not terminate any episodes of AF.

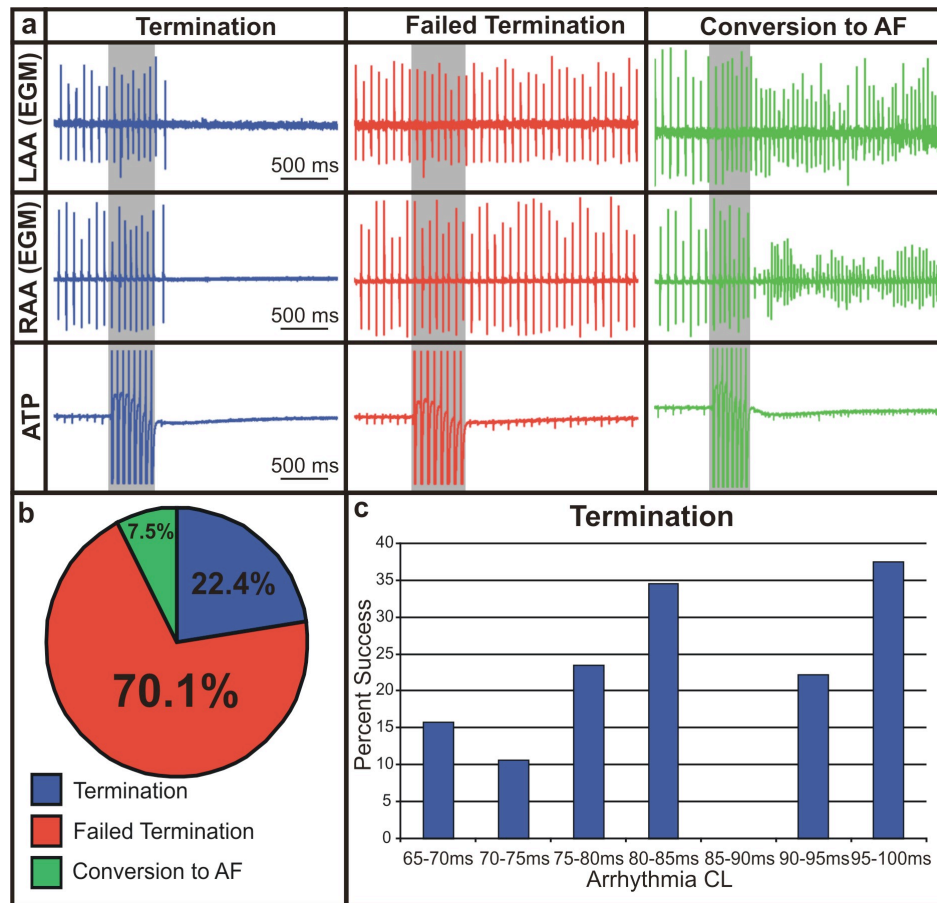


**Figure 5.3:** Application of antitachycardia pacing to AFL. (a) Representative electrograms of termination, failed termination, and conversion to AF upon application of ATP (8 pulses, 50-100% of arrhythmia CL) to AFL from the RAA and lower RA. (b) Distribution of outcome during application of ATP to AFL. (c) Percentage of therapy success as a function of CL. Abbreviations – ATP: antitachycardia pacing; CL: cycle length; EGM: electrogram.

### 5.4.3 Far Field Excitation Threshold

Prior to arrhythmia induction, we applied single shocks to determine the atrial far field excitation threshold (n=7). Figure 5.4a,b show that shocks of opposite polarities resulted in identical atrial activation patterns. Of seven preparations, four demonstrated activation patterns originating from the RAA; however, in two preparations the earliest activation began from the LAA, and in one preparation activity originated from the lower RA. We observed no difference in the atrial far field excitation threshold when comparing opposite polarity shocks ( $0.097 \pm 0.06$  V/cm for both) (Figure 5.4c). Lower voltage shocks (i.e., 0.05 V/cm) resulted in physiological activation of the ventricles via the atrioventricular node and conduction system, whereas higher voltage shocks (i.e., 5 V/cm) resulted in simultaneous activation of both the atria and ventricles (Figure 5.4d,e). The ventricular far field excitation threshold was  $0.43 \pm 0.13$  V/cm.

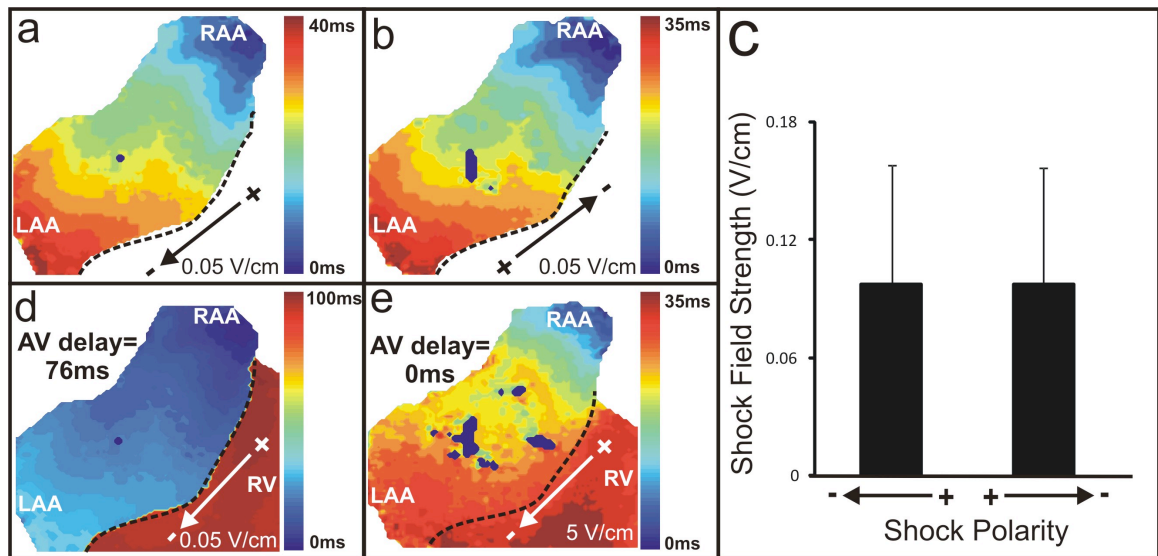


**Figure 5.4:** Far field excitation. (a,b) Activation maps resulting from opposite polarity shocks at a field strength of  $\pm 0.05$  V/cm. The dotted black line demarcates the AV groove. (c) Average shock field strength of both polarities ( $0.097 \pm 0.06$  V/cm). (d) Activation delay of the ventricles at a physiological AV delay (76 ms) caused by far field excitation of the atria with a shock field strength of 0.05 V/cm. (e) Simultaneous activation of the atria and ventricles with a higher-voltage shock.

In the preparation illustrated in both Figure 5.2 and 5.4, the location of earliest activation (RAA; Figure 5.4a,b) corresponded with the location of the dominant rotor maintaining AF (RAA, Figure 5.2d). This, however, was not representative of all experiments. The dominant rotor corresponded to the site of earliest activation via far field shocks in only 50% of the preparations in which both the threshold was measured and AF was induced.

#### **5.4.4 Termination of Atrial Flutter by Low-Voltage Multiple-Shock Therapy**

The efficacy of low-voltage multiple shock therapy was tested during AFl and AF, and then compared with both ATP and the application of single, phase-independent shocks. In the case of AFl, we applied a total of 405 trials of low-voltage multiple-shock therapy: 302 trials were delivered within 1 CL of the arrhythmia and 103 trials were delivered within 2 CLs. Figure 5.5a shows that the defibrillation threshold was significantly decreased during trials in which we applied multiple shocks within 1 CL ( $0.86 \pm 0.73$  V/cm) and 2 CLs ( $0.28 \pm 0.13$  V/cm), as compared to single shocks ( $2.12 \pm 1.31$  V/cm). Despite the significantly decreased defibrillation threshold for multiple shocks delivered over 2 CLs, this therapy resulted in an increased rate of conversion of AFl to sustained AF when compared with multiple shocks delivered over 1 CL (16.5% versus 14.2%,  $p=0.3$ ). Single shocks resulted in AF in 6.4% of therapy applications. Additionally, 54.3% of terminations in the case of multiple shocks delivered over 2 CLs were preceded by a short run of AF. Overall, immediate termination of AFl occurred in 63% of cases, whereas 37% of terminations were preceded by a  $1.46 \pm 0.8$  second run of AF. For multiple shocks delivered within 1 CL, 4 shocks resulted in the lowest overall

defibrillation threshold ( $0.41 \pm 0.22$  V/cm), as compared to 3 ( $0.53 \pm 0.41$  V/cm) and 5 ( $1.26 \pm 0.82$  V/cm) shocks (Figure 5.5b). Preparations in which the length of our experimental protocol allowed for the testing of all numbers of multiple shocks also followed these more global observations as shown in Figure 5.6. Defibrillation of AFI was successful by multiple shocks in 100% of the preparations in which the arrhythmia was induced.

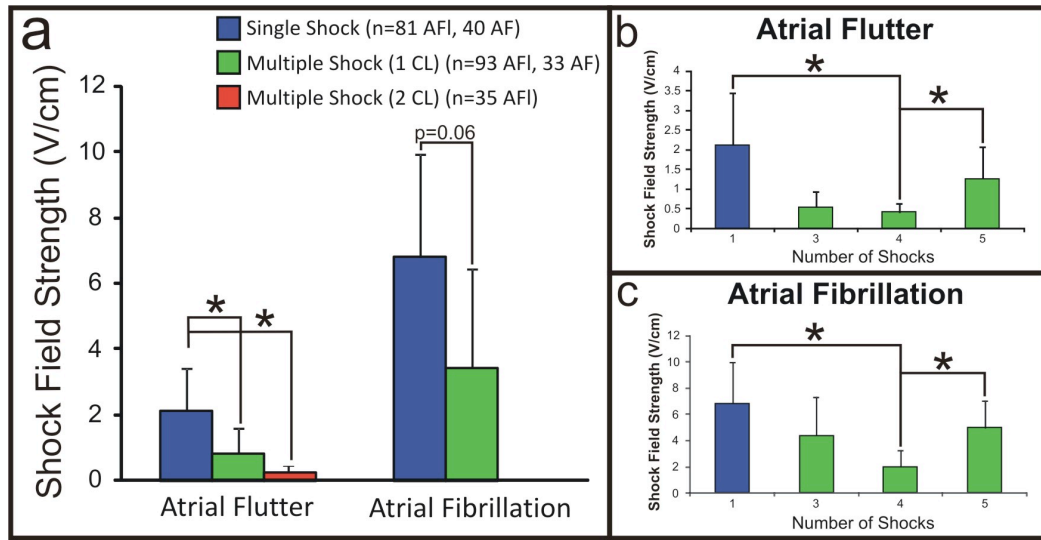


**Figure 5.5:** Defibrillation thresholds. (a) Defibrillation thresholds for single shocks, multiple shocks delivered within 1 CL, and multiple shocks delivered within 2 CLs. (b) Defibrillation thresholds for single shocks and multiple shocks (3 to 5) delivered within 1 arrhythmia CL for AFI and AF, respectively.

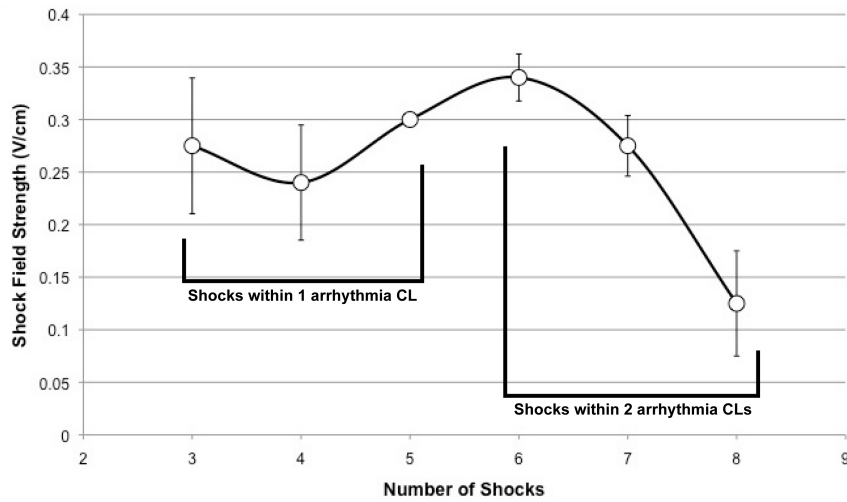


**Figure 5.6:** Shock field strength as a function of number of shocks.

### 5.4.5 Termination of Atrial Fibrillation by Low-Voltage Multiple-Shock Therapy

In the case of AF, we applied a total of 233 trials of low-voltage multiple-shock therapy delivered within 1 CL of the arrhythmia. Once again, defibrillation of AF by multiple shocks was successful in 100% of preparations and the defibrillation threshold was decreased ( $p=0.06$ ) during the trials in which we applied multiple shocks within 1 CL ( $3.46\pm 3$  V/cm), as compared to the application of single shocks ( $6.18\pm 3.12$  V/cm) as shown in Figure 5.5a. For multiple shocks delivered within 1 CL, 4 shocks again resulted in the lowest defibrillation threshold ( $1.97\pm 1.25$  V/cm), as compared to 3 ( $4.38\pm 2.92$  V/cm) and 5 ( $4.97\pm 2.08$  V/cm) shocks in this arrhythmia model (Figure 5.5c).

Figure 5.7 shows the average CLs of AF and AF, which were successfully defibrillated during the course of the study, as a function of defibrillation threshold. There is a trend that AF with longer CLs, require lower shock strengths for defibrillation, however the trend for defibrillation of AF is not as clear.

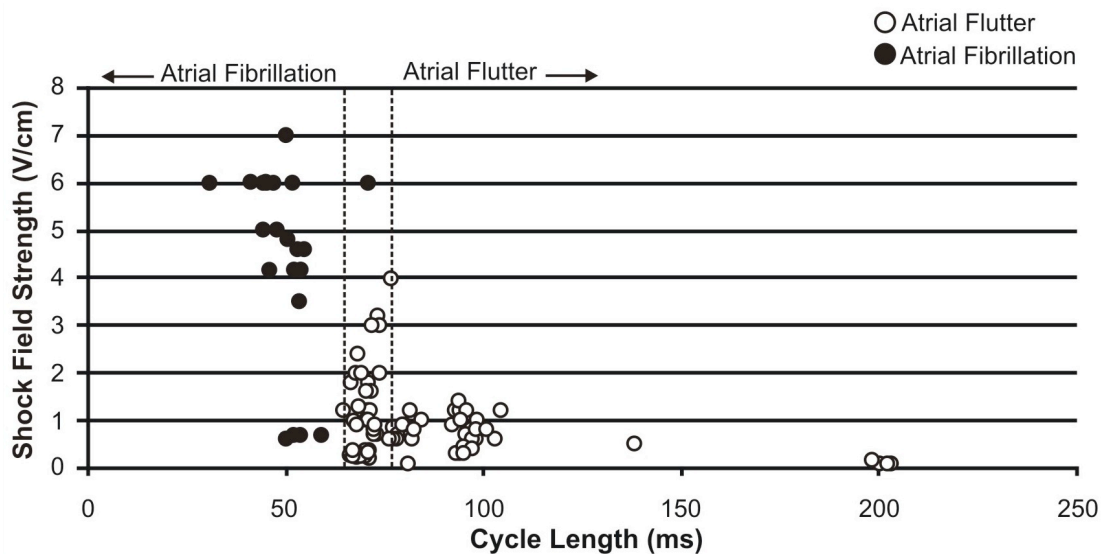


Figure 5.7: Defibrillation threshold as a function of arrhythmia cycle length.



#### 5.4.6 Mechanisms of Termination

Optical data obtained during the application of multiple shocks to AFl and AF revealed that the mechanism of termination relies on the recruitment of a sufficient number of secondary sources of excitation, resulting from virtual electrodes, to effectively terminate all reentrant circuits involved in the arrhythmia. Due to the fact that the maintenance of AFl and AF require different numbers of reentrant circuits, the energy needed to create a sufficient amount of secondary sources varies between the arrhythmias. In addition to the field strength of the shock, the timing of the shock is also important (Ripplinger, Krinsky et al. 2006).

The termination of AFl was achieved through unpinning of the arrhythmia wavefront by a properly timed shock arising from the location of earliest activation corresponding to the region of highest anatomical heterogeneity (Trayanova, Skouibine et al. 1998). In the example of successful termination shown in Figure 5.8a,b the train of multiple shocks was delivered approximately 7 ms earlier than the unsuccessful shock (Figure 5.8c,d) in relation to the rotating arrhythmia wavefront.

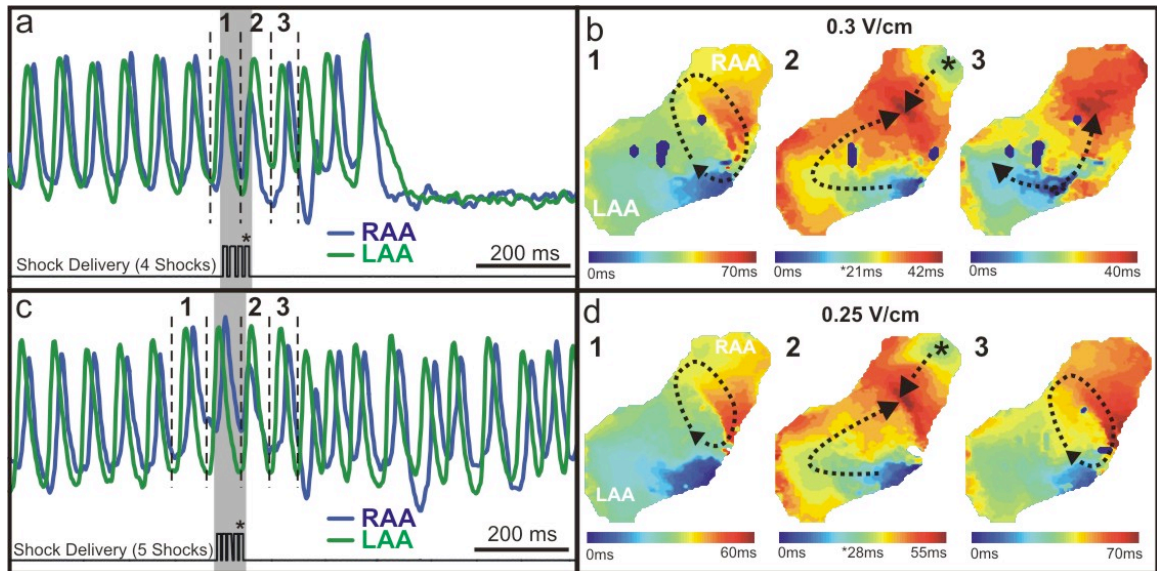


**Figure 5.8:** Application of multiple shocks to atrial flutter. (a) In this example of successful arrhythmia termination, four 10 ms shocks (0.3 V/cm) were applied during 1 CL of AF (70 ms). OAPs are shown from the RAA and LAA before and after termination. (b) Activation maps reconstructed from the  $dV/dt_{max}$  of the OAPs denoted by 1 to 3 in (a). (c) In this example of unsuccessful arrhythmia termination, five 10 ms shocks (0.25 V/cm) were applied during 1 CL of the same arrhythmia. (d) Activation maps reconstructed from the OAPs denoted 1 to 3 in (c). The asterisks (\*) in (b,d) represent the shocks indicated in (a,c).

The termination of AF was achieved by higher strength shocks able to excite and consequently to recruit enough secondary sources to disrupt the multiple rotors maintaining the arrhythmia. As shown in Figure 5.9, successful and unsuccessful terminations of AF relied on the amount of tissue depolarized by one or more shocks in the delivered therapy. In a dramatic example of successful termination of AF, as shown in Figure 5.9a, the first and fourth shocks (10 V/cm) in the series recruited atrial tissue in opposing areas as can be seen at 750 and 800 ms. In this preparation, a shock of <10 V/cm was not sufficient to defibrillate sustained AF. In the example of unsuccessful termination of AF, as shown in Figure 5.9b, from a different preparation, the shocks delivered at 2 V/cm were not strong enough to engage a sufficient amount of atrial tissue and create enough secondary sources for termination. Consequently, the arrhythmia

continued to persist after the shock (Gray, Ayers et al. 1997). Subsequent multiple shock therapy applications in this preparation terminated AF at 6 V/cm.

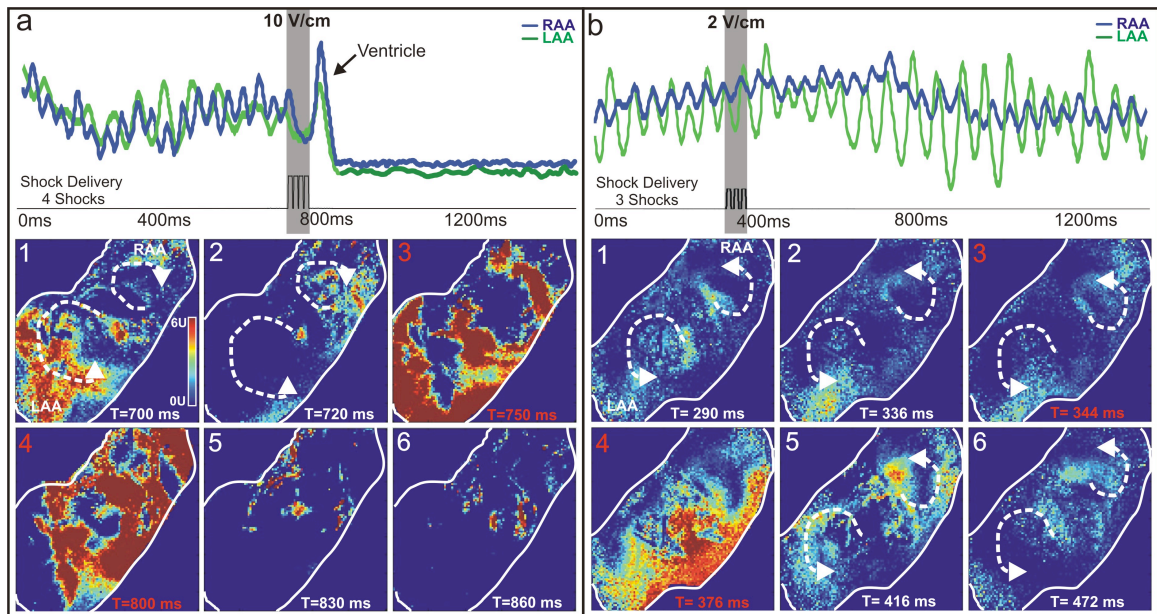


**Figure 5.9:** Application of multiple shocks to atrial fibrillation. (a) In this example of successful arrhythmia termination, four 10 ms shocks (10 V/cm) were applied during 1 arrhythmia CL of AF (55 ms). OAPs are shown from the RAA and LAA before and after termination by the shocks shown. Arrhythmia wavefronts, reconstructed from the  $dV/dt_{max}$ , before, during, and after shock application. (b) In this example of unsuccessful termination, three 10 ms shocks (2 V/cm) were applied during 1 CL of AF (50 ms). Arrhythmia wavefront frames indicated by red lettering represent those reconstructed during shock application.

### 5.4.7 Therapy Safety

During the application of a total of 638 rounds of low-voltage multiple-shock therapy in 17 preparations, no episodes of ventricular flutter or fibrillation were induced. In addition, there was no evidence of atrial electroporation as the majority of shocks were delivered below the atrial electroporation threshold (9.2-13.6 V/cm) (Fedorov, Kosteki et al. 2008).

## 5.5 Discussion

In the present study, a new method of low-voltage multiple-shock therapy was tested in a rabbit model of atrial tachyarrhythmias. We found a significant reduction in the defibrillation thresholds for both AF1 and AF, as compared with single phase-independent shocks, and success rates of 100% as opposed to 66.7% and 0% with ATP for AF1 and AF, respectively. Furthermore, 4 shocks delivered within 1 CL showed the lowest defibrillation threshold for both arrhythmias.

### 5.5.1 Antitachycardia Pacing

The low success rate of ATP in our study, as compared with the 100% success rate of multiple-shock therapy, can be explained by the inability of local excitation to invade the excitable gap of reentry when the pacing electrode is not located close to the core of reentry. On the other hand, multiple-shock therapy, based on the virtual electrode polarization hypothesis (VEP) (Efimov and Ripplinger 2006), uses far field electrical stimuli to produce excitation in larger areas of tissue to destabilize and terminate reentrant tachyarrhythmias (Ripplinger, Krinsky et al. 2006). VEP predicts that, in response to an external electric field, opposite sides of functional and anatomical heterogeneities will experience either hyperpolarization or depolarization (Takagi, Pumar et al. 2004; Ripplinger, Krinsky et al. 2006). The depolarized region of the heterogeneity can then become a secondary source of excitation and collide with the existing reentry, resulting in termination.

### **5.5.2 Monophasic versus Biphasic Shocks**

All shocks delivered in this study were monophasic, chosen because of the results of our previous investigation of ventricular tachycardia in a rabbit model of infarction (Li, Ripplinger et al. 2009). In that study, it was reported that the use of monophasic shocks not only reinforced the VEP response of the tissue, but also terminated ventricular tachycardia with significantly lower energies than multiple biphasic shocks. More importantly, it was found that the second phase of biphasic shocks reversed the VEP effect of the first phase, preventing maintenance of the secondary source of excitation responsible for colliding with and terminating the arrhythmia wavefront.

### **5.5.3 Arrhythmia Organization and Defibrillation**

The spatiotemporal organization of AFI/AF is important to defibrillation studies. Several different animal models of the arrhythmias, based on human states of the disease, have been developed, reflecting differences in such characteristics as dominant frequency, organization, and electrical/structural remodeling (Li, Fareh et al. 1999; Verheule, Wilson et al. 2003; Sharifov, Fedorov et al. 2004; Katsouras, Sakabe et al. 2009). Additionally, Everett, et al (Everett, Wilson et al. 2007) recently showed that higher defibrillation thresholds are directly related to arrhythmia models with higher dominant AF frequencies, such as the cholinergically-induced experimental model used in this study (Mandapati, Skanes et al. 2000).

In our study, with more anatomically defined AFl and more functionally defined AF, we reported increased defibrillation thresholds for AF as opposed to AFl. The mechanisms of defibrillation, as revealed by our optical mapping studies, show that the defibrillation of AFl/AF relies on the ability of the therapy to infiltrate the excitable gap of reentry. In the case of AFl, the long excitable gap associated with a single macro-reentrant circuit was easily penetrated by a properly timed shock originating from the region of highest heterogeneity (Figure 5.8). AF, on the other hand, shows multiple smaller reentrant circuits with higher dominant frequencies, and consequently, smaller excitable gaps. Multiple-shock therapy, in this case, required larger voltage shocks to excite a sufficient amount of tissue to disrupt the multiple motors maintaining that reentry (Figure 5.9).

#### **5.5.4 Patient Pain Perception**

Studies investigating patient pain perception have shown that internal shocks  $>0.1$  J are generally perceived as uncomfortable, although there is a wide variation in perception, perhaps because of varying autonomic tone, the presence of drugs, and the location of the shock electrodes (Ladwig, Marten-Mittag et al. 2003; Mitchell, Spurrell et al. 2004). Additionally, the majority of patients are unable to distinguish the difference among shocks delivered higher than this threshold (Mitchell, Spurrell et al. 2004). During clinical studies in which several intracardiac shocks were delivered about 5 minutes apart, patients perceived later shocks in the series to be more painful than the initial one regardless of the energy delivered (Steinhaus, Cardinal et al. 2002). Clinical testing should be performed to determine how a train of multiple shocks delivered in quick

succession will be perceived, as the overall energy delivered may exceed that of a single shock.

### 5.5.5 Safety

In our study of the intact heart, we induced no episodes of ventricular tachyarrhythmias. As AFI/AF ranged from 50 to 200 ms in our experimental rabbit arrhythmia model, we have the ability to deliver low-voltage multiple-shock therapy safely and effectively within the ventricular refractory period without causing additional arrhythmias (Cheng, Li et al. 2004). Human AFI/AF has been reported to range from 120 to 200 ms (Haissaguerre, Sanders et al. 2004; Kim, Olgin et al. 2009), while the ventricular refractory period is  $\geq 200$  ms (Kong, Goldberger et al. 1995). Moreover, the AFI defibrillation threshold with multiple shocks delivered within 2 CLs was only  $0.28 \pm 0.13$  V/cm and thus about 1.5 times less than the ventricular excitation threshold ( $0.43 \pm 0.13$  V/cm). Consequently, additional *in vivo* experiments should be performed to evaluate this therapy in humans because low-strength atrial defibrillation shocks have been shown to excite the ventricles (Gray and Jalife 1998), and depending on the arrhythmia, may fall within the ventricular refractory period.

A recent study by Fenton, et al proposed and tested a therapy termed “far field antifibrillation pacing” in a canine model of atrial tachyarrhythmia (Fenton, Luther et al. 2009). The therapy, 5 shocks, was applied to coincide with the CL of the arrhythmia in an attempt to synchronize tissue activation and create enough secondary sources of excitation for termination of the arrhythmia. The investigators reported a success rate of

93% amongst 74 therapy trials in 8 coronary-perfused RA/RV preparations at field strengths of 0.9-1.4 V/cm. Since far field shocks were applied at the CL of the arrhythmia, shocks could coincide with the T-wave to induce ventricular arrhythmias in the whole heart (Gray and Jalife 1998), although none were reported in this study. In our study in the intact heart, we also observed no episodes of ventricular tachyarrhythmias. Furthermore, our ability to deliver low-voltage multiple-shock therapy during the ventricular refractory period ensures that we can safely and effectively terminate AFI/AF without causing additional arrhythmias, or the R-on-T phenomenon.

It should also be mentioned that in the Fenton, et al study atrial tachycardia, AFI, and AF were not separated into distinct defibrillation trials making comparison between our studies difficult. In addition, our recent canine atrial defibrillation study performed on the analogous AF canine model in the Fenton, et al study, demonstrated that the single shock defibrillation threshold was significantly lower for AFI versus AF ( $0.19 \pm 0.05$  versus  $7.26 \pm 3.94$  V/cm,  $p < 0.05$ ) (Foyil, Fedorov et al. 2008). Consequently, as we have shown in this study, AFI and AF have distinct spatiotemporal characteristics resulting in varying defibrillation strengths and mechanisms.

## 5.6 Conclusion

Our findings indicate that low-voltage multiple-shock therapy has the potential to serve as a useful treatment for atrial tachyarrhythmias such as AFI and AF. In this study, we have shown that multiple shocks delivered over 1 or 2 CLs significantly reduced the



defibrillation threshold of AF1 and AF, although multiple shocks delivered over 2 CLs resulted in an increased conversion of AF1 to AF. We achieved defibrillation success in all preparations and induced no ventricular arrhythmias. Based on this study, we conclude that low-voltage multiple-shock therapy terminates AF1 with higher efficacy than AF due to the unique spatiotemporal characteristics of the arrhythmias.

## 6 Concluding Remarks and Future Directions

The work presented in this dissertation sought to further understand the molecular and structural substrates of atrial fibrillation and flutter through the use of high-throughput molecular biology techniques (Chapter 2) and the application of optical coherence tomography (Chapters 3 and 4). In Chapter 5, the low-voltage termination of these atrial tachyarrhythmias was addressed based on knowledge of their unique spatiotemporal characteristics.

Since our recent investigations of ATP-sensitive potassium ( $K_{ATP}$ ) channels (as described in Chapter 2, Section 2.4.3.1) revealed profound differences between molecular-level expression and their functional consequences in mouse and human hearts (Glukhov, Flagg et al. 2010; Fedorov, Glukhov et al. 2011), the use of clinically-relevant models of arrhythmia and disease pathology has become increasingly crucial. Consequently, in this investigation we use a variety of animal models with proven clinical relevance. The rabbit model, used for the low-voltage defibrillation studies presented in Chapter 5, has

been repeatedly shown to sustain clinically-relevant arrhythmias, which are typically not observed in other smaller animal species (Panfilov 2006). The canine atrial pacemaker complex, as described in the study presented in Chapter 4, has been shown to functionally behave similar to the human heart (Fedorov, Schuessler et al. 2009; Fedorov, Glukhov et al. 2010) and furthermore is similar in size to the human heart. Finally, we have been afforded the unique opportunity to work with human tissues, as presented in Chapters 2 and 3, although careful consideration must be taken to account for disease pathology and other underlying factors that may confound experimental results.

In Chapter 2, we analyzed relative expression levels of transcripts encoding for various ion channels, calcium handling proteins, and other transporters important in both normal and abnormal cardiac conduction as a function of both gender and disease pathology. While we probed tissues of both the left atrium and ventricle, significant patterns of gender dependent expression only appeared with respect to the atrium. The pathophysiology of atrial fibrillation and congestive heart failure is, however, a complex interplay of long- and short-term molecular mechanisms that have only begun to be unraveled. Continued access to and analysis of human cardiac tissues, such as those studied in this investigation will only serve to increase our understanding of these complex mechanisms. Furthermore, as we have shown, the clinical classification of human tissues is critical in interpretation of results and factors, such as gender, disease, and arrhythmia history must be accounted for.

In this particular study, we analyzed the gene expression patterns in cardiac tissues with multiple distinct populations of cell types, including myocytes, fibroblasts, smooth muscle cells, and neuronal cells. It is highly likely that these various cell types undergo differential remodeling processes and consequently express differential gene expression patterns as a function of gender, disease state, and arrhythmia history. A recent study by Gronich, et al employed laser-capture microdissection in human cardiac tissue preparations to isolate the gene expression patterns of myocytes only (Gronich, Kumar et al. 2010). Their study also focused on identifying alternative RNA splicing events, which could potentially play a key role with respect to gender and arrhythmia susceptibility and thus should be considered in future studies in this direction.

An additional avenue of exploration in molecular cardiac excitability and arrhythmogenesis is the characterization of microRNAs. MicroRNAs, composed of on average 22 nucleic acids, are post-transcriptional regulators that bind directly to mRNA resulting in translational repression and gene silencing. Expression profiles of microRNAs have revealed significant differences in diseased and arrhythmic substrates pointing to their probable role in the pathogenesis of atrial fibrillation and heart failure (Wang 2010; Wang, Lu et al. 2011). However, their role in the gender dependence of arrhythmia susceptibility and heart failure has yet to be elucidated.

Finally, the availability of data sets, such as those produced in Chapter 2, incorporating a variety of tissues across age, gender, disease, and arrhythmia history, provides a wealth of information for computer modeling studies. The development of physiologically-

relevant models (Grandi, Pasqualini et al. 2010; O'Hara, Virag et al. 2011) relies upon the incorporation of clinically-relevant information. In addition, computer models can potentially be used to predict electrophysiological behavior and provide the basis for simulations of drug therapy, for instance, in a wide variety of patient/disease types.

In Chapters 3 and 4, we applied optical coherence tomography, a non-destructive, high-resolution imaging modality, to a series of explanted human and canine hearts. In both studies, we demonstrated the utility of OCT in imaging the cardiac conduction system and other structures crucial to cardiac conduction and arrhythmogenesis. In the canine hearts, we specifically visualized and quantified cardiac fibers in the atrial pacemaker complex, which we have previously shown to be important in the maintenance and generation of atrial flutter and fibrillation (Fedorov, Chang et al. 2010). We identified fiber orientation patterns unique to the crista terminalis, atrial myocardium, sinoatrial node, and block zone. Furthermore, the fiber angle distributions of the crista terminalis, atrial myocardium, and sinoatrial node were able to be distinguished quantitatively.

As we have shown in this dissertation, OCT has many potential applications in cardiology, particularly with respect to arrhythmia diagnostics and ablation guidance. In addition, the development of catheter-based OCT probes has subsequently opened the door for uses beyond the realm of cardiac research. A recent study by Fleming, et al demonstrated the utility of an OCT probe in monitoring the progress of radiofrequency ablation (Fleming, Wang et al. 2010). Based on the studies presented in this dissertation, OCT can also be utilized, for example, to identify and/or monitor atrial fibroses and other

tissue heterogeneities that may play a role in the maintenance of reentrant atrial arrhythmias. In addition, it may also be used for precise structural identification of the elements of the conduction system during electrophysiology studies and ablation procedures. However, before OCT can be applied to clinical practice, several technical limitations must be addressed such as its limiting depth penetration (Bouma, Tearney et al. 1995) and imaging in blood-perfused tissues (Brezinski, Saunders et al. 2001; Xu, Yu et al. 2008).

Finally, Chapter 5 presented a study in which we applied a method for low-voltage defibrillation therapy in a rabbit model of atrial tachyarrhythmias. We demonstrated a significant reduction in defibrillation thresholds when applying multiple shocks within one and two arrhythmia cycle lengths to both atrial flutter and fibrillation. We also used optical mapping to visualize the mechanisms of termination for both arrhythmias. In this study, shocks were applied via far field shock meshes thus creating a uniform field strength across the heart. In reality, clinical shock vectors may not encompass the entire heart and, subsequently, the mechanisms of defibrillation may be altered. Consequently, it is critically important to test these defibrillation sequences in a large animal with clinically-positioned shock coils.

One of the main goals of low-voltage defibrillation therapies is to reduce the overall defibrillation energy, as the energy required for successful endocardial cardioversion still exceeds the pain threshold (Mitchell, Spurrell et al. 2004). Although studies have been completed exploring patient pain perception of multiple shocks, the shocks applied in

these studies were delivered on the order of minutes apart (Steinhaus, Cardinal et al. 2002). It remains to be seen how a train of multiple shocks delivered in quick succession, as delivered in this study, will be perceived.

In summary, it is obvious from this dissertation and multitudes of other studies that atrial fibrillation is an extremely complex arrhythmia resulting from the interplay of a multitude of molecular, structural, and electrophysiological parameters. Consequently, the development of efficacious treatment options is also complex and to date, no one therapy has been 100% successful in abolishing atrial fibrillation with minimal patient discomfort. Only truly integrative approaches, such as those presented in this dissertation, combining efforts in molecular biology and both structural and functional imaging modalities, will continue to unravel the complexities of atrial fibrillation.

## **Appendix A Relative Quantification Data from Failing and Nonfailing Human Hearts of Both Genders**

This appendix contains the raw data, expressed as mean  $\pm$  standard deviation, of the relative quantification (RQ values,  $2^{-\Delta\Delta C_t}$ ) for all targets analyzed in this study. An electronic version of this data will be made available upon publication. Abbreviations are as follows – I F LA: ischemic female left atrium; I F LV: ischemic female left ventricle; I M LA: ischemic male left atrium; NF F LA: nonfailing female left atrium; NF F LV: nonfailing female left ventricle; NF M LA: nonfailing male left atrium; NF M LV: nonfailing male left ventricle; NF F Endo: nonfailing female left ventricular endocardium; NF F Epi: nonfailing female left ventricular epicardium; NF M Endo: nonfailing male left ventricular endocardium; NF M Epi: nonfailing male left ventricular epicardium; NI F Endo: nonischemic female left ventricular endocardium; NI F Epi: nonischemic female left ventricular epicardium; NI M Endo: nonischemic male left ventricular endocardium; and NI M Epi: nonischemic male epicardium.



Gene Name	Common Name	IF LA	IF LV	I M LA	I M LV	NF F LA	NF F LV	NF M LA	NF M LV	NF F Endo	NF F Epi	NF M Endo	NF M Epi	NI F Endo	NI F Epi	NI M Endo	NI M Epi
ABCC8	SUR1	0.8340.33	1.4240.44	1.1410.07	1.3340.52	1.5240.76	1.3340.61	1.591.12	1.691.14	0.940.42	0.7740.34	1.5340.74	1.1940.36	1.4140.23	2.051.18	1.381.12	1.2940.75
ABCC9	SUR2	0.6140.07	0.9940.30	1.0740.23	1.0840.32	0.7140.23	1.0840.16	0.994.12	1.2140.35	0.940.17	1.0840.40	1.0640.46	0.8640.36	1.4140.23	0.8640.26	0.8840.27	0.9440.40
ACTN1	$\alpha$ -actinin	1.840.45	0.9340.54	2.6341.69	0.840.22	2.6741.97	0.9840.63	1.9140.65	1.7940.28	1.3840.37	1.0840.29	0.9240.42	0.9640.37	1.0140.32	2.0540.84	1.6841.15	1.7841.24
ADRA1B	$\alpha$ 1b Adrenergic Receptor	1.6541.08	1.7241.10	2.6441.98	1.640.65	1.9141.97	2.2842.66	1.2840.36	1.9240.88	1.8340.17	1.2240.89	1.4440.40	1.1240.67	1.9241.23	2.0540.84	1.6841.15	1.7841.24
ADRA1D	$\alpha$ 1d Adrenergic Receptor	0.3340.15	0.3440.34	0.6740.54	0.2340.15	0.3640.31	0.3340.15	0.3640.31	0.6140.32	0.6840.65	0.4140.30	0.9641.38	0.2440.41	0.0840.01	0.4240.22	0.0540.03	0.2540.31
ADRB1	$\beta$ 1 Adrenergic Receptor	0.4740.26	1.3941.82	0.9640.72	0.5640.29	0.7140.38	0.6140.32	0.9340.47	0.8540.21	0.6840.36	0.5940.09	0.6440.30	0.6340.50	0.4240.42	0.7340.26	0.4840.19	0.6540.59
ADRB2	$\beta$ 2 Adrenergic Receptor	0.9340.31	1.1940.97	1.3140.75	0.7040.21	0.8240.14	0.8330.33	0.9540.29	0.9440.27	1.3940.45	1.1030.34	0.6840.05	0.6040.09	0.6140.34	0.8040.22	0.8040.36	0.7440.41
ADRB3	$\beta$ 3 Adrenergic Receptor	No target amplified.															
ATP1A1	$\alpha$ 1 subunit of Na/K Pump	0.9640.22	0.9540.14	1.0440.75	0.7640.26	1.3040.94	1.4741.03	1.1540.17	1.2540.32	2.4741.49	2.9242.25	1.0840.45	0.8740.29	1.1540.19	1.2140.14	0.8640.31	0.8040.25
ATP1A2	$\alpha$ 2 subunit of Na/K Pump	0.5040.09	0.9140.42	0.7140.50	0.9240.30	0.7140.24	0.9240.64	1.1440.41	1.5240.56	1.6840.65	1.2140.49	1.3940.52	1.0340.39	1.1840.14	1.2740.21	0.9840.65	0.9540.36
ATP1A3	$\alpha$ 3 subunit of Na/K Pump	0.5340.14	1.5541.43	0.9740.46	0.9740.28	0.7340.33	1.0440.51	1.1640.49	1.4040.51	1.3940.41	1.0140.29	1.3040.48	1.0240.04	0.8640.20	0.8240.23	1.3840.68	1.1940.79
ATP1B1	$\beta$ 1 subunit of Na/K Pump	0.3740.11	0.6740.20	0.5440.14	0.7640.18	0.6940.18	1.1340.33	1.0140.24	1.3440.37	1.3240.55	1.6141.00	0.9840.14	0.8040.28	0.8540.02	0.7340.07	0.7540.12	0.7240.22
ATP1B2	$\beta$ 2 subunit of Na/K Pump	1.540.53	2.0641.65	2.4441.20	2.1741.39	0.8440.36	0.8540.25	0.9840.40	1.2240.38	1.7640.66	1.3140.24	1.4840.23	1.2540.27	2.4241.04	2.5840.49	1.5840.93	1.8540.54
ATP2A2	SERCA2a	0.7740.29	0.5240.08	1.3540.44	0.6340.25	1.1940.59	1.2140.61	1.9841.21	1.4740.66	1.1140.69	0.7940.24	0.8240.25	1.1340.53	0.3540.15	0.2840.12	0.6240.37	0.6540.18
ATP2B4	PMCA2	1.1640.28	1.0540.37	1.6640.85	1.3940.53	1.6241.12	1.4541.64	0.9740.13	1.4240.66	1.6740.71	1.6040.71	0.9240.44	0.8140.21	0.2040.50	2.2140.26	1.0840.41	1.3340.36
CACNA1C	Cav1.2	0.9240.14	1.0940.13	1.2940.51	1.2040.23	1.2540.74	1.4740.76	1.0846.10	1.2440.52	1.1641.06	1.2940.85	0.8640.72	1.4441.32	1.1940.60	1.3740.06	1.8541.84	1.8242.22
CACNA1D	Cav1.3	3.5742.30	1.5241.65	5.5042.54	1.3040.70	9.1446.30	1.4740.76	1.0846.10	1.8140.99	1.8640.92	1.0840.99	1.2541.50	1.2040.90	1.2141.10	2.5340.92	1.1641.09	2.1440.96
CACNA1G	Cav3.1	11.15414.36	1.7242.14	1.1540.95	1.2540.85	27.55417.59	0.8641.20	24.57415.07	1.6140.57	1.7240.51	1.0840.57	1.4140.58	1.3940.15	1.4040.79	0.9640.22	1.2240.71	0.9440.03
CACNA1H	Cav3.2	0.8240.31	0.9540.50	1.1540.40	0.8440.32	1.3140.61	1.4740.87	1.0040.23	0.9140.22	1.0640.21	0.7540.44	0.7640.37	0.6940.31	0.7540.44	0.9040.26	0.7040.32	0.7740.38
CALM3	Calmodulin 3	0.4140.05	0.7540.44	0.9240.52	0.5940.19	0.7640.32	0.7640.37	0.7040.23	1.1740.20	1.2740.27	1.8440.50	1.1640.16	1.1940.15	1.7940.22	2.1240.59	1.4740.54	1.6140.51
CAMK2B	CAM Kinase II Beta	1.2940.19	1.4440.58	1.5540.72	1.1640.26	1.3440.75	0.9640.50	1.3040.28	1.2740.25	1.2540.24	0.9440.15	1.0840.36	0.9940.15	1.4840.28	1.7440.74	1.3240.42	1.4240.06
CASQ2	Calsequestrin 2	1.0440.32	1.1840.27	0.9140.34	1.4840.48	0.9740.54	1.2540.28	1.0740.21	1.2740.25	1.2540.24	0.9440.15	1.0840.36	0.9940.15	1.4840.28	2.0740.50	1.3740.09	1.7640.73
CANV3	Caveolin 3	0.9040.30	0.2840.25	0.8240.30	1.2540.39	1.0740.68	1.5340.71	1.1840.47	1.6440.63	1.6740.30	1.7140.50	1.5140.56	1.3240.16	1.4240.40	2.7040.60	1.2740.09	1.7640.73
CD4		1.2440.68	0.7340.47	2.2951.28	0.6540.20	1.5940.61	1.0540.22	1.1840.41	1.1240.52	0.9340.55	0.8940.42	0.4640.31	0.6840.22	0.4640.11	0.5640.22	0.7040.13	0.6240.44
CHAT	Choline Acetyltransferase	No target amplified.															
CHRM1	M1 Muscarinic Receptor	1.7040.76	1.1940.58	2.8941.23	1.4840.56	1.9040.92	1.1140.49	2.9441.07	1.7040.95	1.3640.75	1.2640.53	1.7540.58	1.3940.15	1.6841.08	2.1040.84	1.3440.71	1.4940.99
CHRM2	M2 Muscarinic Receptor	0.8641.03	0.5643.97	0.7840.90	3.0242.55	1.1241.55	2.7442.80	2.4342.47	2.9441.65	0.9440.60	2.5342.17	1.140.49	1.5442.22	2.8841.96	0.5640.78	1.3441.14	
CHRM3	M3 Muscarinic Receptor	3.1541.75	3.2844.34	9.1841.39	1.5941.17	1.8441.25	1.0741.08	0.5046.90	4.5840.81	3.6344.43	0.8940.69	0.6140.77	1.2341.04	1.3540.92	3.7741.49	3.9045.67	2.7842.96
CHRNA1	Cholinergic Receptor	0.8740.58	0.2440.16	0.8040.51	0.4340.20	1.4341.93	1.1141.42	0.9340.70	0.4640.17	1.1140.68	1.3541.05	0.6740.65	0.6640.54	1.1740.48	1.2840.56	0.2640.16	0.3640.08
GJA1	Connexin 43	1.1640.32	1.3840.64	1.2440.35	1.1440.60	0.9640.38	0.9840.24	1.1840.34	1.3040.31	1.0440.33	1.0440.68	1.0540.34	0.9540.21	0.6540.15	0.8940.16	0.8340.34	0.9540.45
GJA5	Connexin 45	2.8241.19	0.8240.41	6.0943.94	0.8840.18	5.4444.35	1.2140.40	5.7141.80	2.1642.28	4.1143.14	1.0340.31	2.7141.87	0.8040.44	1.6240.81	0.7940.26	2.3341.74	0.9740.36
GJC1	Connexin 45	1.5540.31	1.2440.54	2.0541.42	1.0340.35	2.0040.80	1.3640.84	1.9140.43	3.7545.82	2.1040.70	1.5647.50	1.5740.38	1.2040.36	1.4140.41	1.5640.16	1.3440.67	1.0740.37
HCN1	Hyperpolarization activated cyclic nucleotide-gated channel 1	109.674124.34	1.1740.05	154.92465.83	1.6041.48	219.11484.88	1.4340.62	1.2140.73	2.2141.85	2.3840.32	2.3740.55	5.0543.90	1.8740.44	2.2443.76	0.6540.48	4.3741.29	3.0741.86
HCN2	Hyperpolarization activated cyclic nucleotide-gated channel 2	1.1440.64	2.2541.85	1.7841.67	1.9940.66	1.1940.60	1.4840.62	1.2140.73	2.2141.85	2.3840.32	2.3740.55	1.7640.96	1.1841.05	1.9341.10	1.1840.44	2.2541.54	1.8941.82
HCN4	Hyperpolarization activated cyclic nucleotide-gated channel 4	0.7340.39	0.8041.01	0.7140.74	0.7440.47	0.7740.55	0.7840.41	1.0340.73	1.2540.80	1.4840.24	0.9540.32	1.3840.35	1.0640.83	1.2140.62	0.7840.47	0.7440.30	0.5040.28
IRX3	Inroquin 3	0.0940.06	0.9540.23	0.1240.07	1.1440.47	0.1640.14	1.1540.48	0.1840.13	1.6140.77	2.1742.07	0.8740.44	2.0741.35	0.3940.11	1.8940.63	0.5940.42	1.2640.35	0.6240.45
ITPR1	Inositol 1,4,5-Triphosphate Receptor 1	1.4040.48	1.0540.46	2.3041.15	1.3740.24	1.6340.67	0.8940.17	1.5440.19	1.1840.24	1.7340.43	1.1140.33	1.1840.73	0.9040.48	1.1040.53	0.8840.19	1.1540.61	1.0140.17
ITPR3	Inositol 1,4,5-Triphosphate Receptor 3	0.4140.12	0.6840.81	1.2340.99	0.5340.19	0.7640.39	0.7440.49	0.9140.40	0.8041.29	1.4240.75	1.3841.22	0.8749.65	0.7740.58	0.4940.24	0.5740.28	0.7840.60	0.6840.47
KCNK2	Kv1.2	0.9440.47	1.1440.38	2.3442.70	1.9540.87	1.1440.37	1.0240.54	2.9443.00	2.6041.48	0.8840.39	0.9440.65	1.2640.05	1.6640.45	1.5440.65	1.9840.41	1.1740.63	1.9841.29
KCNK4	Kv1.4	0.7840.36	1.7840.38	1.4440.84	2.2040.63	0.7540.57	1.2040.63	0.8240.58	1.5540.78	2.6040.56	1.4140.85	1.7440.35	0.8640.14	4.7542.28	4.4641.46	2.9742.46	1.8550.90
KCNK6	Kv1.5	16.4446.68	3.0342.08	25.05510.01	2.9540.91	21.05111.62	1.2540.21	36.3346.38	2.1041.51	2.1940.33	1.8640.91	1.4640.46	0.9740.27	2.6641.36	2.0940.65	1.9441.29	1.9741.71
KCNK6	Kv1.6	1.3540.60	1.5241.30	3.4141.69	1.5741.05	2.4741.42	0.8840.52	3.3541.77	1.8841.36	1.0740.45	0.8740.44	0.5040.26	0.740.27	0.9740.59	1.0640.13	1.2740.38	1.3040.44
KCNAB1	Kv $\beta$ 1	1.0840.43	1.2640.71	1.6640.67	1.3440.36	1.0640.54	0.9540.64	1.2640.62	1.1140.46	1.8540.85	1.7041.07	1.0240.23	1.4240.60	1.3640.59	1.6140.24	1.8240.69	1.5740.25
KCNAB2	Kv $\beta$ 2	0.3140.09	1.140.61	0.6040.33	1.3640.62	0.740.22	1.0240.36	0.7040.23	1.2740.39	1.0940.49	0.8740.69	0.6440.24	0.6040.29	0.7340.22	0.8740.68	0.6740.28	0.9640.75
KCNAB3	Kv $\beta$ 3	0.8340.6	0.7140.83	3.0743.18	1.3740.74	1.8641.29	1.1741.24	1.1840.57	0.8540.43	0.5740.16	0.5440.33	0.5440.46	0.6340.50	0.8140.70	0.8140.46	0.5240.33	0.5840.64
KCNB1	Kv2.1	2.3541.92	1.8941.20	5.5241.41	2.1741.25	2.6941.24	2.2940.68	2.6241.4	2.4241.34	2.5741.22	1.941.08	3.1940.92	3.0740.44	3.3741.18	4.9042.32	2.1141.12	2.1741.17
KCNB2	Kv2.2	0.7240.17	0.6940.42	1.3540.66	1.3040.68	0.9540.58	0.6440.60	1.0240.44	0.7340.16	0.7740.22	0.5440.21	0.5940.12	0.6240.36	1.6740.58	1.5140.21	0.8040.28	0.9340.17
KCNB4	Kv3.4	1.3140.08	0.7340.76	2.8743.15	0.2940.16	1.0040.52	0.4140.51	0.9340.66	0.5440.61	0.1440.14	0.2140.20	0.1140.1	0.1740.22	0.3440.38	0.8740.33	0.2740.23	0.4840.41
KCNB5	Kv4.3	0.7740.09	0.9740.57	1.4140.92	0.7640.22	1.1440.42	1.0440.18	1.5440.62	1.2440.41	0.8440.77	1.2140.53	1.5640.12	1.3540.29	0.7940.53	0.8940.24	1.1540.77	0.9540.16
KCNE1	minK	0.7540.29	2.1140.45	1.3741.32	1.0840.46	0.8140.36	0.8340.41	0.8340.62	1.0240.42	1.0840.70	0.9640.43	0.8240.21	0.7940.09	0.9840.35	1.4040.31	0.940.47	1.1940.93
KCNE2																	

Gene Name	Common Name	IF LA	IF LV	I M LA	I M LV	NF LA	NF LV	NF M LA	NF M LV	NF F Endo	NF F Endo	NF EPI	NF M Endo	NF M EPI	NF F Endo	NIF EPI	NI M Endo	NI M EPI
KCNJ8	Ki6.1	0.140.02	0.366.0.17	0.444.0.32	0.580.0.34	0.380.0.30	1.100.0.92	0.420.0.22	0.650.0.37	0.820.0.55	0.720.0.45	0.830.0.37	0.870.0.11	0.760.0.43	0.520.0.16	0.560.0.31	0.710.0.67	0.710.0.67
KCNK1	TWIK1	2.350.0.44	0.640.0.28	3.250.0.88	0.580.0.13	4.310.1.45	0.740.0.14	0.050.1.13	0.740.0.44	1.330.0.74	1.380.1.26	1.300.0.43	0.880.0.44	1.020.0.35	1.190.0.57	1.190.0.57	1.320.0.40	1.320.0.40
KCNK2	TREK1	0.440.0.47	0.490.0.62	1.010.1.04	1.190.1.32	0.550.0.44	1.320.0.99	3.050.5.2	2.860.2.23	1.250.0.93	3.940.5.47	0.360.0.33	0.870.0.20	0.620.0.33	1.510.2.14	2.470.1.43	2.320.1.40	2.320.1.40
KCNK3	TASK1	8.140.2.30	0.340.0.13	14.340.6.66	0.280.0.17	26.440.25.85	1.180.0.84	23.800.3.79	0.890.0.24	2.280.2.25	1.650.1.69	0.510.0.27	0.750.0.19	0.190.0.13	0.540.0.28	0.210.0.02	0.840.0.39	0.840.0.39
KCNK6	TWIK2	0.510.0.3	1.060.0.49	0.630.0.66	0.990.0.53	0.780.0.68	0.960.0.79	0.470.0.18	0.630.0.37	0.460.0.17	0.460.0.10	0.630.0.05	0.740.0.15	0.520.0.20	1.170.0.51	0.820.0.54	1.110.0.85	1.110.0.85
KCNQ1	Kv7.1/KvLQT1	1.140.0.40	1.180.0.69	1.560.0.76	0.910.0.19	1.460.0.47	1.220.0.54	1.470.0.28	1.170.0.27	1.770.0.29	1.270.0.12	1.320.0.59	1.180.0.21	1.230.0.39	1.510.0.56	1.140.0.52	1.360.0.29	1.360.0.29
NPPA	ANP	808.940.187.32	26.740.22.15	1130.060.1134.56	49.130.668.11	847.240.487.84	5.140.2.96	669.365.14	1.930.2.33	11.910.5.59	7.370.6.99	7.010.6.29	1.460.1.33	74.490.67.59	1.210.1.03	72.780.65.98	11.610.8.47	11.610.8.47
PANX1	Pannexin 1	1.240.2.27	1.040.0.33	1.060.0.35	1.280.0.40	1.180.0.74	1.780.1.56	1.020.0.33	1.360.0.33	1.700.1.05	1.670.1.12	1.020.0.22	0.770.0.12	1.640.1.16	1.440.0.34	0.990.0.33	1.070.0.37	1.070.0.37
PANX2	Pannexin 2	2.340.1.54	2.910.3.57	5.070.4.37	0.830.0.88	4.630.2.46	0.620.0.77	6.510.5.48	1.030.0.61	1.000.0.92	0.200.0.14	0.740.0.43	1.390.0.73	1.440.1.46	1.300.1.44	1.590.0.33	0.570.0.93	0.570.0.93
PIAS3	KChAP	0.680.0.13	1.070.0.59	1.350.0.72	1.030.0.25	1.060.0.40	1.100.0.51	1.050.0.19	1.110.0.30	1.460.0.39	1.080.0.49	0.850.0.14	0.790.0.27	1.450.0.35	1.100.0.38	0.980.0.42	0.980.0.42	0.980.0.42
PLA2G4C	Phospholipase A2	0.880.0.20	0.920.0.28	0.860.0.43	1.070.0.50	0.760.0.52	0.750.0.46	0.840.0.21	0.960.0.22	0.720.0.25	0.690.0.31	0.930.0.41	1.040.0.24	1.390.0.58	1.830.0.43	1.160.0.71	1.160.0.71	1.160.0.71
PLA2G6	Phospholipase A2	1.540.0.25	1.910.1.23	2.420.0.90	1.510.0.31	1.590.0.6	1.090.0.26	1.450.0.38	1.420.0.39	2.320.1.01	1.480.0.47	2.080.1.11	1.830.0.41	2.330.0.98	2.090.0.45	2.480.0.89	1.900.0.61	1.900.0.61
PLN	Protein Phosphatase 3	0.760.0.18	0.920.0.26	0.940.0.25	1.490.0.32	0.670.0.23	1.010.0.13	0.890.0.13	1.230.0.15	1.310.0.52	1.620.0.92	1.080.0.24	0.970.0.31	1.170.0.37	1.180.0.14	0.880.0.1	1.050.0.04	1.050.0.04
PTK2B	PKC2	1.190.0.48	0.890.0.2	2.150.1.89	0.960.0.24	1.090.0.2	1.030.0.33	1.190.0.22	1.070.0.18	1.440.0.34	1.540.0.45	1.130.0.34	1.060.0.26	1.150.0.46	1.270.0.44	1.130.0.35	1.260.0.36	1.260.0.36
PTK2B	PKC2	0.920.0.69	0.460.0.26	1.830.1.43	0.410.0.09	1.550.1.12	0.660.0.31	1.710.1.14	0.630.0.22	0.760.0.11	0.620.0.1	0.490.0.4	0.510.0.15	0.430.0.18	0.470.0.24	0.670.0.46	0.670.0.46	0.670.0.46
RTR2	Ryanodine Receptor 2	0.950.0.17	1.180.0.23	0.730.0.19	1.330.0.46	0.840.0.22	0.970.0.35	0.910.0.39	1.290.0.26	1.260.0.45	1.270.0.68	1.020.0.39	0.960.0.31	1.060.0.19	1.390.0.31	1.190.0.51	1.240.0.25	1.240.0.25
RTR3	Ryanodine Receptor 3	3.060.2.38	1.460.1.61	4.770.4.73	1.410.0.83	1.370.0.79	3.130.3.69	1.220.0.50	3.940.3.42	2.270.1.19	2.240.2.0	3.170.1.67	2.340.1.66	1.980.2.34	0.430.0.38	3.240.2.14	1.230.1.33	1.230.1.33
SCN1A	Nav1.1	2.020.1.71	0.970.0.88	2.980.1.20	0.760.0.17	2.650.0.94	0.790.0.28	2.510.0.73	1.090.0.31	1.860.1.03	1.080.0.45	1.510.0.96	1.390.0.69	1.240.0.37	0.740.0.18	1.610.1.28	1.230.0.92	1.230.0.92
SCN2B	Nav2	0.420.0.09	1.260.0.53	0.60.0.33	1.040.0.35	0.330.0.19	0.60.0.36	0.540.0.35	0.790.0.39	0.970.0.44	0.890.0.69	0.920.0.66	0.680.0.25	1.340.1.16	1.690.0.37	1.290.0.61	1.430.0.85	1.430.0.85
SCN3B	Nav3	0.580.0.29	0.600.0.21	0.970.0.33	0.860.0.33	0.740.0.34	0.940.0.17	0.550.0.15	0.650.0.25	0.930.0.45	0.810.0.41	0.760.0.09	0.520.0.12	1.200.0.27	1.050.0.13	0.930.0.66	0.820.0.06	0.820.0.06
SCN5A	Nav1.5	0.660.0.17	1.030.0.76	0.970.0.64	0.980.0.35	0.880.0.4	0.960.0.35	1.060.0.22	1.370.0.34	1.860.0.4	1.240.0.36	1.430.0.67	0.830.0.26	1.260.0.13	1.170.0.24	1.350.0.55	1.320.0.62	1.320.0.62
SCN7A	Nav2.1	1.420.0.79	1.490.0.93	1.500.0.29	1.840.0.51	1.030.0.55	1.250.0.24	1.670.0.84	1.670.0.48	0.870.0.36	1.130.0.64	1.830.0.41	1.650.0.44	2.180.0.45	2.100.0.68	1.430.0.51	1.520.0.58	1.520.0.58
SCN8A	Nav1.7	0.660.0.36	0.470.0.27	1.690.1.59	0.610.0.31	1.120.0.77	0.660.0.38	1.140.0.42	1.190.0.25	1.370.0.09	1.580.0.04	1.140.0.39	1.070.0.09	1.780.0.39	1.060.0.11	0.650.0.5	0.480.0.37	0.480.0.37
SLC8A1	NCX1	0.740.0.03	1.040.0.09	1.040.0.35	1.230.0.30	0.760.0.24	1.020.0.5	0.960.0.1	0.920.1.09	2.050.2.10	0.210.0.16	1.710.1.83	0.270.0.28	1.010.42	0.910.0.41	1.960.0.8	2.310.0.36	2.310.0.36
SUN	Sarcoplasm	6.360.2.80	0.560.0.46	19.630.7.54	6.690.3.38	52.930.65.15	0.490.0.28	59.480.24.02	0.820.1.09	2.050.2.10	0.210.0.16	1.710.1.83	0.270.0.28	1.010.42	0.910.0.41	1.960.0.8	2.310.0.36	2.310.0.36
TBX2	T-box 2	0.450.0.13	1.090.1.32	1.060.0.59	0.890.0.34	0.820.0.4	1.040.0.73	0.940.0.32	1.080.0.32	1.370.0.56	1.110.0.11	1.050.0.21	0.890.0.19	0.610.0.21	0.670.0.05	1.060.0.69	1.260.1.02	1.260.1.02
TBX20	T-box 20	0.950.0.19	0.480.0.13	0.860.0.35	0.660.0.33	0.570.0.22	0.720.0.29	1.030.0.28	0.940.0.3	0.890.0.27	1.040.0.2	0.910.0.25	1.160.0.41	0.960.0.39	0.760.0.21	0.480.0.13	0.660.0.16	0.660.0.16
TBX3	T-box 3	0.310.0.12	0.360.0.25	0.770.0.46	0.820.0.42	0.650.0.28	0.760.0.39	0.950.0.39	1.220.0.35	1.160.0.01	1.250.0.89	0.940.0.42	0.650.0.15	0.990.0.12	0.250.0.03	0.540.0.22	0.170.0.34	0.170.0.34
TBX5	T-box 5	3.380.1.15	1.050.0.14	7.060.4.93	1.530.0.57	5.320.24	1.340.0.81	6.080.6.7	1.890.0.92	1.710.0.48	1.810.0.51	1.660.0.18	2.070.0.90	1.660.0.77	1.400.0.44	1.440.0.47	1.510.0.36	1.510.0.36
TH	Tyrosine Hydroxylase	0.450.0.24	0.890.0.74	0.530.0.56	0.690.1.03	0.610.0.27	0.540.0.77	0.460.0.58	0.330.0.35	0.820.1.21	0.680.0.55	0.250.0.39	0.220.0.17	0.220.0.15	0.950.0.53	0.120.0.15	0.320.0.21	0.320.0.21
VIM	Vimentin	2.270.1.15	1.310.0.86	3.660.3.57	0.890.0.22	2.250.0.43	1.230.0.49	1.710.0.43	0.920.0.14	1.650.0.25	1.210.0.26	1.120.0.57	0.960.0.06	1.120.0.37	0.940.0.12	1.730.0.90	1.550.0.19	1.550.0.19



## **Appendix B Master-8 Pacing and Acquisition Control Program**

The acquisition of data in Chapter 5 (Termination of Sustained Atrial Flutter and Fibrillation Using Low-Voltage Multiple-Shock Therapy) required the coordination of multiple experimental systems, including stimulation protocols, optical data acquisition, and shock delivery. Consequently, a pacing and acquisition control program was designed using LabVIEW 7.1 (National Instruments) and a Master-8 programmable stimulator (A.M.P.I., Jerusalem). In addition to delivering a variety of pacing protocols, the stimulator was also used to deliver appropriately-timed impulses to trigger both shock delivery and optical data acquisition as described in this Appendix.

### **B.1 Components of the Low-Voltage Defibrillation Setup**

For the analysis performed in Chapter 5, we needed to be able to initiate arrhythmias, delivery therapy (in the form of both antitachycardia pacing and multiple monophasic

shocks), and record electrograms and changes in membrane fluorescence. A Master-8 programmable stimulator (A.M.P.I., Jerusalem) was used for overall coordination and delivery of a variety of pacing protocols. A MiCAM ULTIMA-L CMOS camera system was used to record optical data and a dual Kepko-based defibrillator (Ripplinger, Lou et al. 2009) was used for shock delivery. An overall schematic of the system is shown in Figure B.1.

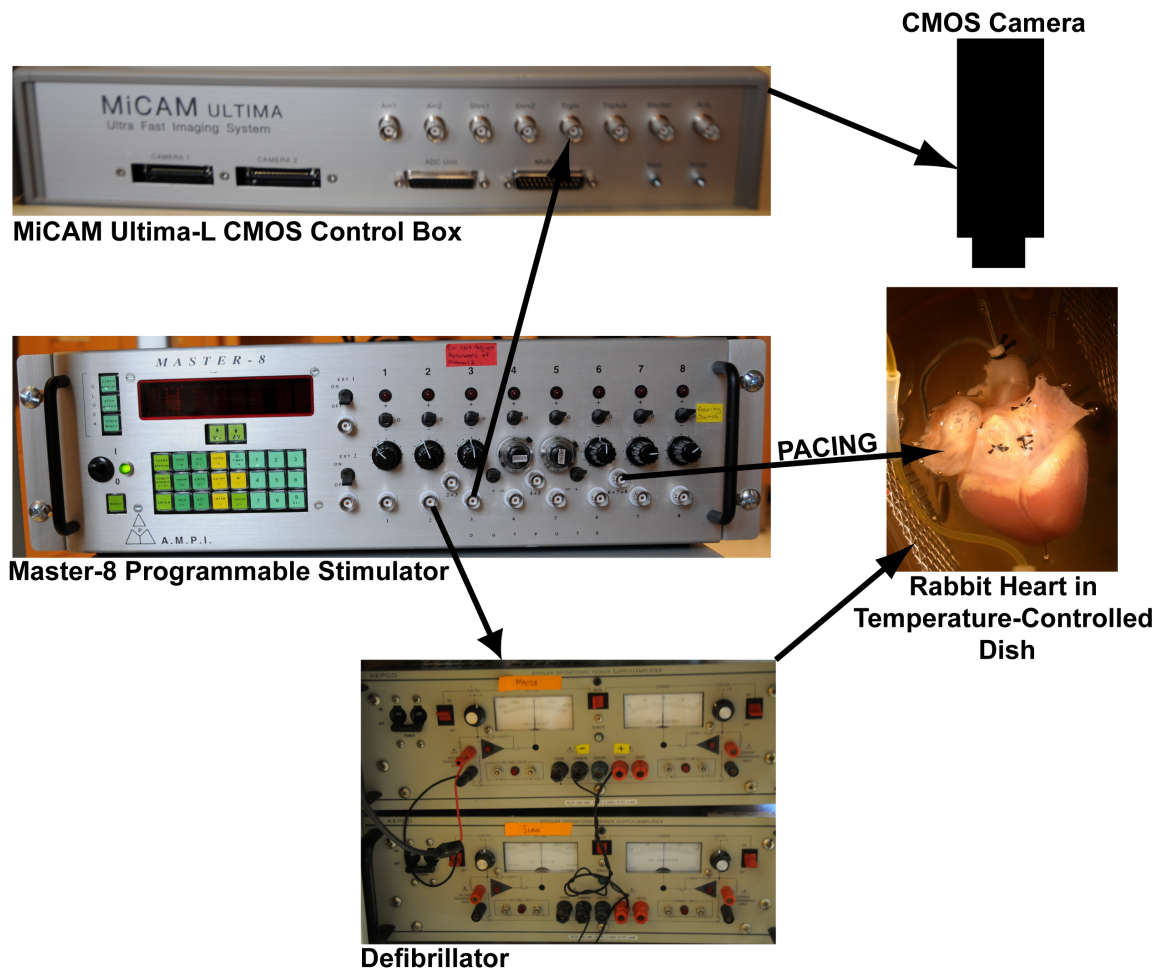


**Figure B.1:** Schematic of the overall experimental system for defibrillation study.

The Master-8 programmable stimulator has a total of 8 independent channels capable of delivering repetitive, single, and train outputs with variable pulse durations, delays, and intervals. Each channel delivers pulses ranging from -10 to +10 V with a maximum

current of 20 mA. For this configuration, we use a total of five Master-8 channels for pacing and trigger delivery. Channel 2 is used to trigger shock delivery. Channel 3 is used to trigger the acquisition of optical data through the MiCAM Ultima-L system. Channels 6 through 8 are used to deliver various pacing protocols, including continuous pacing, burst pacing, and single and dual prematurities.

## B.2 LabVIEW Software Configuration

### B.2.1 User Interface

The user interface for the pacing and acquisition control program is shown in Figure B.2.

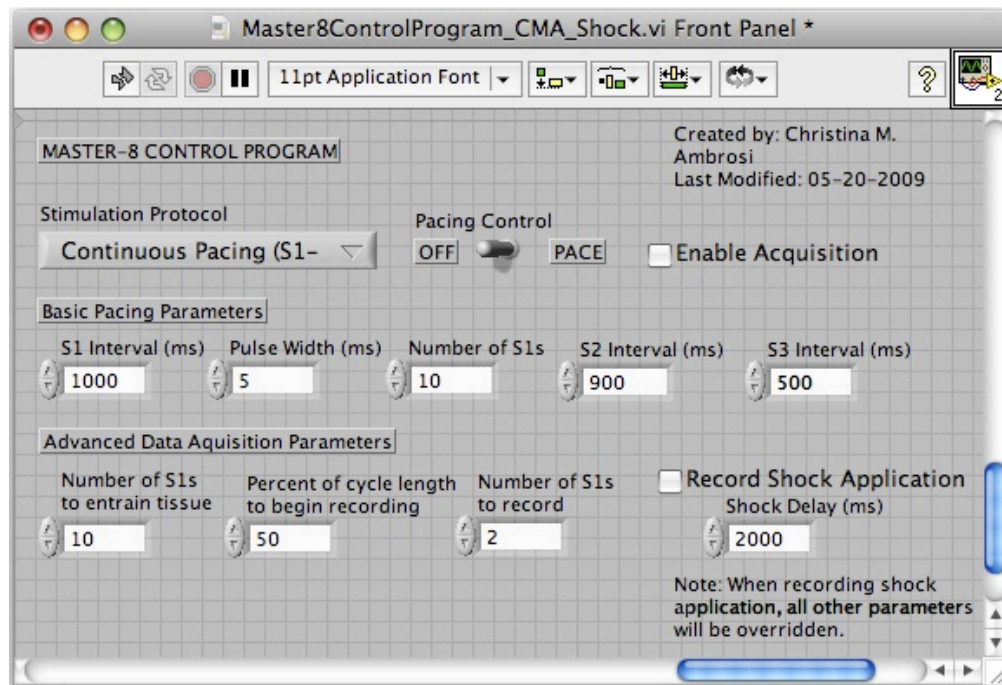


**Figure B.2:** User interface for LabVIEW program used to coordinate pacing protocols, shock delivery, and optical data acquisition.

As described previously, there are four pacing paradigms available to the user – Continuous Pacing (S1-S1), Burst Pacing, Single Prematurity (S1-S2) and Dual Prematurity (S1-S2-S3). Each pacing paradigm is available with and without the option to simultaneously record optical data by triggering the MiCAM Ultima-L system. When “Enable Acquisition” is checked, a low voltage TTL pulse (3.3 V) is delivered from channel 3 of the Master-8 to the MiCAM Ultima-L system according to the Advanced Data Acquisition Parameters located at the bottom of the LabVIEW interface. If no pacing paradigms are enabled, acquisition will occur without delay.

Once an arrhythmia is initiated and low-voltage multiple-shock therapy is ready to be delivered to the preparation through the stainless steel mesh electrodes located in the tissue bath, “Record Shock Application” should be checked on the LabVIEW user interface. When this option is enabled, all other parameters associated with pacing protocols will be overwritten and the system will start by triggering data acquisition. Then at a specified Shock Delay (in ms) a TTL pulse (5.0 V) will be sent to the defibrillator to signal therapy delivery. This ensures that appropriate optical recordings before, during, and after shock application are recorded.

### **B.2.2 LabVIEW Code**

The underlying LabVIEW code for the pacing and acquisition control program consists of a nested series of loops differentially activated based on the parameters specified and options enabled on the program user interface. Figure B.3 shows an example loop activated when Dual Prematurity (S1-S2-S3) is chosen as the pacing paradigm and

“Enable Acquisition” is activated. Figure B.4 shows another loop activated when “Record Shock Application” is enabled.

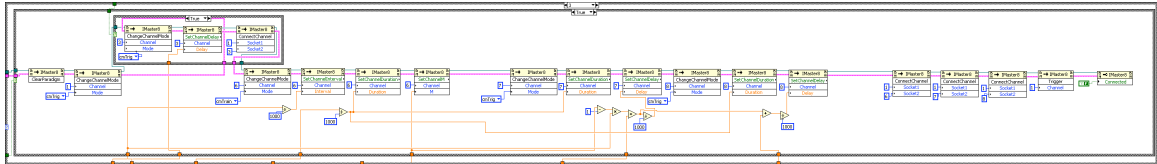


**Figure B.3:** LabVIEW block diagram for application of dual prematurity and optical data acquisition.

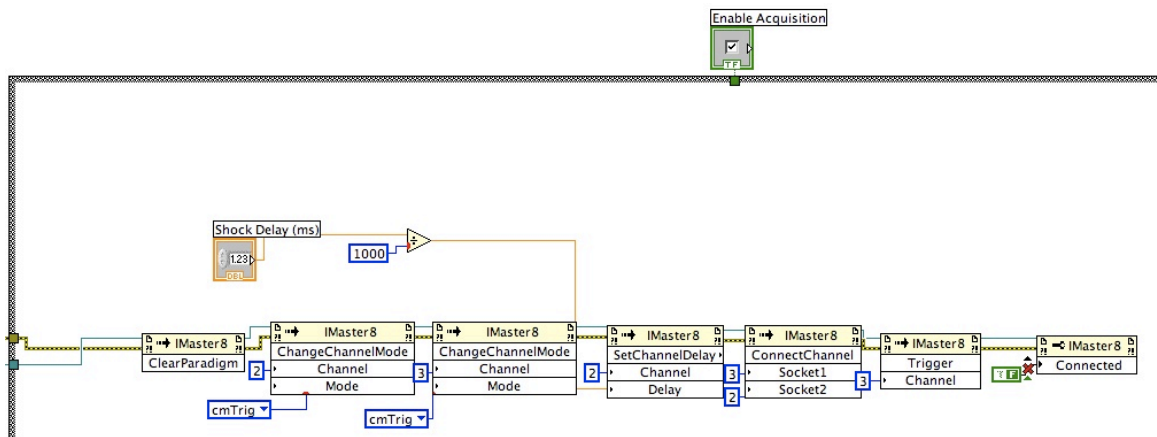


**Figure B.4:** LabVIEW block diagram for delivery of defibrillation therapy and optical data acquisition.

### B.3 Conclusion and Additional Applications

This Appendix describes the coordination of pacing protocols, optical data acquisition, and shock delivery using LabVIEW and a Master-8 programmable stimulator. This experimental system was designed specifically for the study described in Chapter 5 of this dissertation, however variations on this particular system can provide mainstreamed data collection during complicated optical mapping experiments.

As described previously, the Master-8 stimulator has a total of 8 channels that can be programmed for a variety of applications. For instance, it may be desirable to incorporate triggers into the system that will turn on light-emitting diodes necessary for optical data acquisition or to turn off perfusion/superfusion pumps so as not to record motion artifacts with optical data. In addition, a trigger can also be incorporated to activate a National Instruments data acquisition card if a larger number of electrograms are to be recorded in a particular experiment.



## References

- Abi-Gerges, N., K. Philp, C. Pollard, I. Wakefield, T. G. Hammond and J. P. Valentin (2004). "Sex differences in ventricular repolarization: from cardiac electrophysiology to Torsades de Pointes." Fundam Clin Pharmacol **18**(2): 139-51.
- Ahrens-Nicklas, R. C. and D. J. Christini (2009). "Anthropomorphizing the mouse cardiac action potential via a novel dynamic clamp method." Biophys J **97**(10): 2684-92.
- Aiba, T. and G. F. Tomaselli (2010). "Electrical remodeling in the failing heart." Curr Opin Cardiol **25**(1): 29-36.
- Akar, F. G., R. D. Nass, S. Hahn, E. Cingolani, M. Shah, G. G. Hesketh, D. DiSilvestre, R. S. Tunin, D. A. Kass and G. F. Tomaselli (2007). "Dynamic changes in conduction velocity and gap junction properties during development of pacing-induced heart failure." Am J Physiol Heart Circ Physiol **293**(2): H1223-30.
- Allessie, M., W. J. E. P. Lammers, F. I. M. Bonke and J. Hollen, Eds. (1985). Experimental evaluation of Moe's multiple wavelet hypothesis of atrial fibrillation. Cardiac Electrophysiology and Arrhythmias. Orlando, Grune & Stratton.
- Alt, E., R. Ammer, C. Schmitt, F. Evans, G. Lehmann, J. Pasquantonio and A. Schomig (1997). "A comparison of treatment of atrial fibrillation with low-energy intracardiac cardioversion and conventional external cardioversion." Eur Heart J **18**(11): 1796-804.
- Antzelevitch, C. (2007). "Heterogeneity and cardiac arrhythmias: an overview." Heart Rhythm **4**(7): 964-72.
- Antzelevitch, C. and J. Fish (2001). "Electrical heterogeneity within the ventricular wall." Basic Res Cardiol **96**(6): 517-27.
- Antzelevitch, C., W. Shimizu, G. X. Yan, S. Sicouri, J. Weissenburger, V. V. Nesterenko, A. Burashnikov, J. Di Diego, J. Saffitz and G. P. Thomas (1999). "The M cell: its contribution to the ECG and to normal and abnormal electrical function of the heart." J Cardiovasc Electrophysiol **10**(8): 1124-52.

- Ausma, J., M. Wijffels, F. Thone, L. Wouters, M. Allesie and M. Borgers (1997). "Structural changes of atrial myocardium due to sustained atrial fibrillation in the goat." Circulation **96**(9): 3157-63.
- Balana, B., D. Dobrev, E. Wettwer, T. Christ, M. Knaut and U. Ravens (2003). "Decreased ATP-sensitive K(+) current density during chronic human atrial fibrillation." J Mol Cell Cardiol **35**(12): 1399-405.
- Bartlett, J. M. and D. Stirling (2003). "A short history of the polymerase chain reaction." Methods Mol Biol **226**: 3-6.
- Benjamin, E. J., D. Levy, S. M. Vaziri, R. B. D'Agostino, A. J. Belanger and P. A. Wolf (1994). "Independent risk factors for atrial fibrillation in a population-based cohort. The Framingham Heart Study." JAMA **271**(11): 840-4.
- Biermann, M., M. Rubart, A. Moreno, J. Wu, A. Josiah-Durant and D. P. Zipes (1998). "Differential effects of cytochalasin D and 2,3 butanedione monoxime on isometric twitch force and transmembrane action potential in isolated ventricular muscle: implications for optical measurements of cardiac repolarization." J Cardiovasc Electrophysiol **9**(12): 1348-57.
- Bleeker, W. K., A. J. Mackaay, M. Masson-Pevet, L. N. Bouman and A. E. Becker (1980). "Functional and morphological organization of the rabbit sinus node." Circ Res **46**(1): 11-22.
- Boheler, K. R., M. Volkova, C. Morrell, R. Garg, Y. Zhu, K. Margulies, A. M. Seymour and E. G. Lakatta (2003). "Sex- and age-dependent human transcriptome variability: implications for chronic heart failure." Proc Natl Acad Sci U S A **100**(5): 2754-9.
- Boineau, J. P., T. E. Canavan, R. B. Schuessler, M. E. Cain, P. B. Corr and J. L. Cox (1988). "Demonstration of a widely distributed atrial pacemaker complex in the human heart." Circulation **77**(6): 1221-37.
- Borlak, J. and T. Thum (2003). "Hallmarks of ion channel gene expression in end-stage heart failure." FASEB J **17**(12): 1592-608.
- Bosch, R. F., X. Zeng, J. B. Grammer, K. Popovic, C. Mewis and V. Kuhlkamp (1999). "Ionic mechanisms of electrical remodeling in human atrial fibrillation." Cardiovasc Res **44**(1): 121-31.

- Bouma, B. E., G. J. Tearney, I. P. Bilinsky, B. Golubovic and J. G. Fujimoto (1996). "Self-phase-modulated Kerr-lens mode-locked Cr:forsterite laser source for optical coherence tomography." Opt Lett **21**(22): 1839-1841.
- Bouma, B. E., G. J. Tearney, S. A. Boppart, M. R. Hee, M. E. Brezinski and J. G. Fujimoto (1995). "High-resolution optical coherence tomographic imaging using a mode-locked Ti:Al<sub>2</sub>O<sub>3</sub> laser source." Opt Lett **20**(13): 1486-1488.
- Boyett, M. R., H. Honjo and I. Kodama (2000). "The sinoatrial node, a heterogeneous pacemaker structure." Cardiovasc Res **47**(4): 658-87.
- Boyett, M. R., S. Inada, S. Yoo, J. Li, J. Liu, J. Tellez, I. D. Greener, H. Honjo, R. Billeter, M. Lei, H. Zhang, I. R. Efimov and H. Dobrzynski (2006). "Connexins in the sinoatrial and atrioventricular nodes." Adv Cardiol **42**: 175-97.
- Boyle, N. G. and K. Shivkumar (2009). "Atrial fibrillation in congestive heart failure: current management." Cardiol Clin **27**(1): 79-93, viii-ix.
- Brandt, M. C., L. Priebe, T. Bohle, M. Sudkamp and D. J. Beuckelmann (2000). "The ultrarapid and the transient outward K(+) current in human atrial fibrillation. Their possible role in postoperative atrial fibrillation." J Mol Cell Cardiol **32**(10): 1885-96.
- Brezinski, M., K. Saunders, C. Jessor, X. Li and J. Fujimoto (2001). "Index matching to improve optical coherence tomography imaging through blood." Circulation **103**(15): 1999-2003.
- Brezinski, M. E. (2006). Optical Coherence Tomography: Principles and Applications. New York, Elsevier.
- Brezinski, M. E. (2007). "Applications of optical coherence tomography to cardiac and musculoskeletal diseases: bench to bedside?" J Biomed Opt **12**(5): 051705.
- Brezinski, M. E., G. J. Tearney, B. E. Bouma, J. A. Izatt, M. R. Hee, E. A. Swanson, J. F. Southern and J. G. Fujimoto (1996). "Optical coherence tomography for optical biopsy. Properties and demonstration of vascular pathology." Circulation **93**(6): 1206-13.

- Bromberg, B. I., D. E. Hand, R. B. Schuessler and J. P. Boineau (1995). "Primary negativity does not predict dominant pacemaker location: implications for sinoatrial conduction." Am J Physiol **269**(3 Pt 2): H877-87.
- Brundel, B. J., R. H. Henning, H. H. Kampinga, I. C. Van Gelder and H. J. Crijns (2002). "Molecular mechanisms of remodeling in human atrial fibrillation." Cardiovasc Res **54**(2): 315-24.
- Brundel, B. J., I. C. Van Gelder, R. H. Henning, R. G. Tieleman, A. E. Tuinenburg, M. Wietses, J. G. Grandjean, W. H. Van Gilst and H. J. Crijns (2001a). "Ion channel remodeling is related to intraoperative atrial effective refractory periods in patients with paroxysmal and persistent atrial fibrillation." Circulation **103**(5): 684-90.
- Brundel, B. J., I. C. Van Gelder, R. H. Henning, A. E. Tuinenburg, M. Wietses, J. G. Grandjean, A. A. Wilde, W. H. Van Gilst and H. J. Crijns (2001b). "Alterations in potassium channel gene expression in atria of patients with persistent and paroxysmal atrial fibrillation: differential regulation of protein and mRNA levels for K<sup>+</sup> channels." J Am Coll Cardiol **37**(3): 926-32.
- Bui, A. L., T. B. Horwich and G. C. Fonarow (2011). "Epidemiology and risk profile of heart failure." Nat Rev Cardiol **8**(1): 30-41.
- Burke, J. H., J. J. Goldberger, F. A. Ehlert, J. T. Kruse, M. A. Parker and A. H. Kadish (1996). "Gender differences in heart rate before and after autonomic blockade: evidence against an intrinsic gender effect." Am J Med **100**(5): 537-43.
- Bustin, S. A. (2000). "Absolute quantification of mRNA using real-time reverse transcription polymerase chain reaction assays." J Mol Endocrinol **25**(2): 169-93.
- Calkins, H., M. R. Reynolds, P. Spector, M. Sondhi, Y. Xu, A. Martin, C. J. Williams and I. Sledge (2009). "Treatment of atrial fibrillation with antiarrhythmic drugs or radiofrequency ablation: two systematic literature reviews and meta-analyses." Circ Arrhythm Electrophysiol **2**(4): 349-61.
- Cerbai, E., L. Sartiani, P. DePaoli, R. Pino, M. Maccherini, F. Bizzarri, F. DiCiolla, G. Davoli, G. Sani and A. Mugelli (2001). "The properties of the pacemaker current I(F) in human ventricular myocytes are modulated by cardiac disease." J Mol Cell Cardiol **33**(3): 441-8.

- Chan, K. W., A. Wheeler and L. Csanady (2008). "Sulfonylurea receptors type 1 and 2A randomly assemble to form heteromeric KATP channels of mixed subunit composition." J Gen Physiol **131**(1): 43-58.
- Chandler, N., O. Aslanidi, D. Buckley, S. Inada, S. Birchall, A. Atkinson, D. Kirk, O. Monfredi, P. Molenaar, R. Anderson, V. Sharma, D. Sigg, H. Zhang, M. Boyett and H. Dobrzynski (2011). "Computer three-dimensional anatomical reconstruction of the human sinus node and a novel paranodal area." Anat Rec (Hoboken) **294**(6): 970-9.
- Chandler, N. J., I. D. Greener, J. O. Tellez, S. Inada, H. Musa, P. Molenaar, D. Difrancesco, M. Baruscotti, R. Longhi, R. H. Anderson, R. Billeter, V. Sharma, D. C. Sigg, M. R. Boyett and H. Dobrzynski (2009). "Molecular architecture of the human sinus node: insights into the function of the cardiac pacemaker." Circulation **119**(12): 1562-75.
- Chang, R. and D. L. Budenz (2008). "New developments in optical coherence tomography for glaucoma." Curr Opin Ophthalmol **19**(2): 127-35.
- Chen, P. S., C. C. Chou, A. Y. Tan, S. Zhou, M. C. Fishbein, C. Hwang, H. S. Karagueuzian and S. F. Lin (2006). "The mechanisms of atrial fibrillation." J Cardiovasc Electrophysiol **17 Suppl 3**: S2-7.
- Chen, Z., T. E. Milner, S. Srinivas, X. Wang, A. Malekafzali, M. J. van Gemert and J. S. Nelson (1997). "Noninvasive imaging of in vivo blood flow velocity using optical Doppler tomography." Opt Lett **22**(14): 1119-21.
- Cheng, Y., L. Li, V. Nikolski, D. W. Wallick and I. R. Efimov (2004). "Shock-induced arrhythmogenesis is enhanced by 2,3-butanedione monoxime compared with cytochalasin D." Am J Physiol Heart Circ Physiol **286**(1): H310-8.
- Cheng, Y., K. Mowrey, I. R. Efimov, D. R. Van Wagoner, P. J. Tchou and T. N. Mazgalev (1997). "Effects of 2,3-butanedione monoxime on atrial-atrioventricular nodal conduction in isolated rabbit heart." J Cardiovasc Electrophysiol **8**(7): 790-802.
- Cohen, L. B., B. M. Salzberg, H. V. Davila, W. N. Ross, D. Landowne, A. S. Waggoner and C. H. Wang (1974). "Changes in axon fluorescence during activity: molecular probes of membrane potential." J Membr Biol **19**(1): 1-36.

- Cohen, M. and G. V. Naccarelli (2008). "Pathophysiology and disease progression of atrial fibrillation: importance of achieving and maintaining sinus rhythm." J Cardiovasc Electrophysiol **19**(8): 885-90.
- Coro, L., P. Delise, E. Bertaglia, M. G. Mozzato, M. Fantinel, G. Bilardo, D. D'Este and P. Pascotto (2001). "The duration of atrial fibrillation influences the long-term efficacy of low-energy internal cardioversion." Ital Heart J **2**(5): 388-93.
- Costa, R. A., M. Skaf, L. A. Melo, Jr., D. Calucci, J. A. Cardillo, J. C. Castro, D. Huang and M. Wojtkowski (2006). "Retinal assessment using optical coherence tomography." Prog Retin Eye Res **25**(3): 325-53.
- Coumel, P. (1994a). "Paroxysmal atrial fibrillation: a disorder of autonomic tone?" Eur Heart J **15 Suppl A**: 9-16.
- Coumel, P. (1994b). "Paroxysmal atrial fibrillation: role of autonomic nervous system." Arch Mal Coeur Vaiss **87 Spec No 3**: 55-62.
- Cox, J. L. and T. M. Sundt, 3rd (1997). "The surgical management of atrial fibrillation." Annu Rev Med **48**: 511-23.
- Coyne, K. S., C. Paramore, S. Grandy, M. Mercader, M. Reynolds and P. Zimetbaum (2006). "Assessing the direct costs of treating nonvalvular atrial fibrillation in the United States." Value Health **9**(5): 348-56.
- Crandall, M. A., B. D. Horne, J. D. Day, J. L. Anderson, J. B. Muhlestein, B. G. Crandall, J. P. Weiss, J. S. Osborne, D. L. Lappe and T. J. Bunch (2009). "Atrial fibrillation significantly increases total mortality and stroke risk beyond that conveyed by the CHADS2 risk factors." Pacing Clin Electrophysiol **32**(8): 981-6.
- Davila, H. V., B. M. Salzberg, L. B. Cohen and A. S. Waggoner (1973). "A large change in axon fluorescence that provides a promising method for measuring membrane potential." Nat New Biol **241**(109): 159-60.
- Dhala, A., D. Underwood, R. Leman, E. Madu, D. Baugh, Y. Ozawa, Y. Kasamaki, Q. Xue and S. Reddy (2002). "Signal-averaged P-wave analysis of normal controls and patients with paroxysmal atrial fibrillation: a study in gender differences, age dependence, and reproducibility." Clin Cardiol **25**(11): 525-31.

- Dhar, S., P. Lidhoo, D. Koul, M. Bakhshi and F. T. Deger (2009). "Current concepts and management strategies in atrial flutter." South Med J **102**(9): 917-22.
- Dobrev, D. and S. Nattel (2010). "New antiarrhythmic drugs for treatment of atrial fibrillation." Lancet **375**(9721): 1212-23.
- Dobrev, D., E. Wettwer, A. Kortner, M. Knaut, S. Schuler and U. Ravens (2002). "Human inward rectifier potassium channels in chronic and postoperative atrial fibrillation." Cardiovasc Res **54**(2): 397-404.
- Dobrzynski, H., J. Li, J. Tellez, I. D. Greener, V. P. Nikolski, S. E. Wright, S. H. Parson, S. A. Jones, M. K. Lancaster, M. Yamamoto, H. Honjo, Y. Takagishi, I. Kodama, I. R. Efimov, R. Billeter and M. R. Boyett (2005). "Computer three-dimensional reconstruction of the sinoatrial node." Circulation **111**(7): 846-54.
- Doppalapudi, H., T. Yamada and G. N. Kay (2009). "Complications during catheter ablation of atrial fibrillation: Identification and prevention." Heart Rhythm **6**(12, Supplement 1): S18-S25.
- Dosdall, D. J. and R. E. Ideker (2007). "Intracardiac atrial defibrillation." Heart Rhythm **4**(3 Suppl): S51-6.
- Drexler, W. (2004). "Ultrahigh-resolution optical coherence tomography." J Biomed Opt **9**(1): 47-74.
- Drexler, W. and J. G. Fujimoto (2008). "State-of-the-art retinal optical coherence tomography." Prog Retin Eye Res **27**(1): 45-88.
- Drexler, W., U. Morgner, F. X. Kartner, C. Pitris, S. A. Boppart, X. D. Li, E. P. Ippen and J. G. Fujimoto (1999). "In vivo ultrahigh-resolution optical coherence tomography." Opt Lett **24**(17): 1221-3.
- Ebert, S. N., X. K. Liu and R. L. Woosley (1998). "Female gender as a risk factor for drug-induced cardiac arrhythmias: evaluation of clinical and experimental evidence." J Womens Health **7**(5): 547-57.
- Efimov, I. and C. M. Ripplinger (2006). "Virtual electrode hypothesis of defibrillation." Heart Rhythm **3**(9): 1100-2.

- Eisen, M. B., P. T. Spellman, P. O. Brown and D. Botstein (1998). "Cluster analysis and display of genome-wide expression patterns." Proc Natl Acad Sci U S A **95**(25): 14863-8.
- Ellinghaus, P., R. J. Scheubel, D. Dobrev, U. Ravens, J. Holtz, J. Huetter, U. Nielsch and H. Morawietz (2005). "Comparing the global mRNA expression profile of human atrial and ventricular myocardium with high-density oligonucleotide arrays." J Thorac Cardiovasc Surg **129**(6): 1383-90.
- Everett, T. H. t., E. E. Wilson and J. E. Olgin (2007). "Effects of atrial fibrillation substrate and spatiotemporal organization on atrial defibrillation thresholds." Heart Rhythm **4**(8): 1048-56.
- Fedorov, V. V., R. Chang, A. V. Glukhov, G. Kostecki, D. Janks, R. B. Schuessler and I. R. Efimov (2010). "Complex Interactions Between the Sinoatrial Node and Atrium During Reentrant Arrhythmias in the Canine Heart." Circulation **122**: 782-789.
- Fedorov, V. V., A. V. Glukhov, C. M. Ambrosi, G. Kostecki, R. Chang, D. Janks, R. B. Schuessler, N. Moazami, C. G. Nichols and I. R. Efimov (2011). "Effects of K(ATP) channel openers diazoxide and pinacidil in coronary-perfused atria and ventricles from failing and non-failing human hearts." J Mol Cell Cardiol **51**(2): 215-25.
- Fedorov, V. V., A. V. Glukhov, R. Chang, G. Kostecki, H. Aferol, W. J. Hucker, J. P. Wuskell, L. M. Loew, R. B. Schuessler, N. Moazami and I. R. Efimov (2010). "Optical mapping of the isolated coronary-perfused human sinus node." J Am Coll Cardiol **56**(17): 1386-94.
- Fedorov, V. V., W. J. Hucker, H. Dobrzynski, L. V. Rosenshtraukh and I. R. Efimov (2006). "Postganglionic nerve stimulation induces temporal inhibition of excitability in rabbit sinoatrial node." Am J Physiol Heart Circ Physiol **291**(2): H612-23.
- Fedorov, V. V., G. Kostecki, M. Hemphill and I. R. Efimov (2008). "Atria are more susceptible to electroporation than ventricles: implications for atrial stunning, shock-induced arrhythmia and defibrillation failure." Heart Rhythm **5**(4): 593-604.
- Fedorov, V. V., I. T. Lozinsky, E. A. Sosunov, E. P. Anyukhovskiy, M. R. Rosen, C. W. Balke and I. R. Efimov (2007). "Application of blebbistatin as an excitation-



contraction uncoupler for electrophysiologic study of rat and rabbit hearts." Heart Rhythm **4**(5): 619-26.

Fedorov, V. V., R. B. Schuessler, M. Hemphill, C. M. Ambrosi, R. Chang, A. S. Voloshina, K. Brown, W. J. Hucker and I. R. Efimov (2009). "Structural and functional evidence for discrete exit pathways that connect the canine sinoatrial node and atria." Circ Res **104**(7): 915-23.

Fenton, F. H., S. Luther, E. M. Cherry, N. F. Otani, V. Krinsky, A. Pumir, E. Bodenschatz and R. F. Gilmour, Jr. (2009). "Termination of atrial fibrillation using pulsed low-energy far-field stimulation." Circulation **120**(6): 467-76.

Fercher, A. F., C. K. Hitzenberger, G. Kamp and S. Y. El-Zaiat (1995). "Measurement of intraocular distances by backscattering spectral interferometry." Opt Commun **117**: 43-48.

Filas, B. A., I. R. Efimov and L. A. Taber (2007). "Optical coherence tomography as a tool for measuring morphogenetic deformation of the looping heart." Anat Rec (Hoboken) **290**(9): 1057-68.

Flagg, T. P., H. T. Kurata, R. Masia, G. Caputa, M. A. Magnuson, D. J. Lefer, W. A. Coetzee and C. G. Nichols (2008). "Differential structure of atrial and ventricular KATP: atrial KATP channels require SUR1." Circ Res **103**(12): 1458-65.

Flagg, T. P. and C. G. Nichols (2005). "Sarcolemmal K(ATP) channels: what do we really know?" J Mol Cell Cardiol **39**(1): 61-70.

Fleming, C. P., C. M. Ripplinger, B. Webb, I. R. Efimov and A. M. Rollins (2008). "Quantification of cardiac fiber orientation using optical coherence tomography." J Biomed Opt **13**(3): 030505.

Fleming, C. P., H. Wang, K. J. Quan and A. M. Rollins (2010). "Real-time monitoring of cardiac radio-frequency ablation lesion formation using an optical coherence tomography forward-imaging catheter." J Biomed Opt **15**(3): 030516.

Fluhler, E., V. G. Burnham and L. M. Loew (1985). "Spectra, membrane binding, and potentiometric responses of new charge shift probes." Biochemistry **24**(21): 5749-55.

- Foyil, K. V., V. V. Fedorov, C. M. Ripplinger, R. B. Schuessler and I. R. Efimov (2008). Demonstration and mechanisms of low-voltage multiple pulse defibrillation in a canine model of atrial flutter and fibrillation. Heart Rhythm. San Francisco. **5(5S)**: S111.
- Fujimoto, J. G. (2003). "Optical coherence tomography for ultrahigh resolution in vivo imaging." Nat Biotechnol **21**(11): 1361-7.
- Furukawa, T. and J. Kurokawa (2007). "Regulation of cardiac ion channels via non-genomic action of sex steroid hormones: implication for the gender difference in cardiac arrhythmias." Pharmacol Ther **115**(1): 106-15.
- Gaborit, N., S. Le Bouter, V. Szuts, A. Varro, D. Escande, S. Nattel and S. Demolombe (2007). "Regional and tissue specific transcript signatures of ion channel genes in the non-diseased human heart." J Physiol **582**(Pt 2): 675-93.
- Gaborit, N., M. Steenman, G. Lamirault, N. Le Meur, S. Le Bouter, G. Lande, J. Leger, F. Charpentier, T. Christ, D. Dobrev, D. Escande, S. Nattel and S. Demolombe (2005). "Human atrial ion channel and transporter subunit gene-expression remodeling associated with valvular heart disease and atrial fibrillation." Circulation **112**(4): 471-81.
- Gaborit, N., A. Varro, S. Le Bouter, V. Szuts, D. Escande, S. Nattel and S. Demolombe (2010). "Gender-related differences in ion-channel and transporter subunit expression in non-diseased human hearts." J Mol Cell Cardiol **49**(4): 639-46.
- Gambichler, T., G. Moussa, M. Sand, D. Sand, P. Altmeyer and K. Hoffmann (2005). "Applications of optical coherence tomography in dermatology." J Dermatol Sci **40**(2): 85-94.
- Garrey, W. E. (1914). "The nature of fibrillatory contraction of the heart: its relation to tissue mass and form." Am J Physiol **33**: 397-414.
- Garrey, W. E. (1924). "Auricular fibrillation." Physiol Rev **4**: 215-50.
- Gautier, P., J. P. Bertrand and P. Guiraudou (1991). "Effects of SR 44866, a potassium channel opener, on action potentials of rabbit, guinea pig, and human heart fibers." J Cardiovasc Pharmacol **17**(5): 692-700.

- Gillis, A. M., J. Koehler, M. Morck, R. Mehra and D. A. Hettrick (2005). "High atrial antitachycardia pacing therapy efficacy is associated with a reduction in atrial tachyarrhythmia burden in a subset of patients with sinus node dysfunction and paroxysmal atrial fibrillation." Heart Rhythm **2**(8): 791-6.
- Glukhov, A. V., V. V. Fedorov, Q. Lou, V. K. Ravikumar, P. W. Kalish, R. B. Schuessler, N. Moazami and I. R. Efimov (2010). "Transmural dispersion of repolarization in failing and nonfailing human ventricle." Circ Res **106**(5): 981-91.
- Glukhov, A. V., T. P. Flagg, V. V. Fedorov, I. R. Efimov and C. G. Nichols (2010). "Differential K(ATP) channel pharmacology in intact mouse heart." J Mol Cell Cardiol **48**(1): 152-60.
- Go, A. S., E. M. Hylek, K. A. Phillips, Y. Chang, L. E. Henault, J. V. Selby and D. E. Singer (2001). "Prevalence of diagnosed atrial fibrillation in adults: national implications for rhythm management and stroke prevention: the AnTicoagulation and Risk Factors in Atrial Fibrillation (ATRIA) Study." JAMA **285**(18): 2370-5.
- Grandi, E., F. S. Pasqualini and D. M. Bers (2010). "A novel computational model of the human ventricular action potential and Ca transient." J Mol Cell Cardiol **48**(1): 112-21.
- Gray, R. A., G. Ayers and J. Jalife (1997). "Video imaging of atrial defibrillation in the sheep heart." Circulation **95**(4): 1038-47.
- Gray, R. A. and J. Jalife (1998). "Effects of atrial defibrillation shocks on the ventricles in isolated sheep hearts." Circulation **97**(16): 1613-22.
- Gronich, N., A. Kumar, Y. Zhang, I. R. Efimov and N. M. Soldatov (2010). "Molecular remodeling of ion channels, exchangers and pumps in atrial and ventricular myocytes in ischemic cardiomyopathy." Channels (Austin) **4**(2): 101-7.
- Guagliumi, G. and V. Sirbu (2008). "Optical coherence tomography: high resolution intravascular imaging to evaluate vascular healing after coronary stenting." Catheter Cardiovasc Interv **72**(2): 237-47.
- Gupta, M., A. M. Rollins, J. A. Izatt and I. R. Efimov (2002). "Imaging of the atrioventricular node using optical coherence tomography." J Cardiovasc Electrophysiol **13**(1): 95.

- Haissaguerre, M., M. Hocini, P. Sanders, Y. Takahashi, M. Rotter, F. Sacher, T. Rostock, L. F. Hsu, A. Jonsson, M. D. O'Neill, P. Bordachar, S. Reuter, R. Roudaut, J. Clementy and P. Jais (2006). "Localized sources maintaining atrial fibrillation organized by prior ablation." Circulation **113**(5): 616-25.
- Haissaguerre, M., P. Jais, D. C. Shah, A. Takahashi, M. Hocini, G. Quiniou, S. Garrigue, A. Le Mouroux, P. Le Metayer and J. Clementy (1998). "Spontaneous initiation of atrial fibrillation by ectopic beats originating in the pulmonary veins." N Engl J Med **339**(10): 659-66.
- Haissaguerre, M., P. Sanders, M. Hocini, L. F. Hsu, D. C. Shah, C. Scavee, Y. Takahashi, M. Rotter, J. L. Pasquie, S. Garrigue, J. Clementy and P. Jais (2004). "Changes in atrial fibrillation cycle length and inducibility during catheter ablation and their relation to outcome." Circulation **109**(24): 3007-13.
- Ho, S. Y., R. H. Anderson and D. Sanchez-Quintana (2002). "Atrial structure and fibres: morphologic bases of atrial conduction." Cardiovasc Res **54**(2): 325-36.
- Holland, P. M., R. D. Abramson, R. Watson and D. H. Gelfand (1991). "Detection of specific polymerase chain reaction product by utilizing the 5'----3' exonuclease activity of *Thermus aquaticus* DNA polymerase." Proc Natl Acad Sci U S A **88**(16): 7276-80.
- Hu, Z. and A. M. Rollins (2005). "Quasi-telecentric optical design of a microscope-compatible OCT scanner." Optics Express **13**(17): 6407-6415.
- Huang, C., B. Liu and M. E. Brezinski (2008). "Ultrasound-enhanced optical coherence tomography: improved penetration and resolution." J Opt Soc Am A Opt Image Sci Vis **25**(4): 938-46.
- Huang, D., E. A. Swanson, C. P. Lin, J. S. Schuman, W. G. Stinson, W. Chang, M. R. Hee, T. Flotte, K. Gregory, C. A. Puliafito and et al. (1991). "Optical coherence tomography." Science **254**(5035): 1178-81.
- Hucker, W. J., M. L. McCain, J. I. Laughner, P. A. Iaizzo and I. R. Efimov (2008). "Connexin 43 expression delineates two discrete pathways in the human atrioventricular junction." Anat Rec (Hoboken) **291**(2): 204-15.

- Hucker, W. J., C. M. Ripplinger, C. P. Fleming, V. V. Fedorov, A. M. Rollins and I. R. Efimov (2008). "Bimodal biophotonic imaging of the structure-function relationship in cardiac tissue." J Biomed Opt **13**(5): 054012.
- Iacobas, D. A., S. Iacobas, N. Thomas and D. C. Spray (2010). "Sex-dependent gene regulatory networks of the heart rhythm." Funct Integr Genomics **10**(1): 73-86.
- James, A. F., S. C. Choisy and J. C. Hancox (2007). "Recent advances in understanding sex differences in cardiac repolarization." Prog Biophys Mol Biol **94**(3): 265-319.
- James, T. N. (1962). "Anatomy of the sinus node of the dog." Anat Rec **143**: 251-65.
- Janse, M. J. (2004). "Electrophysiological changes in heart failure and their relationship to arrhythmogenesis." Cardiovasc Res **61**(2): 208-17.
- Jenkins, M., R. S. Wade, Y. Cheng, A. M. Rollins and I. R. Efimov (2005). "Optical coherence tomography imaging of the purkinje network." J Cardiovasc Electrophysiol **16**(5): 559-60.
- Jenkins, M. W., O. Q. Chughtai, A. N. Basavanahally, M. Watanabe and A. M. Rollins (2007). "In vivo gated 4D imaging of the embryonic heart using optical coherence tomography." J Biomed Opt **12**(3): 030505.
- Kaab, S., J. Dixon, J. Duc, D. Ashen, M. Nabauer, D. J. Beuckelmann, G. Steinbeck, D. McKinnon and G. F. Tomaselli (1998). "Molecular basis of transient outward potassium current downregulation in human heart failure: a decrease in Kv4.3 mRNA correlates with a reduction in current density." Circulation **98**(14): 1383-93.
- Kannel, W. B. and E. J. Benjamin (2009). "Current perceptions of the epidemiology of atrial fibrillation." Cardiol Clin **27**(1): 13-24, vii.
- Kannel, W. B., P. A. Wolf, E. J. Benjamin and D. Levy (1998). "Prevalence, incidence, prognosis, and predisposing conditions for atrial fibrillation: population-based estimates." Am J Cardiol **82**(8A): 2N-9N.
- Katsouras, G., M. Sakabe, P. Comtois, A. Maguy, B. Burstein, P. G. Guerra, M. Talajic and S. Nattel (2009). "Differences in atrial fibrillation properties under vagal

nerve stimulation versus atrial tachycardia remodeling." Heart Rhythm **6**(10): 1465-72.

Kettlewell, S., N. L. Walker, S. M. Cobbe, F. L. Burton and G. L. Smith (2004). "The electrophysiological and mechanical effects of 2,3-butane-dione monoxime and cytochalasin-D in the Langendorff perfused rabbit heart." Exp Physiol **89**(2): 163-72.

Khan, I. A. (2003). "Atrial stunning: basics and clinical considerations." Int J Cardiol **92**(2-3): 113-28.

Khasnis, A. and R. K. Thakur (2009). "Atrial fibrillation: a historical perspective." Cardiol Clin **27**(1): 1-12, vii.

Kim, A. M., J. E. Olgin and T. H. t. Everett (2009). "Role of atrial substrate and spatiotemporal organization in atrial fibrillation." Heart Rhythm **6**(8 Suppl): S1-7.

Kligfield, P., K. G. Lax and P. M. Okin (1996). "QT interval-heart rate relation during exercise in normal men and women: definition by linear regression analysis." J Am Coll Cardiol **28**(6): 1547-55.

Kong, T. Q., Jr., J. J. Goldberger, M. Parker, T. Wang and A. H. Kadish (1995). "Circadian variation in human ventricular refractoriness." Circulation **92**(6): 1507-16.

Koster, R. W., P. Dorian, F. W. Chapman, P. W. Schmitt, S. G. O'Grady and R. G. Walker (2004). "A randomized trial comparing monophasic and biphasic waveform shocks for external cardioversion of atrial fibrillation." Am Heart J **147**(5): e20.

Koumi, S., C. L. Backer and C. E. Arentzen (1995). "Characterization of inwardly rectifying K<sup>+</sup> channel in human cardiac myocytes. Alterations in channel behavior in myocytes isolated from patients with idiopathic dilated cardiomyopathy." Circulation **92**(2): 164-74.

Koumi, S. I., R. L. Martin and R. Sato (1997). "Alterations in ATP-sensitive potassium channel sensitivity to ATP in failing human hearts." Am J Physiol **272**(4 Pt 2): H1656-65.

- Ladwig, K. H., B. Marten-Mittag, G. Lehmann, H. Gundel, H. Simon and E. Alt (2003). "Absence of an impact of emotional distress on the perception of intracardiac shock discharges." Int J Behav Med **10**(1): 56-65.
- Lauschke, J. and B. Maisch (2009). "Athlete's heart or hypertrophic cardiomyopathy?" Clin Res Cardiol **98**(2): 80-8.
- Lee, A. M., S. J. Melby and R. J. Damiano, Jr. (2009). "The surgical treatment of atrial fibrillation." Surg Clin North Am **89**(4): 1001-20, x-xi.
- Lewis, T. (1909). "Auricular fibrillation: a common clinical condition." Br Med J **2**: 1528.
- Lewis, T. (1912a). "Evidences of auricular fibrillation, treated historically." Br Med J **13**: 59.
- Lewis, T. (1912b). "The relation of regular tachycardias of auricular origin to auricular fibrillation." Heart **3**: 173-93.
- Li, D., S. Fareh, T. K. Leung and S. Nattel (1999). "Promotion of atrial fibrillation by heart failure in dogs: atrial remodeling of a different sort." Circulation **100**(1): 87-95.
- Li, J. and L. Wang (2006). "Catheter ablation of atrial fibrillation originating from superior vena cava." Arch Med Res **37**(3): 415-8.
- Li, W., C. M. Ripplinger, Q. Lou and I. R. Efimov (2009). "Multiple monophasic shocks improve electrotherapy of ventricular tachycardia in a rabbit model of chronic infarction." Heart Rhythm **6**(7): 1020-7.
- Lip, G. Y. and D. G. Beevers (1995). "ABC of atrial fibrillation. History, epidemiology, and importance of atrial fibrillation." BMJ **311**(7016): 1361-3.
- Liu, Y., G. Ren, B. O'Rourke, E. Marban and J. Seharaseyon (2001). "Pharmacological comparison of native mitochondrial K(ATP) channels with molecularly defined surface K(ATP) channels." Mol Pharmacol **59**(2): 225-30.

- Livak, K. J. and T. D. Schmittgen (2001). "Analysis of relative gene expression data using real-time quantitative PCR and the 2(-Delta Delta C(T)) Method." Methods **25**(4): 402-8.
- Lloyd-Jones, D., R. J. Adams, T. M. Brown, M. Carnethon, S. Dai, G. De Simone, T. B. Ferguson, E. Ford, K. Furie, C. Gillespie, A. Go, K. Greenlund, N. Haase, S. Hailpern, P. M. Ho, V. Howard, B. Kissela, S. Kittner, D. Lackland, L. Lisabeth, A. Marelli, M. M. McDermott, J. Meigs, D. Mozaffarian, M. Mussolino, G. Nichol, V. L. Roger, W. Rosamond, R. Sacco, P. Sorlie, T. Thom, S. Wasserthiel-Smoller, N. D. Wong and J. Wylie-Rosett (2010). "Heart disease and stroke statistics--2010 update: a report from the American Heart Association." Circulation **121**(7): e46-e215.
- Locati, E. H., W. Zareba, A. J. Moss, P. J. Schwartz, G. M. Vincent, M. H. Lehmann, J. A. Towbin, S. G. Priori, C. Napolitano, J. L. Robinson, M. Andrews, K. Timothy and W. J. Hall (1998). "Age- and sex-related differences in clinical manifestations in patients with congenital long-QT syndrome: findings from the International LQTS Registry." Circulation **97**(22): 2237-44.
- Lu, H. R., P. Remeysen, K. Somers, A. Saels and F. De Clerck (2001). "Female gender is a risk factor for drug-induced long QT and cardiac arrhythmias in an in vivo rabbit model." J Cardiovasc Electrophysiol **12**(5): 538-45.
- Luczak, E. D. and L. A. Leinwand (2009). "Sex-based cardiac physiology." Annu Rev Physiol **71**: 1-18.
- Luo, W., D. L. Marks, T. S. Ralston and S. A. Boppart (2006). "Three-dimensional optical coherence tomography of the embryonic murine cardiovascular system." J Biomed Opt **11**(2): 021014.
- Maisel, W. H. and L. W. Stevenson (2003). "Atrial fibrillation in heart failure: epidemiology, pathophysiology, and rationale for therapy." Am J Cardiol **91**(6A): 2D-8D.
- Mandapati, R., A. Skanes, J. Chen, O. Berenfeld and J. Jalife (2000). "Stable microreentrant sources as a mechanism of atrial fibrillation in the isolated sheep heart." Circulation **101**(2): 194-9.
- Marionneau, C., B. Couette, J. Liu, H. Li, M. E. Mangoni, J. Nargeot, M. Lei, D. Escande and S. Demolombe (2005). "Specific pattern of ionic channel gene expression



associated with pacemaker activity in the mouse heart." J Physiol **562**(Pt 1): 223-34.

Markus, M. R., H. F. Freitas, P. R. Chizzola, G. T. Silva, A. C. Lima and A. J. Mansur (2004). "Left ventricular mass in patients with heart failure." Arq Bras Cardiol **83**(3): 232-6; 227-31.

Mary-Rabine, L., A. Albert, T. D. Pham, A. Hordof, J. J. Fenoglio, Jr., J. R. Malm and M. R. Rosen (1983). "The relationship of human atrial cellular electrophysiology to clinical function and ultrastructure." Circ Res **52**(2): 188-99.

McKee, P. A., W. P. Castelli, P. M. McNamara and W. B. Kannel (1971). "The natural history of congestive heart failure: the Framingham study." N Engl J Med **285**(26): 1441-6.

McMichael, J. (1982). "History of atrial fibrillation 1628-1819 Harvey - de Senac - Laennec." Br Heart J **48**(3): 193-7.

Mines, G. R. (1913). "On dynamic equilibrium in the heart." J Physiol **46**: 349-82.

Mitchell, A. R., P. A. Spurrell, L. E. Boodhoo and N. Sulke (2004). "Long-term care of the patient with the atrial defibrillator." Am Heart J **147**(2): 210-7.

Miyasaka, Y., M. E. Barnes, B. J. Gersh, S. S. Cha, K. R. Bailey, W. P. Abhayaratna, J. B. Seward and T. S. Tsang (2006). "Secular trends in incidence of atrial fibrillation in Olmsted County, Minnesota, 1980 to 2000, and implications on the projections for future prevalence." Circulation **114**(2): 119-25.

Moe, G. K. (1968). "A conceptual model of atrial fibrillation." J Electrocardiol **1**(2): 145-6.

Monfredi, O., H. Dobrzynski, T. Mondal, M. R. Boyett and G. M. Morris (2010). "The anatomy and physiology of the sinoatrial node--a contemporary review." Pacing Clin Electrophysiol **33**(11): 1392-406.

Morad, M. and G. Salama (1979). "Optical probes of membrane potential in heart muscle." J Physiol **292**: 267-95.

- Nassif, N., B. Cense, B. H. Park, S. H. Yun, T. C. Chen, B. E. Bouma, G. J. Tearney and J. F. de Boer (2004). "In vivo human retinal imaging by ultrahigh-speed spectral domain optical coherence tomography." Optics Letters **29**(5): 480-482.
- Nattel, S. (1998). "Experimental evidence for proarrhythmic mechanisms of antiarrhythmic drugs." Cardiovasc Res **37**(3): 567-77.
- Nattel, S., B. Burstein and D. Dobrev (2008). "Atrial remodeling and atrial fibrillation: mechanisms and implications." Circ Arrhythm Electrophysiol **1**(1): 62-73.
- Nattel, S., Y. Frelin, N. Gaborit, C. Louault and S. Demolombe (2009). "Ion-channel mRNA-expression profiling: Insights into cardiac remodeling and arrhythmic substrates." J Mol Cell Cardiol **48**(1): 96-105.
- Nerbonne, J. M. (2004). "Studying cardiac arrhythmias in the mouse--a reasonable model for probing mechanisms?" Trends Cardiovasc Med **14**(3): 83-93.
- Nerbonne, J. M. and R. S. Kass (2005). "Molecular physiology of cardiac repolarization." Physiol Rev **85**(4): 1205-53.
- Noma, A. (1983). "ATP-regulated K<sup>+</sup> channels in cardiac muscle." Nature **305**(5930): 147-8.
- O'Hara, T., L. Virag, A. Varro and Y. Rudy (2011). "Simulation of the undiseased human cardiac ventricular action potential: model formulation and experimental validation." PLoS Comput Biol **7**(5): e1002061.
- Oh, W. Y., S. H. Yun, B. J. Vakoc, M. Shishkov, A. E. Desjardins, B. H. Park, J. F. de Boer, G. J. Tearney and B. E. Bouma (2008). "High-speed polarization sensitive optical frequency domain imaging with frequency multiplexing." Opt Express **16**(2): 1096-103.
- Oren, R. V. and C. E. Clancy (2010). "Determinants of heterogeneity, excitation and conduction in the sinoatrial node: a model study." PLoS Comput Biol **6**(12): e1001041.
- Padrini, R., S. Bova, G. Cargnelli, D. Piovan and M. Ferrari (1992). "Effects of pinacidil on guinea-pig isolated perfused heart with particular reference to the proarrhythmic effect." Br J Pharmacol **105**(3): 715-9.

- Panfilov, A. V. (2006). "Is heart size a factor in ventricular fibrillation? Or how close are rabbit and human hearts?" Heart Rhythm **3**(7): 862-4.
- Pellman, J., R. C. Lyon and F. Sheikh (2010). "Extracellular matrix remodeling in atrial fibrosis: mechanisms and implications in atrial fibrillation." J Mol Cell Cardiol **48**(3): 461-7.
- Pelzmann, B., P. Schaffer, E. Bernhart, P. Lang, H. Machler, B. Rigler and B. Koidl (2001). "Effects of K<sup>+</sup> channel openers on I K(ATP) of human atrial myocytes at physiological temperatures." Naunyn Schmiedebergs Arch Pharmacol **363**(2): 125-32.
- Pinto, T. L. and R. Waksman (2006). "Clinical applications of optical coherence tomography." J Interv Cardiol **19**(6): 566-73.
- Pountney, D. J., Z. Q. Sun, L. M. Porter, M. N. Nitabach, T. Y. Nakamura, D. Holmes, E. Rosner, M. Kaneko, T. Manaris, T. C. Holmes and W. A. Coetzee (2001). "Is the molecular composition of K(ATP) channels more complex than originally thought?" J Mol Cell Cardiol **33**(8): 1541-6.
- Povazay, B., K. Bizheva, A. Unterhuber, B. Hermann, H. Sattmann, A. F. Fercher, W. Drexler, A. Apolonski, W. J. Wadsworth, J. C. Knight, P. S. Russell, M. Vetterlein and E. Scherzer (2002). "Submicrometer axial resolution optical coherence tomography." Opt Lett **27**(20): 1800-2.
- Raeis, V., P. Philip-Couderc, A. Roatti, W. Habre, J. Sierra, A. Kalangos, M. Beghetti and A. J. Baertschi (2010). "Central venous hypoxemia is a determinant of human atrial ATP-sensitive potassium channel expression: evidence for a novel hypoxia-inducible factor 1alpha-Forkhead box class O signaling pathway." Hypertension **55**(5): 1186-92.
- Ramaekers, D., H. Ector, A. E. Aubert, A. Rubens and F. Van de Werf (1998). "Heart rate variability and heart rate in healthy volunteers. Is the female autonomic nervous system cardioprotective?" Eur Heart J **19**(9): 1334-41.
- Ripplinger, C. M., V. I. Krinsky, V. P. Nikolski and I. R. Efimov (2006). "Mechanisms of unpinning and termination of ventricular tachycardia." Am J Physiol Heart Circ Physiol **291**(1): H184-92.

- Ripplinger, C. M., Q. Lou, W. Li, J. Hadley and I. R. Efimov (2009). "Panoramic imaging reveals basic mechanisms of induction and termination of ventricular tachycardia in rabbit heart with chronic infarction: implications for low-voltage cardioversion." Heart Rhythm **6**(1): 87-97.
- Roden, D. M. and S. Kopperschmidt (1999). "From genes to channels: normal mechanisms." Cardiovasc Res **42**(2): 318-26.
- Rollins, A. M., S. Yazdanfar, J. K. Barton and J. A. Izatt (2002). "Real-time in vivo color Doppler optical coherence tomography." J Biomed Opt **7**(1): 123-9.
- Ross, W. N., B. M. Salzberg, L. B. Cohen, A. Grinvald, H. V. Davila, A. S. Waggoner and C. H. Wang (1977). "Changes in absorption, fluorescence, dichroism, and Birefringence in stained giant axons: : optical measurement of membrane potential." J Membr Biol **33**(1-2): 141-83.
- Salama, G. and B. R. Choi (2000). "Images of Action Potential Propagation in Heart." News Physiol Sci **15**: 33-41.
- Salama, G. and M. Morad (1976). "Merocyanine 540 as an optical probe of transmembrane electrical activity in the heart." Science **191**(4226): 485-7.
- Sanchez-Quintana, D., J. A. Cabrera, J. Farre, V. Climent, R. H. Anderson and S. Y. Ho (2005). "Sinus node revisited in the era of electroanatomical mapping and catheter ablation." Heart **91**(2): 189-94.
- Sanders, P., J. B. Morton, P. M. Kistler, S. J. Spence, N. C. Davidson, A. Hussin, J. K. Vohra, P. B. Sparks and J. M. Kalman (2004). "Electrophysiological and electroanatomic characterization of the atria in sinus node disease: evidence of diffuse atrial remodeling." Circulation **109**(12): 1514-22.
- Schenk, J. O. and M. E. Brezinski (2002). "Ultrasound induced improvement in optical coherence tomography (OCT) resolution." Proc Natl Acad Sci U S A **99**(15): 9761-4.
- Schoels, W., C. D. Swerdlow, W. Jung, K. M. Stein, K. Seidl and C. J. Haffajee (2001). "Worldwide clinical experience with a new dual-chamber implantable cardioverter defibrillator system." J Cardiovasc Electrophysiol **12**(5): 521-8.

- Schuessler, R. B. (2003). "Abnormal sinus node function in clinical arrhythmias." J Cardiovasc Electrophysiol **14**(2): 215-7.
- Seiler, J. and W. G. Stevenson (2010). "Atrial fibrillation in congestive heart failure." Cardiol Rev **18**(1): 38-50.
- Severs, N. J., A. F. Bruce, E. Dupont and S. Rothery (2008). "Remodelling of gap junctions and connexin expression in diseased myocardium." Cardiovasc Res **80**(1): 9-19.
- Shanmugam, M., C. E. Molina, S. Gao, R. Severac-Bastide, R. Fischmeister and G. J. Babu (2011). "Decreased sarcolipin protein expression and enhanced sarco(endo)plasmic reticulum Ca(2+) uptake in human atrial fibrillation." Biochem Biophys Res Commun **410**(1): 97-101.
- Sharifov, O. F., V. V. Fedorov, G. G. Beloshapko, A. V. Glukhov, A. V. Yushmanova and L. V. Rosenshtraukh (2004). "Roles of adrenergic and cholinergic stimulation in spontaneous atrial fibrillation in dogs." J Am Coll Cardiol **43**(3): 483-90.
- Silverman, M. E. (1994). "From rebellious palpitations to the discovery of auricular fibrillation: contributions of Mackenzie, Lewis and Einthoven." Am J Cardiol **73**(5): 384-9.
- Sipido, K. R., T. Stankovicova, W. Flameng, J. Vanhaecke and F. Verdonck (1998). "Frequency dependence of Ca<sup>2+</sup> release from the sarcoplasmic reticulum in human ventricular myocytes from end-stage heart failure." Cardiovasc Res **37**(2): 478-88.
- Soltysinska, E., S. P. Olesen, T. Christ, E. Wettwer, A. Varro, M. Grunnet and T. Jespersen (2009). "Transmural expression of ion channels and transporters in human nondiseased and end-stage failing hearts." Pflugers Arch **459**(1): 11-23.
- Steinhaus, D. M., D. S. Cardinal, L. Mongeon, S. K. Musley, L. Foley and S. Corrigan (2002). "Internal defibrillation: pain perception of low energy shocks." Pacing Clin Electrophysiol **25**(7): 1090-3.
- Stiles, M. K., C. X. Wong, B. John, P. Kuklik, A. G. Brooks, D. H. Lau, H. Dimitri, L. Wilson, G. D. Young and P. Sanders (2010). "Characterization of atrial remodeling studied remote from episodes of typical atrial flutter." Am J Cardiol **106**(4): 528-34.

- Takagi, S., A. Pumir, D. Pazo, I. Efimov, V. Nikolski and V. Krinsky (2004). "Unpinning and removal of a rotating wave in cardiac muscle." Phys Rev Lett **93**(5): 058101.
- Tamargo, J., R. Caballero and E. Delpon (2004). "Pharmacological approaches in the treatment of atrial fibrillation." Curr Med Chem **11**(1): 13-28.
- Tearney, G. J., M. E. Brezinski, S. A. Boppart, B. E. Bouma, N. Weissman, J. F. Southern, E. A. Swanson and J. G. Fujimoto (1996). "Images in cardiovascular medicine. Catheter-based optical imaging of a human coronary artery." Circulation **94**(11): 3013.
- Tearney, G. J., M. E. Brezinski, B. E. Bouma, S. A. Boppart, C. Pitris, J. F. Southern and J. G. Fujimoto (1997). "In vivo endoscopic optical biopsy with optical coherence tomography." Science **276**(5321): 2037-9.
- Tearney, G. J., I. K. Jang and B. E. Bouma (2006). "Optical coherence tomography for imaging the vulnerable plaque." J Biomed Opt **11**(2): 021002.
- Tearney, G. J., H. Yabushita, S. L. Houser, H. T. Aretz, I. K. Jang, K. H. Schlendorf, C. R. Kauffman, M. Shishkov, E. F. Halpern and B. E. Bouma (2003). "Quantification of macrophage content in atherosclerotic plaques by optical coherence tomography." Circulation **107**(1): 113-9.
- Tellez, J., M. Maczewski, J. Yanni, P. Sutyagin, U. Mackiewicz, A. Atkinson, S. Inada, A. Beresewicz, R. Billeter, H. Dobrzynski and M. R. Boyett (2011). "Ageing-Dependent Remodelling of Ion Channel and Ca<sup>2+</sup> Clock Genes Underlying Sinoatrial Node Pacemaking." Exp Physiol.
- Tomaselli, G. F. and E. Marban (1999). "Electrophysiological remodeling in hypertrophy and heart failure." Cardiovasc Res **42**(2): 270-83.
- Trayanova, N., K. Skouibine and F. Aguel (1998). "The role of cardiac tissue structure in defibrillation." Chaos **8**(1): 221-233.
- Unterhuber, A., B. Povazay, K. Bizheva, B. Hermann, H. Sattmann, A. Stingl, T. Le, M. Seefeld, R. Menzel, M. Preusser, H. Budka, C. Schubert, H. Reitsamer, P. K. Ahnelt, J. E. Morgan, A. Cowey and W. Drexler (2004). "Advances in broad bandwidth light sources for ultrahigh resolution optical coherence tomography." Phys Med Biol **49**(7): 1235-46.

- Valderrabano, M. (2007). "Influence of anisotropic conduction properties in the propagation of the cardiac action potential." Prog Biophys Mol Biol **94**(1-2): 144-68.
- Valderrabano, M., M. H. Lee, T. Ohara, A. C. Lai, M. C. Fishbein, S. F. Lin, H. S. Karagueuzian and P. S. Chen (2001). "Dynamics of intramural and transmural reentry during ventricular fibrillation in isolated swine ventricles." Circ Res **88**(8): 839-48.
- Van Gelder, I. C., H. J. Crijns, W. H. Van Gilst, R. Verwer and K. I. Lie (1991). "Prediction of uneventful cardioversion and maintenance of sinus rhythm from direct-current electrical cardioversion of chronic atrial fibrillation and flutter." Am J Cardiol **68**(1): 41-6.
- Van Gelder, I. C., A. E. Tuinenburg, B. S. Schoonderwoerd, R. G. Tieleman and H. J. Crijns (1999). "Pharmacologic versus direct-current electrical cardioversion of atrial flutter and fibrillation." Am J Cardiol **84**(9A): 147R-151R.
- Van Wagoner, D. R. (2003). "Electrophysiological remodeling in human atrial fibrillation." Pacing Clin Electrophysiol **26**(7 Pt 2): 1572-5.
- Van Wagoner, D. R., A. L. Pond, M. Lamorgese, S. S. Rossie, P. M. McCarthy and J. M. Nerbonne (1999). "Atrial L-type Ca<sup>2+</sup> currents and human atrial fibrillation." Circ Res **85**(5): 428-36.
- Van Wagoner, D. R., A. L. Pond, P. M. McCarthy, J. S. Trimmer and J. M. Nerbonne (1997). "Outward K<sup>+</sup> current densities and Kv1.5 expression are reduced in chronic human atrial fibrillation." Circ Res **80**(6): 772-81.
- VanGuilder, H. D., K. E. Vrana and W. M. Freeman (2008). "Twenty-five years of quantitative PCR for gene expression analysis." Biotechniques **44**(5): 619-26.
- Verheule, S., E. Wilson, T. t. Everett, S. Shanbhag, C. Golden and J. Olgin (2003). "Alterations in atrial electrophysiology and tissue structure in a canine model of chronic atrial dilatation due to mitral regurgitation." Circulation **107**(20): 2615-22.
- Verkerk, A. O., A. Baartscheer, J. R. de Groot, R. Wilders and R. Coronel (2011). "Etiology-dependency of ionic remodeling in cardiomyopathic rabbits." Int J Cardiol **148**(2): 154-60.

- Verkerk, A. O., M. W. Veldkamp, N. de Jonge, R. Wilders and A. C. van Ginneken (2000). "Injury current modulates afterdepolarizations in single human ventricular cells." Cardiovasc Res **47**(1): 124-32.
- Vozzi, C., E. Dupont, S. R. Coppens, H. I. Yeh and N. J. Severs (1999). "Chamber-related differences in connexin expression in the human heart." J Mol Cell Cardiol **31**(5): 991-1003.
- Waldo, A. L. (2003). "Inter-relationships between atrial flutter and atrial fibrillation." Pacing Clin Electrophysiol **26**(7 Pt 2): 1583-96.
- Waldo, A. L. and G. K. Feld (2008). "Inter-relationships of atrial fibrillation and atrial flutter mechanisms and clinical implications." J Am Coll Cardiol **51**(8): 779-86.
- Wang, T. J., M. G. Larson, D. Levy, R. S. Vasan, E. P. Leip, P. A. Wolf, R. B. D'Agostino, J. M. Murabito, W. B. Kannel and E. J. Benjamin (2003). "Temporal relations of atrial fibrillation and congestive heart failure and their joint influence on mortality: the Framingham Heart Study." Circulation **107**(23): 2920-5.
- Wang, Z. (2010). "The role of microRNA in cardiac excitability." J Cardiovasc Pharmacol **56**(5): 460-70.
- Wang, Z., Y. Lu and B. Yang (2011). "MicroRNAs and atrial fibrillation: new fundamentals." Cardiovasc Res **89**(4): 710-21.
- Weiner, N. and A. Rosenbluth (1946). "The mathematical formulation of the problem of conduction of impulses in a network of connected excitable elements." Arch Inst Cardiol Mex **16**: 205-65.
- Welzel, J. (2001). "Optical coherence tomography in dermatology: a review." Skin Res Technol **7**(1): 1-9.
- Wijffels, M. C., C. J. Kirchhof, R. Dorland and M. A. Allessie (1995). "Atrial fibrillation begets atrial fibrillation. A study in awake chronically instrumented goats." Circulation **92**(7): 1954-68.
- Wilde, A. A., D. Escande, C. A. Schumacher, D. Thuringer, M. Mestre, J. W. Fiolet and M. J. Janse (1990). "Potassium accumulation in the globally ischemic mammalian heart. A role for the ATP-sensitive potassium channel." Circ Res **67**(4): 835-43.



- Wojtkowski, M., R. Leitgeb, A. Kowalczyk, T. Bajraszewski and A. F. Fercher (2002). "In vivo human retinal imaging by Fourier domain optical coherence tomography." J Biomed Opt **7**(3): 457-63.
- Wolbrette, D., G. Naccarelli, A. Curtis, M. Lehmann and A. Kadish (2002). "Gender differences in arrhythmias." Clin Cardiol **25**(2): 49-56.
- Workman, A. J. (2010). "Cardiac adrenergic control and atrial fibrillation." Naunyn Schmiedebergs Arch Pharmacol **381**(3): 235-49.
- Workman, A. J., K. A. Kane and A. C. Rankin (2008). "Cellular bases for human atrial fibrillation." Heart Rhythm **5**(6 Suppl): S1-6.
- Wu, G., C. X. Huang, Y. H. Tang, H. Jiang, J. Wan, H. Chen, Q. Xie and Z. R. Huang (2005). "Changes of IK, ATP current density and allosteric modulation during chronic atrial fibrillation." Chin Med J (Engl) **118**(14): 1161-6.
- Xu, X., L. Yu and Z. Chen (2008). "Optical clearing of flowing blood using dextrans with spectral domain optical coherence tomography." J Biomed Opt **13**(2): 021107.
- Yang, P. C., J. Kurokawa, T. Furukawa and C. E. Clancy (2010). "Acute effects of sex steroid hormones on susceptibility to cardiac arrhythmias: a simulation study." PLoS Comput Biol **6**(1): e1000658.
- Yue, L., J. Feng, R. Gaspo, G. R. Li, Z. Wang and S. Nattel (1997). "Ionic remodeling underlying action potential changes in a canine model of atrial fibrillation." Circ Res **81**(4): 512-25.
- Yun, S. H., G. J. Tearney, J. F. de Boer, N. Iftimia and B. E. Bouma (2003). "High-speed optical frequency-domain imaging." Optics Express **11**(22): 2953-2963.
- Zhang, H., T. P. Flagg and C. G. Nichols (2010). "Cardiac sarcolemmal K(ATP) channels: Latest twists in a queuing tale!" J Mol Cell Cardiol **48**(1): 71-5.
- Zicha, S., L. Xiao, S. Stafford, T. J. Cha, W. Han, A. Varro and S. Nattel (2004). "Transmural expression of transient outward potassium current subunits in normal and failing canine and human hearts." J Physiol **561**(Pt 3): 735-48.

## CV

Christina Marie Ambrosi

Date of Birth: May 21, 1981

August 2011, Ph.D. in Biomedical Engineering, Washington University in St. Louis

May 2004, M.S. in Biomedical Engineering, Washington University in St. Louis

M.S. Thesis: "Comparison of the Response of the Human Aortic Endothelial Cell to Cyclic Stretch and Compression", prepared under the supervision of Dr. Frank C-P. Yin

May 2004, B.S. in Biomedical Engineering, Washington University in St. Louis

### ***Publications***

*Ambrosi CM, Fedorov VV, Schuessler RB, Rollins AM, Efimov IR. Quantification of fiber orientation in the canine atrial pacemaker complex using optical coherence tomography. Submitted to Circulation Imaging. Submitted, 2011.*

Fedorov VV, *Ambrosi CM*, Kostecki G, Huckler WJ, Glukhov AV, Wuskell JP, Loew LM, Moazami N, Efimov IR. Anatomical localization and autonomic modulation of AV junctional rhythm in failing human hearts. *Circ Arrhythm Electrophysiol.* 4(4): 515-25, Aug 2011.

Fedorov VV, Glukhov AV, *Ambrosi CM*, Kostecki G, Chang R, Janks D, Schuessler RB, Moazami N, Nichols CG, Efimov IR. Effects of  $K_{ATP}$  channel openers diazoxide and pinacidil in coronary-perfused atria and ventricles from failing and nonfailing human hearts. *J Mol Cell Cardiol.* 51(2): 215-25, Aug 2011.

*Ambrosi CM*, Ripplinger CM, Efimov IR, Fedorov VV. Termination of sustained atrial flutter and fibrillation using a low-voltage multiple-shock therapy. *Heart Rhythm.* 8(1): 101-8, Jan 2011.

Kurian T, *Ambrosi C*, Huckler WJ, Fedorov VV, Efimov IR. Anatomy and electrophysiology of the human AV node. *Pacing Clin Electrophysiol.* 33(6): 754-62, June 2010.

*Ambrosi CM*, Moazami N, Rollins AM, Efimov IR. Virtual histology of the human heart using optical coherence tomography. *J Biomed Optics.* 14(5): 054002, Sept-Oct 2009.

Fedorov VV, Schuessler RB, Hemphill M, *Ambrosi CM*, Chang R, Voloshina AS, Brown K, Huckler WJ, Efimov IR. Structural and functional evidence for discrete exit pathways that connect the canine sinoatrial node and atria. *Circ Res.* 104(7): 915-23, April 2009.

Wille JJ, *Ambrosi CM*, Yin FCP. Comparison of the effects of cyclic stretching and compression on endothelial cell morphological responses. *J Biomech Eng.* 126(5): 545-51, Oct 2004.

## ***Abstracts and Proceedings***

*Ambrosi CM, Moazami N, Nerbonne JM, Efimov IR. Gender-dependent differences in molecular electrophysiological targets in failing and nonfailing human hearts. Heart Rhythm. 8(5S): S320, May 2011.*

*Ambrosi CM, Moazami N, Nerbonne JM, Efimov IR. Molecular electrophysiological differences between genders in the nonfailing human heart. Proceedings of the Biomedical Engineering Society. Oct 2010.*

*Efimov IR, Fedorov VV, Glukhov A, Lou Q, Ambrosi C, Janks D, Hucker WJ, Schuessler RB, Moazami N. Multiscale imaging of the human heart: Building the foundation for human systems physiology and translational medicine. Conf Proc IEEE Eng Med Biol Sci. 1: 5177-80, 2010.*

*Ambrosi CM, Ripplinger CM, Efimov IR, Fedorov VV. Multiple low-energy shock therapy terminates atrial flutter and fibrillation more effectively than ATP. Heart Rhythm. 6(11): 1686-7, Nov 2009.*

*Ambrosi CM, Moazami N, Rollins AM, Efimov IR. Virtual histology of the human heart using optical coherence tomography. Heart Rhythm. 6(5S): S421, May 2009.*

*Fedorov VV, Ambrosi CM, Hucker WJ, Glukhov AV, Foyil KV, Wuskell J, Loew LM, Moazami N, Efimov IR. Human AV junctional pacemaker shift due to cholinergic and adrenergic stimulations: Optical imaging with a novel long wavelength voltage-sensitive dye. Circulation. 118(Suppl): 520, Oct 2008.*

*Fedorov VV, Schuessler RB, Ambrosi CM, Hucker WJ, Glukhov AV, Efimov IR. Structure-function correlation in the mammalian sinoatrial node: Implications for engineering a biological pacemaker. Proceedings of the Biomedical Engineering Society. Oct 2008.*

*Ambrosi CM, Fedorov VV, Hucker WJ, Fleming CP, Schuessler RB, Rollins AM, Efimov IR. Optical coherence tomography of the canine sinoatrial node. Proceedings of the Biomedical Engineering Society. Oct 2008.*

*Fedorov VV, Hucker WJ, Ambrosi CM, Foyil KV, Glukhov AV, Schuessler RB, Moazami N, Efimov IR. Arrhythmogenesis due to alternans of anisotropy in isolated coronary-perfused human ventricles with dilated cardiomyopathy. Heart Rhythm. 5(5S): S112, May 2008.*

*Fedorov VV, Ripplinger CM, Voloshina AS, Ambrosi CM, Wolfe C, Foyil KV, Schuessler RB, Efimov IR. Sinoatrial reentry is a mechanism of atrial flutter. Heart Rhythm. 5(5S): S59, May 2008.*

*Ambrosi CM, Huckler WJ, Fedorov VV, Wuskell J, Loew LM, Moazami N, Efimov IR. Bimodal biophotonic imaging of the human atrioventricular junction. Heart Rhythm. 5(5S): S58, May 2008.*

Fedorov VV, Schuessler RB, Huckler WJ, *Ambrosi CM*, Foyil KV, Ripplinger CM, Efimov IR. Dual-modal biophotonic imaging of the canine sinoatrial nodal structure and function. *Circulation*. 116(Suppl II): 119, Nov 2007.

*Ambrosi CM, Chuang J, Yin FCP. Comparison of endothelial cell gene expression to cyclic stretching versus compression. Proceedings of the Biomedical Engineering Society. Oct 2003.*

*Ambrosi CM, Wille JJ, Yin FCP. Reorientation response of endothelial cells to cyclic compression: comparison with cyclic stretching. Proceedings of the Biomedical Engineering Society. Oct 2002.*